Design and Control of Hydraulic Power Take-Offs for Wave Energy Converters

Cargo, Christopher

Award date:
2013

Awarding institution:
University of Bath

Design and Control of Hydraulic Power Take-Offs for Wave Energy Converters

submitted by

Christopher Cargo

for the degree of Doctor of Philosophy

of the

University of Bath

Department of Mechanical Engineering

December 2012

SUMMARY

Renewable marine energy has attracted considerable interest in recent years, especially in the UK due to its excellent location to take advantage of this sustainable energy source. Different types of device have been developed over several decades to capture the energy of sea waves but they all need to be able to convert this mechanical energy into electrical energy. The success of wave energy converters (WECs) depends on their efficiency, reliability and their ability to react to the variable wave conditions. Although a number of simulation studies have been undertaken, these have used significantly simplified models and any experimental data is scarce.

This work considers a heaving point absorber with a hydraulic power take-off unit. It employs a common hydraulic power take-off design, which uses the heaving motion of the buoy to drive an actuator that behaves like a linear pump. Energy storage is used to provide power smoothing in an attempt to give a constant power output from a hydraulic motor coupled to a generator. Although this design has been presented before, the inefficiencies and dynamics of the components have not been investigated in detail.

The aim of this work is to create an understanding of the non-linear dynamics of a hydraulic power take-off unit and how these affect the hydrodynamic behaviour of the WEC. A further aim is to predict the efficiency of the power take-off unit and determine tuning and control methods which will improve the power generation. In order to do this and test the device in different wave conditions, a full hydrodynamic and hydraulic model is developed using the Simulink and SimHydraulics software package.

The model is initially tested with regular waves to determine the behaviour of the power take-off unit and a method for adjusting the hydraulic motor displacement depending on the frequency of the incoming wave is investigated. The optimal effective PTO damping to maximise power generation is found to be dependent on the significant wave frequency and the values of PTO damping are significantly different to previous work using a linear power take-off model which emphasises the importance of including the inefficiencies of the hydraulic components. The model is then analysed with irregular waves to predict the behaviour and power levels in realistic wave conditions. Power generation reduces in comparison to regular waves but a similar tuning method to maximise power generation still exists.

A hydraulic motor speed control method is shown to increase power generation in irregular waves by maintaining the motor speed within an acceptable working range. Wave data from the Atlantic Ocean is then used to investigate the benefits of an adaptive tuning method which uses estimated wave parameters for a number of different sea conditions. Results show only minimal gains from using active tuning methods over a passive method. However, results revealed significant power losses in both calm and rough sea conditions with the PTO most efficient, at approximately 60%, in an average sea power.

A scaled experimental power take-off unit is developed to help validate the simulation results. The power take-off unit is tested using a hardware-in-the-loop system in which the hydrodynamic behaviour of the WEC is predicted by a real-time simulation model. The experimental results show good agreement to the simulation with the PTO showing similar characteristics and tuning trends for maximising power generation.

ACKNOWLEDGEMENTS

I would like to thank my supervisors Professor Andrew Plummer and Dr Andrew Hillis for their support and guidance throughout the project and also their understanding when I required time away from Bath for hockey commitments. Furthermore, I would like to show my gratitude to Dr Derek Tilley and Dr Michael Schlotter for their supervision at different times during the project. Derek presented the project to me as an undergraduate and I am very grateful to him for the wonderful opportunity.

I would also like to thank my friends in 8 East for their help and camaraderie during the last few years. Alan Jefferies, my technician, has been invaluable in helping to build the experimental rig and relocate it a few times after the many rearrangements of the laboratories.

Finally, I would like to thank my parents for their amazing support throughout my time at Bath. They have been a constant driving force and support in balancing my thesis and playing international sport and I could not have done either without their continual help.

CONTENTS

LIST OF FIGURES

LIST OF TABLES

NOMENCLATURE

Listed below are the main parameters and variables used throughout this thesis. Additional subscripted versions of these variable may also be found in the document to describe more specific parts of the system, which are not listed here. Where this occurs, the meaning of these parameters will be clearly stated in the approriate section.

$A(\omega)$	frequency dependent added mass	[kg]
A_p	piston area	[m^2]
A_∞	added mass at infinite frequency	[kg]
a	buoy radius	[m]
B_o	bulk modulus of hydraulic fluid	[bar]
$B(\omega)$	frequency dependent radiation damping coefficient	[Ns/m]
C	viscous damping coefficient	[N/(m/s)]
C_f	motor coulomb friction coefficient	[-]
C_g	generator damping coefficient	[Nm/(rad/s)]
C_{opt}	optimum viscous damping coefficient	[Ns/m)]
C_s	motor slip coefficient	[-]
C_v	motor viscous friction coefficient	[-]
D_m	motor capacity	[cc/rev]
d	pipe diameter	[m]
E_A	accumulator 'A' energy	[J]
E_B	accumulator 'B' energy	[J]
E_m	motor energy	[J]
$F_m(s)$	Laplace transform of mechanical force	[N]
f	pipe friction factor	[-]

f_c	coulomb friction	[N]
f_e	wave excitation force	[N]
f_{fr}	cylinder friction	[N]
f_h	wave force	[N]
f_{hs}	wave hydrostatic force	[N]
f_m	mechanical force	[N]
f_{rig}	mechanical force produced by the rig	[N]
f_v	viscous friction coefficient	[Ns/m]
f_p	peak wave frequency	[rad/s]
f_r	wave radiation force	[N]
$F_e(s)$	Laplace transform of wave excitation force	[N]
g	gravitational acceleration	[ms^{-2}]
H	wave height	[m]
H_s	significant wave height	[m]
j	imaginary unit, $\sqrt{-1}$	[-]
J	generator inertia	[kgm^2]
K	PTO spring constant	[N/m]
K_i	proportioanl gain	[-]
K_p	integral gain	[-]
K_v	valve coefficient	[m^3/s bar]
k	wave number	[m^{-1}]
k_z	displacement scaling factor	[-]
k_ω	frequency scaling factor	[-]
L	pipe length	[m]
$L(t)$	radiation impulse response function	[Ns/m]
l	half height of buoy	[m]
m	mass of buoy	[kg]
m_a	frequency moment of the variance spectrum	[-]
n	number of wave components	[-]
p	pressure	[bar]
p_i	piston chamber pressure (i = 1,2)	[bar]
p_A	accumulator 'A' pressure	[bar]
p_B	accumulator 'B' pressure	[bar]
p_o	initial accumulator pressure	[bar]
$\bar{P_{cap}}$	average captured power	[kW]
P_{cap}	captured power	[kW]
P_{flux}	wave power flux	[kW/m]
P_{gen}	generated power	[kW]
P_{max}	maximum average captured power	[kW]
P_{trans}	transmitted power	[kW]
P_{wave}	wave power	[kW]
q	flow rate	[m^3/s]

q_m	flow rate to the motor	[m^3/s]
q_r	rectified flow rate	[m^3/s]
S	buoy cross sectional area	[m^2]
S_n	spectral density	[m^2s]
t	time	[s]
T_e	energy period	[s]
T_m	motor torque	[Nm]
T_p	peak period	[s]
U_f	mean fluid velocity	[m/s]
$U(j\omega)$	velocity in the frequency domain	[m/s]
U_{opt}	optimum buoy velocity amplitude	[m/s]
V_i	piston chamber oil volume (i = 1,2)	[m^3]
V_A	accumulator 'A' oil volume	[m^3]
V_B	accumulator 'B' oil volume	[m^3]
V_o	initial oil volume in accumulators	[m^3]
x	buoy displacement	[m]
$\dot{x}$	buoy velocity	[m/s]
$\ddot{x}$	buoy acceleration	[m/s^2]
x_m	fraction of motor displacement	[-]
$\bar{x_m}$	average fraction of motor displacement	[-]
x_r	rig displacement	[m]
$X(s)$	Laplace transform of position, x(t)	[m]
X_w	wave amplitude	[m]
α	PTO damping	[Ns/m]
α_{opt}	optimum PTO damping	[Ns/m]
Δp	pressure drop	[bar]
Δt	wave cycle time	[s]
$\Delta\omega$	wave frequency band	[rad/s]
ϵ	Havelock's coefficient	[-]
η	wave surface elevation	[m]
η_{cap}	buoy capture efficiency	[%]
η_m	motor efficiency	[%]
η_{pto}	PTO efficiency	[%]
η_{tot}	total PTO efficiency	[%]
η_{trans}	transmission efficiency	[%]
η_{wec}	overall WEC efficiency	[%]
γ	adiabatic index	[-]
$\Gamma(\omega)$	wave excitation force coefficient	[N/m]
μ	oil dynamic viscosity	[Ns/m^2]
ρ	water density	[kg/m^3]
ρ_o	oil density	[kg/m^3]

τ	time constant	[s]
Φ	PTO force	[N]
Φ_{opt}	optimum PTO force amplitude	[N]
ω	wave frequency	[rad/s]
ω_m	angular motor velocity	[rad/s]
$\bar{\omega_m}$	average motor angular velocity	[rad/s]
ω_{max}	maximum frequency	[rad/s]
ω_{min}	minimum frequency	[rad/s]
ω_n	natural frequency	[rad/s]
ω_r	rig frequency	[rad/s]
ω_s	generator synchronous speed	[rad/s]
ω_{var}	motor speed variation	[rad/s]
φ	wave phase component	[s]

CHAPTER 1

INTRODUCTION

To reduce the world's dependence on fossil fuels and tackle the important global issue of climate change and rising CO_2 levels, the focus on generating electricity from renewable sources is an important area of development. There are many types of renewable energy, such as wind, solar, tidal and hydro but for the most part wave has remained unexploited until now. Most people recognise the vast amounts of power that the sea contains but it is normally only demonstrated during destructive events such as tsunamis and storms with people being unable to harness it effectively on a regular basis to date.

1.1 Potential

Wave energy is a form of solar energy with the sun producing temperature differences across the earth which causes winds to be blown over the ocean surfaces. This results in ocean swells, which are waves that can travel for great distances with virtually no energy loss [11]. These waves are very different to the breaking waves seen near shore because when waves reach shallow water and break this results in a large energy loss. Therefore, ocean swells represent an attractive energy source and it is an advantage to harvest the energy from the waves at greater sea depths before these energy losses occur. However, there is an economic trade-off between the higher wave energy available offshore and the extra cost associated with the additional distance to grid and port [12]. The main advantages of wave energy are:

- Sea waves offer the highest energy density among renewable sources [13].

Solar power intensity is typically 0.1-0.3 kW/m^2 but near surface wave power has an average typical intensity of 2-3 kW/m^2 through a vertical plane perpendicular to wave travel [14].

- Waves can travel for large distances with little energy loss. The ocean acts as an integrator, meaning that winds in practically any part of the Central or Northern Atlantic will generate waves incident on the shores of the UK [15].
- Limited negative environmental impact when device in use.
- It is estimated that wave power devices can generate power up to 90% of the time, compared to approximately 20-30% for wind and solar power devices [16].

The energy of each wave depends on its height and frequency with the power being proportional to the period and square of the height. Figure 1-1 illustrates the wide variations in average wave power at different locations around the world with the Western coastline of Europe having a large potential for wave energy sites due to the large wave power levels in this area. Cruz [13] estimates that the resource worldwide is around 2TW which is a similar magnitude to the worlds electricity generation and that 10-25% of this could be extracted as a conservative estimate. This is supported by a Carbon Trust report [12], which indicates that wave and tidal energy could supply around 20% of the current UK electricity consumption with offshore wave energy having a practical resource of 50TWh/year. These figures suggest that producing electricity from wave power could go a long way in contributing to the electricity generation required by renewable sources and reduce the dependence on fossil fuels and therefore reduce CO_2 emissions.

1.2 History

Wave energy has been investigated since the late 18th Century with the first patent registered in Paris in 1799 by Girard père et fils [17]. Now there are thousands of registered patents with most of the development coming in the last forty years through pioneers like Yoshio Masuda (Japan), Stephen Salter (UK) and Michael McCormick (USA). Research in the UK primarily began in the 1970s due to the oil crisis of 1973, which prompted an increase in interest in alternative energy resources like wave energy. The major British pioneer was Stephen Salter

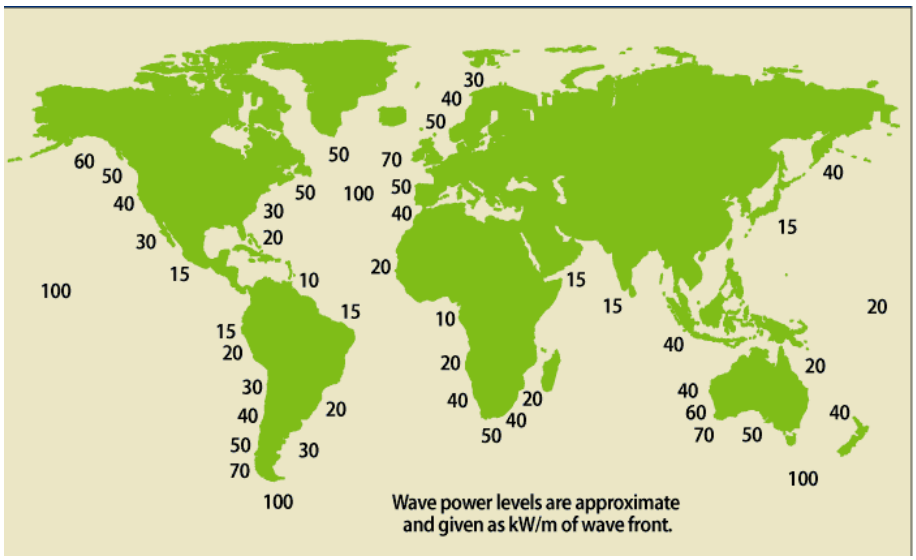

Figure 1-1: *Global wave power distribution [1]*

from the University of Edinburgh who conceived the concept of the 'Salter Duck' that claimed to have an efficiency of 90% for extracting energy from sea waves [11, 17]. Research funding, however, was cut in the early 1980's, as the government decided to move towards funding large generating systems rated at 2GW, like coal fired and nuclear power stations. This practically stopped all research in the area [17]. Since the 1990s, with the threat of global warming and the increased price of fossil fuels, government funding has increased again, resulting in an increased level of research and development. This has meant that the knowledge and understanding in the area has greatly increased, similar to the wind industry 30 years ago. However, there are still many different concepts that developers have devised to convert the energy of ocean waves into electricity. These include devices with different principles of operation and power take-off mechanisms and there is yet to be a convergence to one particular device configuration, which is the occurrence in most developing industries.

1.3 Device Classification

All companies in this field, regardless of device type, face the same main engineering problems when designing and building these devices. Twidell and Weir [18] have described some of the challenges associated with the wave resource that condition the development of wave energy converters (WECs):

- The irregularity of a sea state in terms of amplitude, phase and direction

- Efficient power conversion of variable power levels
- The conversion of slow (approximately 0.1 Hz) irregular and oscillatory motion into useful motion to drive an electrical generator with a grid connection frequency of 50 Hz.
- Necessity to predict and survive storms and other extreme conditions when wave power levels can exceed 2000 kW/m^2.
- More attractive resource is located offshore which provides maintenance problems
- The requirement to be highly reliable and have maintenance intervals of several years to be commercially viable.
- The lack of robustness in rough seas has often prevented long term sea trial measurements to be made

In an attempt to solve these problems, developers have applied many different concepts and theories. Currently, there are a wide range of WECs being developed. Devices can be categorised by their location; shoreline, nearshore and offshore, and the manner in which they capture energy from the waves. An extensive review of the many methods proposed to perform this are available in [9] and [19]. Below is a summary of the different designs which are under development:

1. **Point Absorber**- These are floating structures which capture energy from waves in all directions through their movement at the water surface. They are generally axisymmetric about a vertical axis with a small horizontal dimension compared to wavelength. They consist of a float oscillating in heave at the water surface connected to a relatively stationary surface with the relative motion between the two driving a power take-off unit. Examples of this device type include Wavebob, Wavestar and the OPT Powerbuoy, see Figure 1-2.
2. **Submerged Pressure Differential**- These devices have a similar mode of operation to point absorbers but they are attached to the sea bed and are completely submerged. The wave motion creates a pressure differential in the device which causes the body to oscillate in heave and the relative motion drives a power take-off unit. Being submerged has the advantage of reducing the visual impact of the device and the probability of storm

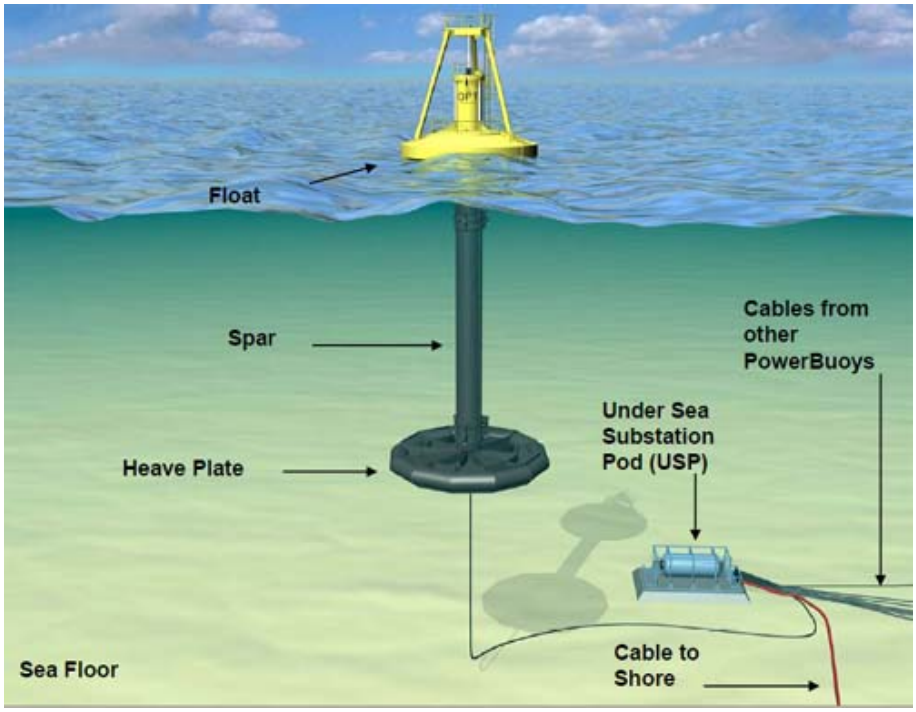

Figure 1-2: *OPT Powerbuoy [2]*

damage. However, it will probably increase maintenance and installation costs. AWS ocean energy's 'Archimedes Wave Swing' device is an example of this type, see Figure 1-3.

3. **Attenuator**- These are also floating devices but they have a significant dimension relative to the wavelength so they span multiple wave crests. They are aligned to the incoming wave direction so their mode of operation is to 'ride' the incoming wave. They are generally jointed devices so they flex as the waves pass along their length and they use the relative motion between the sections to generate power. An example is the Pelamis device, see Figure 1-4.

4. **Terminator**- These devices have their main dimension perpendicular to the incoming wave direction and appear to 'block' the wave. An example is Salter's Duck [20], see Figure 1-5.

5. **Oscillating wave surge converters**- These are a nearshore form of a terminator device which extract energy from the horizontal component of the wave. They consist of a flap which oscillates as a pendulum mounted on a pivot joint at the sea bed and this motion drives a a power take-off unit. An example is Aquamarine Power's Oyster device, see Figure 1-6.

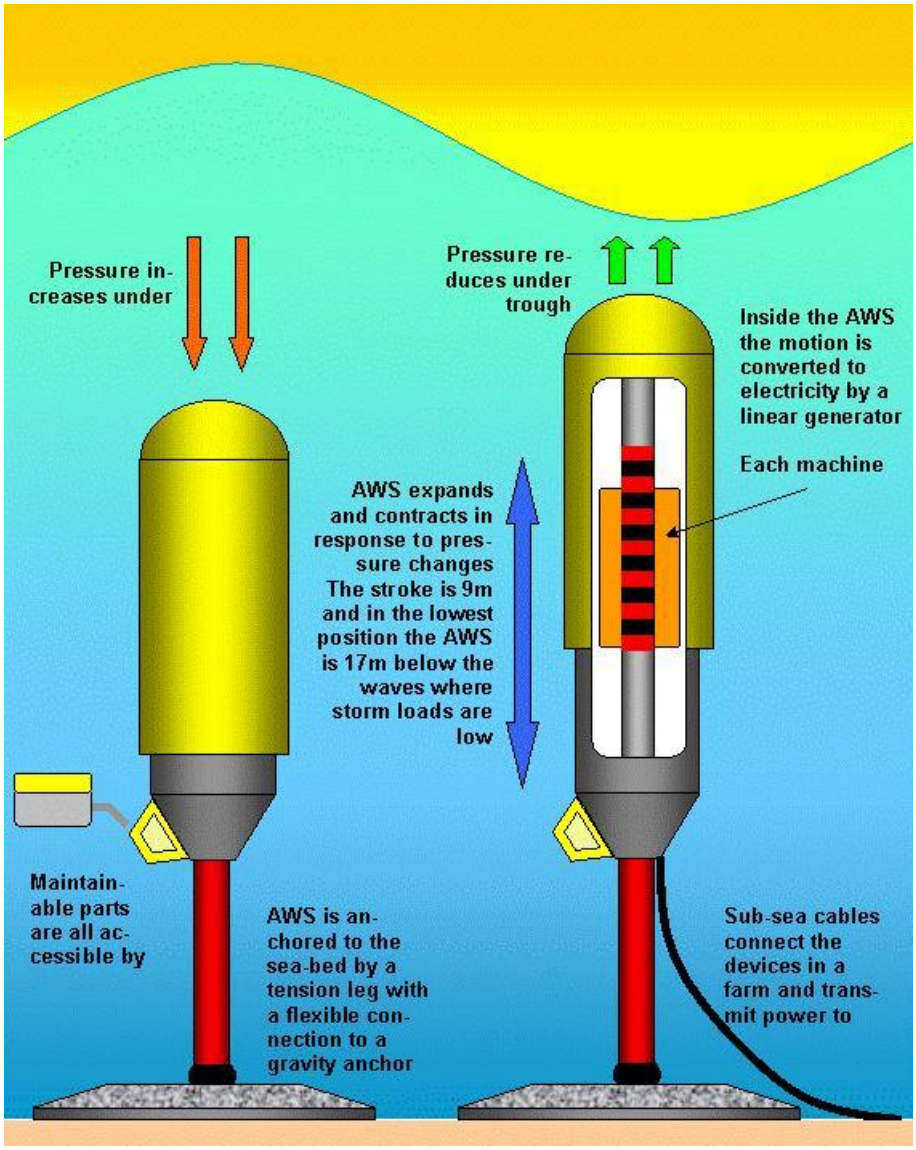

Figure 1-3: *Archimedes Wave Swing [3]*

Figure 1-4: *Pelamis [4]*

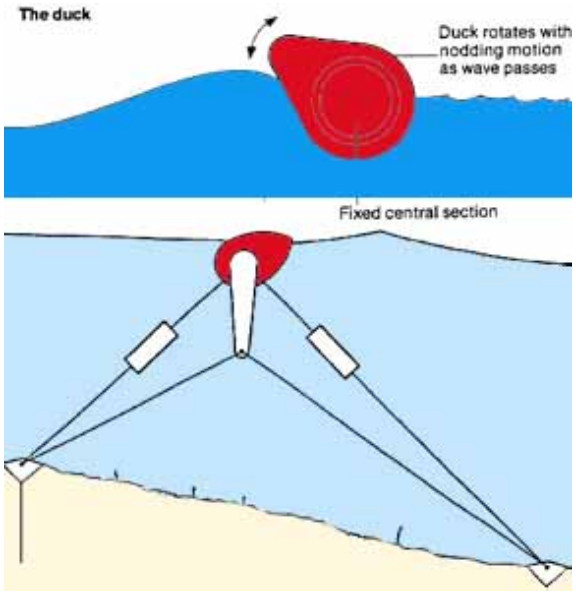

Figure 1-5: *Salter's Duck [5]*

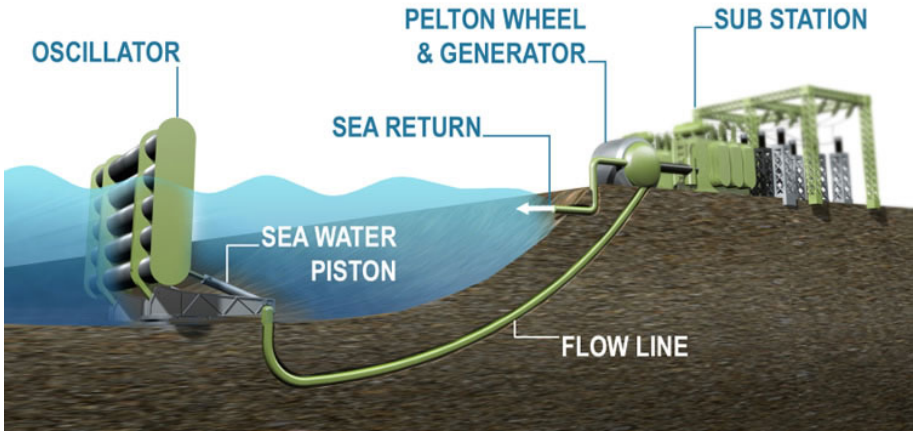

Figure 1-6: *Aquamarine Power Oyster [6]*

6. **Oscillating Water Column**- These are partially submerged, hollow structure devices, which comprise a trapped volume of air above the water surface. The rise and fall of the water level compresses and decompresses the air column which forces air through a Wells turbine, as shown in Figure 1-7. They can be offshore or onshore devices such as Wavegen's Limpet device at Islay, Scotland.

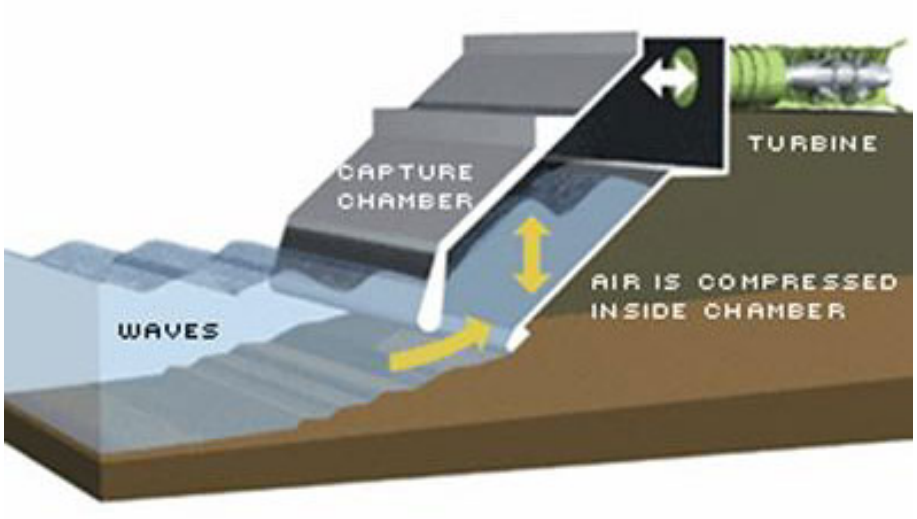

Figure 1-7: *Oscillating water column [7]*

7. **Overtopping device**- These devices rely on the physical capture of water from waves into a reservoir which is above sea level. The water is then gravity fed through turbines in the bottom of the structure back into the sea, see (Figure 1-8). Wavedragon have developed a prototype based on this device type.

1.4 Power Take-Off Unit

Current WEC designs differ widely in their energy extraction method but all require a power take-off unit (PTO) to convert the irregular mechanical motion of the primary wave interface into a smoothed electrical output. The main PTO options are shown in Figure 1-9. Turbine systems will not be investigated as the focus is on harvesting energy from moving devices.

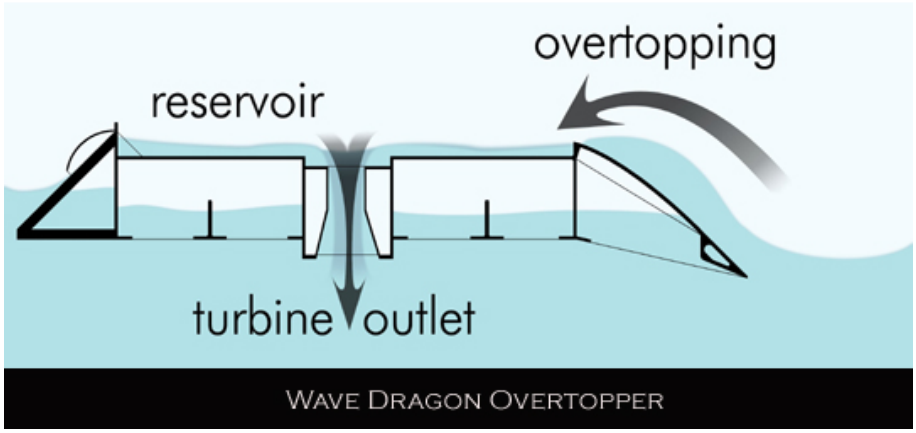

Figure 1-8: *Overtopping device [8]*

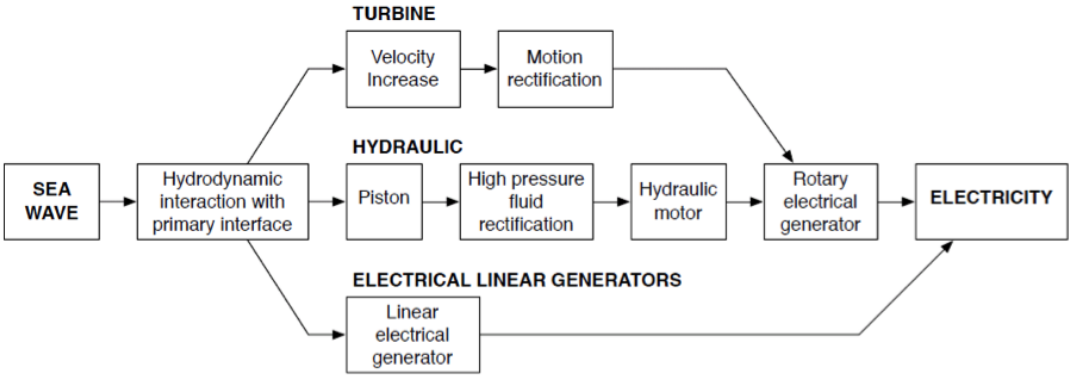

Figure 1-9: *Alternative PTO concepts [9]*

1.4.1 Linear Electrical Generators

Linear electrical generators directly convert the motion of the primary interface (eg. buoy) into electrical energy. There are advantages such as reduced intermediate conversion steps and system complexity. The basic concept of a linear generator connected to a point absorber is to mount the magnets with alternating polarity on the translator, which is directly coupled to the heaving buoy, see Figure 1-10. The stator containing the windings is then mounted on a relatively stationary structure. Generators are most efficient with a low force, high speed input and in a WEC the generator will encounter much lower speeds than typical high-speed rotary generators. With an expected peak air gap speed between the rotor and stator of 2 m/s, and average considerably less, compared to conventional rotary generators, where speeds are upwards of 50 m/s, there are obvious challenges to overcome [21]. This means that there is a requirement for a physically larger machine to achieve reasonable efficiencies and the required damping force [19, 22]. Therefore, early research concluded that machines would be too heavy, inefficient and expensive [20].

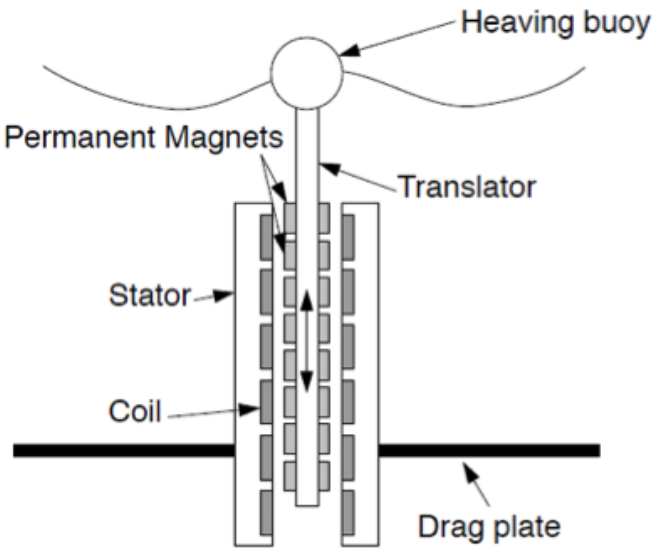

Figure 1-10: *Schematic of a Linear Electrical Generator [9]*

However, since the reduced costs of frequency converter electronics and new rare-earth permanent magnet materials being developed this idea is now being reconsidered. The huge size of a device was exemplified in a trial conducted using the Archimedes Wave Swing and a linear permanent magnet generator [23]. The generator had a 7 m stroke, 1 MN maximum force, 2.2 m/s maximum velocity

and a total mass of 400 tonnes with an average electrical power output of 200 kW predicted based on trial results [24].

The design of electrical generators for direct drive WECs was examined by Mueller [21]. The findings identified transverse flux machines to have more potential than longitudinal flux permanent magnet machine due to the higher power density and efficiency despite the higher shear stresses [25]. Since then work has been ongoing to try and learn more about these devices through simulation [26]. Modified designs are being investigated that use springs attached to the armature to produce higher speed movements with initial results indicating power improvements from smaller and cheaper magnets [22].

1.4.2 High Speed Rotary Electrical Generators

Traditional power stations use synchronous generators operated at virtually constant speed to match the frequency of the grid connection. However, depending on the PTO design of a WEC, generators may need to cope with a variable speed input. There are four main generator types:

1. Doubly Fed Induction Generators (DFIG)
2. Squirrel Cage Induction Generators
3. Permanent Magnet Synchronous Generators
4. Field Wound Synchronous Generators

Wind turbines have solved the same problem of a variable speed input by using either a DFIG and gear box arrangement or a direct drive synchronous generator with power electronic converters where the variable frequency current produced is converted to DC and back to AC to match the grid frequency and voltage. This technology requires costly equipment and can introduce some power losses but the turbine is able to capture a larger percentage of the available wind energy. A DFIG is able to control its rotor voltage and current so that the machine remains synchronous with the grid but the speed of the wind turbine can still vary. Furthermore, the efficiency of such a machine is high and the cost is low due to the overall design. For wave energy however, O'Sullivan and Lewis [27] conclude that a synchronous generator is the preferred option due to its higher energy yield, weight and controllability despite the requirement for a full frequency converter between the PTO and the grid connection.

1.4.3 Hydraulic Units

Currently the most common form of PTO is a hydraulic unit. It converts the slow, high force motion of the WEC into a high speed rotating motion to produce electricity, using hydraulic pistons and motors to drive an electrical generator. Hydraulic PTOs are selected as they are well suited to the low frequency, high force wave inputs and they have a high power density and robustness; an advantage for offshore operation, where maintenance costs are high [28, 29, 30]. Hydraulic units can also produce larger forces in comparison to the best electrical machines for the same size of unit.

Currently there is no standard industry design for a hydraulic PTO with some companies attempting to use a simple system with limited energy storage to drive a variable speed generator. Others are trying a more complex hydraulic system with energy storage integrated in an attempt to drive a synchronous generator. Figure 1-11 shows the most common approach currently with large gas accumulators used to provide the energy storage required to smooth out the irregular power captured from the waves. One-way valves rectify the flow from the piston to ensure the motor rotates in the same direction irrespective of the motion of the buoy. The operation of this type of hydraulic PTO has been demonstrated in the Pelamis device [28]. The PTO in the Pelamis device uses cylinders to pump the fluid, via control manifolds, into high pressure accumulators. These accumulators provide energy storage and in turn provide flow to hydraulic motors which drive grid-connected generators. The energy storage enables the generating equipment to be rated to the mean incident power.

There are some other issues, which must be considered when deciding on and designing hydraulic units.

1. **Fluid containment**- It is important to ensure these devices will be water tight. It is not desirable to have an ingress of sea water, which could damage the internal workings of the device, cause corrosion, adjust the buoyancy and even sink the device. Likewise, if oil is used as the working fluid in the PTO, (which would be the natural choice) it would not be desirable for there to be an oil leak that could have a detrimental environmental effect on the surrounding waters.

2. **Maintenance**- It is an expensive and risky job to carry out maintenance on a marine device, especially if it is far offshore. Maintenance can only be carried out during weather dependent time windows using specialist

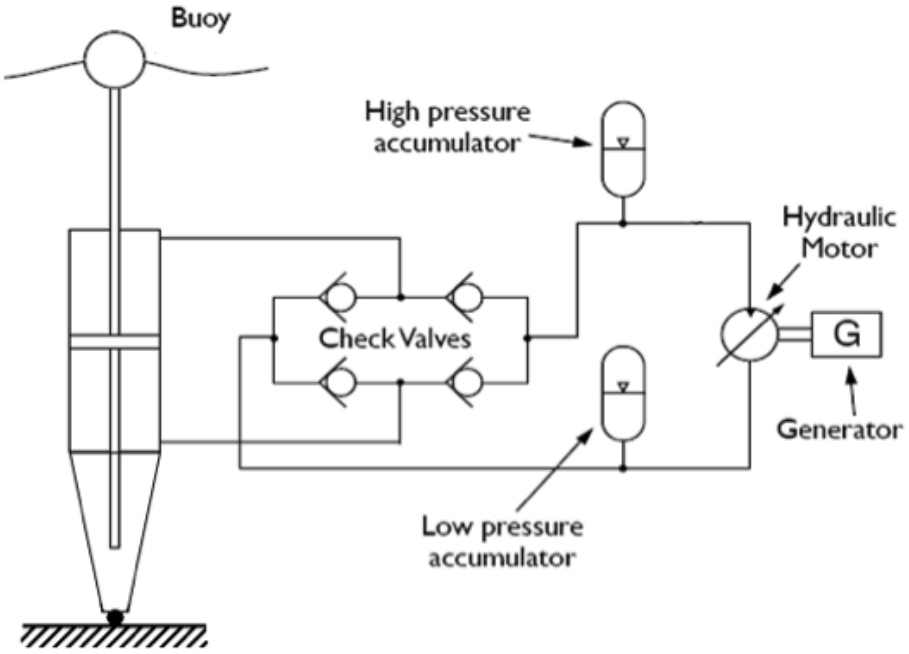

Figure 1-11: *Typical hydraulic PTO (with energy storage) [9]*

boats and engineers to do the work. This can mean high costs so there must be a design thought when considering more complicated hydraulic devices which require more moving parts and could require more regular maintenance. Therefore, the notion of having the PTO onshore, like the Oyster device, has been investigated but there is then the problem of long, costly and inefficient pipework to pump the fluid to shore. One of the major advantages over the other options is that the operation of hydraulic units has also been shown in other applications, such as mobile and industrial machinery, so components are commercially available and the technology is proven.

3. **Efficiency**- The efficiency of the PTO is its ability to turn the energy it captures from the sea into electricity which can be supplied to the grid. Hydrostatic transmissions normally use a coupled variable displacement pump and motor, which has an ideal operating point with a peak efficiency of approximately 60% [28]. However, their efficiency can be low when the system is far away from this point at part load due to the losses associated with leakage, friction and compressibility in hydraulic machines. It is therefore important to discover the duty cycle a device will be used with, as this will give a better indication of the overall efficiency instead of a rated value. An example of this design is shown in Figure 1-12, where an over centre mo-

tor coupled to a variable displacement pump can be used to provide force control but part load losses can be very high [31].

The design of the PTO is highly important as it affects both the hydrodynamics of energy capture and generation of electrical energy. A balance must be found between designing a simple, inefficient PTO that should require minimal maintenance and a complex but more efficient PTO that could require more regular maintenance.

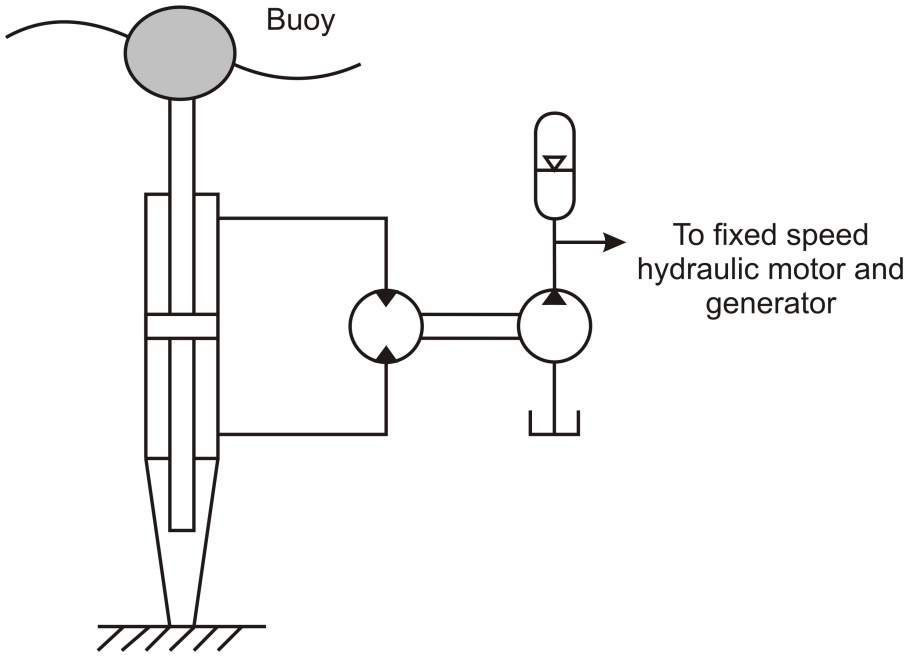

Figure 1-12: *Hydraulic Transformer*

1.5 The Industry

As in any industry, it is necessary to follow the normal development stages for any device. Development begins with computer simulation, concept testing in wave tanks before following on to part scale testing, full scale sea tests and finally commercial deployment. However, creating test sites at sea is not a simple matter due to the electrical grid connections required that require kilometres of underwater cabling and electrical substations in remote parts of the country. Test sites must provide this electrical grid connection point and real time monitoring of the sea conditions.

With this in mind two main sites have been created in the UK to help developers test their devices. The major test site in the UK is the European Marine

Energy Centre (EMEC) off the coast of Orkney. The site consists of four test berths in an area with one of the highest wave energy potentials in Europe, if not the world [32]. In 2004, using the Pelamis device, it was the site of the world's first successful electricity generation to the National Grid from wave energy. It has since been the testing site for other devices and there are plans for more second generation devices to be situated here in the future. The other test site in the UK, Wavehub, located approximately 20 miles off the coast of Cornwall, was completed in 2010 and has plans to test the OPT PowerBuoy technology in the coming years. There are other sites around Europe, which include Agucadoura in Portugal, where in 2008, three Pelamis 750 kW machines were part of the world's first commercial wave farm. The project only lasted a few months but it helped to prove that units of a commercial order could be successfully installed and integrated into the local grid. Furthermore, it provided invaluable experimental data for the company to verify data from computer simulations. The second generation Pelamis design is now being tested at EMEC and there are plans for larger farms in the near future around Europe [33].

1.6 Energy Cost

The current estimates for baseline wave devices put the cost of energy from the first wave farms at 38 p/kWh to 48 p/kWh [12]. This estimate has increased from the value given in the Carbon Trust report in 2006 [34] of 22 p/kWh to 25 p/kWh because the difficulties in the industry and technology are now better understood. This price is expected to reduce significantly as knowledge increases and improvements are made in performance, installation, survivability, maintenance and grid connections. The current price estimate is higher than energy generation from other renewable sources such as tidal and wind energy but this is expected due to the earlier stages of the technology. However, it is believed that with continued development wave energy will be competitive with offshore wind energy in terms of unit cost of electrical energy in the future. One of the major areas with the greatest capacity for improvement, even with small changes, is energy capture. This can be simply improved by implementing better control systems and optimising PTO designs to enlarge the bandwidth of the design with little or even no change to the device structure [30].

1.7 Scope

There are many problems associated with wave energy at this time such as high production cost, service life, health monitoring, reliability and low efficiencies. However, a major problem that has been highlighted is that WECs must operate in a wide range of operating conditions, and it is vital to maintain high efficiencies in all these conditions whilst using a PTO which is easy to control.

From the literature, it is noticeable that there is a lack of research using a realistic PTO model, with most device models focussing on the hydrodynamic interactions or control methods which assume an idealised PTO. Most of the published work demonstrates the capability of WECs to produce large amounts of energy but it does not include the losses which will occur in real devices, even though it is realised that power capture will be degraded by the imperfect operation of non-linear PTOs [35]. Furthermore, the control methods are simulated with idealised PTOs which assume neither energy loss, time delay nor force limits. Finally, there are very few test results for models to be verified against so confidence in simulation results is currently low.

Therefore there is a need to investigate the hydrodynamic interaction of a WEC with the behaviour of a realistic hydraulic PTO including losses. This would provide an important tool to better understand WEC behaviour, ways to maximise power generation and the limitations of certain control methods. In addition, it would provide a better knowledge of the effect on power generation of a well or poorly optimised device. Finally, the verification of a computer based model against experimental results would provide a greater overall confidence in the research.

1.8 Objectives

The objectives of the research are to:

- Build a hydrodynamic simulation model for a generic point absorber
- Combine the hydrodynamic model with a linear PTO simulation model to provide 'base-line' results
- Build a realistic hydraulic PTO simulation model
- Combine the hydrodynamic simulation model with the hydraulic PTO simulation model

- Investigate control and tuning of the overall device in simulation to maximise power generation
- Design and build a physical hydraulic PTO and test rig
- Validate simulation model results with physical model data

1.9 Novel Contribution

This is an original investigation on hydraulic power take-off design and control in wave energy converters. It uses a more accurate model, which includes component losses and dynamics, to better determine how the hydraulic unit would behave and how it would interact with a moving buoy. This model is used to determine tuning and control methods to maximise, and predict, power generation in different wave conditions by taking into account hydraulic component efficiency. Furthermore, these simulation results are supported by experimental results using a scaled power take-off unit.

1.10 Outline of the Thesis

The work presented in this thesis is divided into eight chapters.

Chapter 1 includes a general introduction to the area of wave energy dealing with the resource potential, history, current status of development and a description of the many different device concepts. The scope of the project, the project objectives, the novel contribution to the field and the outline of the thesis are also presented.

Chapter 2 provides a literature review with sections concentrating on the hydrodynamic modelling and the different control methods which have been investigated. Previous work is summarised which uses linear and hydraulic PTO models.

The principles of the mathematical modelling are presented in Chapter 3. The hydrodynamic modelling of the device, the modelling of a linearised PTO and the modelling of a realistic hydraulic PTO are all presented with results showing the behaviour of the different PTOs in regular waves. The component losses in the hydraulic PTO are presented.

Chapter 4 presents a method to tune a PTO to maximise power generation in regular waves for a linear PTO, an idealised hydraulic PTO and a hydraulic

PTO including losses. The three models are compared to reveal the difference in power generation, optimal damping and optimal PTO force magnitude.

Irregular waves are investigated in Chapter 5. Wave spectra and the creation of irregular wave profiles are presented, which are then used to investigate the behaviour of the device in these more realistic conditions. The tuning trends to maximise power generation for a linear and hydraulic PTO are presented and compared to the results for regular waves. Furthermore, a closed loop speed control strategy is implemented to maximise the transmittable power and a smaller PTO is incorporated to improve PTO efficiency.

Chapter 6 investigates real sea conditions. It presents the wave parameters for two separate months, which are calculated from the raw data. This information is used to determine the tuning trends for real sea conditions before an open loop tuning algorithm is presented to maximise power generation.

The experimental work is presented in Chapter 7. The design and construction of the experimental rig is presented with the initial results verified against simulation. A hardware-in-the-loop system is presented, which is used to investigate PTO tuning to maximise power generation for regular waves.

The conclusions are drawn in Chapter 8 and the suggested areas of further work are described.

CHAPTER 2

LITERATURE REVIEW

This chapter is a review of the literature on wave energy. It considers the hydrodynamic modelling of devices and presents the wave theory which will be adopted for this work. The different control strategies which have been investigated on a simulation model are introduced. Particular attention is drawn to recent papers on force control strategies with a hydraulic PTO. Finally, an overview of research on wave estimation for use with the control strategies is presented.

2.1 Hydrodynamics

An early general overview of the subject is presented by McCormick [11]. It describes the basic concepts and techniques of ocean wave energy conversion and the supporting materials, without going in to a high degree of mathematical analysis. It uses the author's experience working in the area of wave-powered navigation aids with the U.S. Coast Guard to describe the properties of waves and the different possible methods to mathematically model a water wave. Linear, nonlinear and random waves are considered.

Initial work analysing the behaviour of devices in waves was presented at a conference held at the University of Edinburgh in 1979. Greenhow [36] found that the hydrodynamic forces acting on a spherical buoy from surface waves and the added mass and damping terms could be predicted from theory and closely matched to experimental results. Furthermore, Jeffreys [37] introduced the theory that frequency domain models will not be valid for modelling these devices as there are substantial non-linearities, and therefore investigation using

a modelling technique to represent the hydrodynamic interactions of a WEC in the time domain was presented.

In deep water, for a wave height to wavelength ratio of 1:50 or less, linear wave theory is expected to give excellent accuracy for predicting the kinematic properties of the waves [11] and it provides the basic theory which underlies hydrodynamic modelling. Linear wave theory makes the following assumptions:

- Waves are two dimensional
- The fluid is incompressible
- There are no viscous losses
- There is no underlying current
- Small amplitude body motions
- Wave height is much smaller than water depth or wave length

A thorough investigation of the interaction between waves and oscillating bodies in the sea, assuming linear wave theory, is presented by Falnes [38]. It provides a comprehensive analysis of the hydrodynamic forces acting on an oscillating WEC. The method uses the approach applied to ships, which was developed by Cummins [39], and was then adapted to model WECs in the time domain by Jeffreys [37] and Falnes [38]. Time domain modelling is an important part in the evaluation of devices due to the need for information on the device's transient response due to the many non-linearities in the system, which include PTOs, moorings and control systems [40]. The method developed by Jeffreys and Falnes, from linear wave theory, is the conventional hydrodynamic modelling technique for work on WECs [41] [42] [43] [44] [45].

2.2 WEC Farms

In the future it is expected that WECs will be deployed in farms with a number of devices using the same electrical grid connections, taking advantage of the same energetic sites and minimising any adverse visual impact. It is therefore important to understand the interaction of multiple devices in farms and to optimise their configuration to maximise power capture. The layout effects, the power capture and an optimal design is dependent on wave conditions including direction

with positive interference between devices increasing overall performance [46]. Power take-off characteristics are also shown to affect the optimum configuration of devices in [46], but the results are for a linear PTO with reactive control, so it represents an optimum case with high power levels. Other work has shown an improvement in power capture by splitting an array into two independent clusters. This gives a larger increase in power capture when the clusters are not aligned to the incoming wave direction because there is a reduction in the 'masking' effect for the devices at the back of the array [47]. Single farm arrangements can also be optimised to give greater power capture than would be achieved by the same number of WECs in single operation, with a power capture increase of 45% for the optimal configuration over the worst configuration of point absorbers [48].

2.3 Control Strategies

A variety of control concepts to maximise energy capture and generation have been investigated and they will be described below. It is important to understand their logic and any practical limitations in their implementation. Generally, energy is captured most efficiently when the undamped natural frequency of a WEC is close to the dominant frequency of the incoming wave [49]. If the damping of the device is too large then the motion of the device will be limited so power captured is reduced. Likewise if the damping is too small then little power is captured so it is important to have a correctly damped system. There will be a requirement for a device to continually adapt to the changing wave conditions because wave height and frequency constantly vary.

2.3.1 Reactive Phase control

Reactive control is an attempt to achieve resonance by matching the characteristics (natural frequency) of a WEC to the predominant frequency of the incoming wave. In a linearised PTO model, which consists of a linear spring and damper, it is simply achieved by adjusting the spring term or the mass of the device [20]. The spring force component gives reactive power which averages to zero over one wave cycle whilst the damping force component relates to the resistive captured power. Due to the size of these devices and the predominant frequency of the waves, this spring term must normally be negative. Reactive control represents an optimal control strategy but it is difficult to implement in practice as it re-

quires the instantaneous power flow to be reversed, meaning that the WEC is applying energy to the waves for small fractions of the oscillation cycle [50]. This can be theoretically achieved by using a hydraulic machine which can act as a pump and motor. However there may be large energy losses involved with this energy re-circulation, and it also means large reactive forces are applied externally on the device, which may be a practical problem [51]. However, results show that if this is possible and the dominant wave frequency can be estimated in irregular waves that the power capture with a tuned PTO can be up to 50% of the available power [10].

2.3.2 Phase control by latching

Another form of reactive control is phase control by latching which was first introduced by Budal and Falnes in 1980 [52]. It is a sub-optimal strategy which consists of locking the oscillating body in position at the instant when its velocity vanishes and releasing it after a certain delay such that the wave force is in phase with the body velocity to maximise the oscillation amplitude. It is applicable to devices with resonant frequencies higher than the wave frequency, which is the normal situation, and the latching duration effectively increases the resonant period of the device to match the frequency of the wave. Figure 2-1 shows the theory of latching. Curve 'a' represents the wave elevation, curve 'b' the displacement of a resonant WEC and curve 'c' the displacement of a non-resonant WEC with latching.

Latching control gives power capture improvement of up to 300% in regular and irregular waves of any frequency, with strategies to maximise buoy amplitude or to maintain buoy velocity and wave excitation force in phase giving similar improvements [44]. This work models the PTO as a linear viscous damper and it requires the prediction of the future wave excitation force so the optimal latching time can be determined. The release time of the body represents the control variable and work has been undertaken to determine the optimal release time with future prediction of the wave excitation force necessary, meaning that it is an anti-causal strategy. Power capture has been shown to improve by a factor of two for a four degree of freedom WEC in irregular waves, but there is the need for the prediction of the wave excitation force signal about 100 seconds in the future [53]. Therefore, the real time implementation of such a method in full scale devices could be a difficult task.

Latching control can be theoretically applied to a hydraulic PTO with a simple algorithm to hold the buoy until the wave force exceeds a multiple of the PTO force [43]. This gives increased energy capture in irregular waves especially when the natural frequency of the device is much larger than the significant frequency of the incoming waves. It is important to have a latching system which holds and releases the WEC at the correct instant so the system must have a quick reaction time, which is easily achievable with a hydraulic PTO [20]. Furthermore, the only external force required will be to lock the actuator which may be easier to implement than other control strategies [51]. Using a hydraulic PTO model with latching control gives an approximate doubling of the generated power in irregular waves [54] using the strategy developed by Falcão [43].

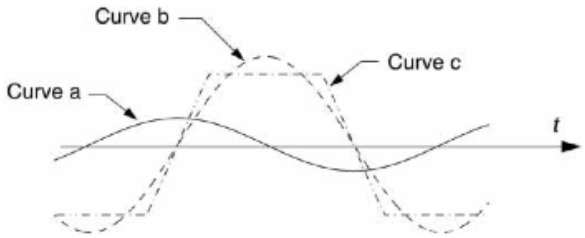

Figure 2-1: *Latching Control*

2.3.3 Declutching

Another sub-optimal method which has been investigated is called active bi-polar damping, unlatching or declutching control. This method tries to perform two tasks. Firstly it removes the induced body stall which occurs when the hydrodynamic forces are less than the force from a hydraulic PTO for part of the wave cycle, as noticed in [42]. This stall means that the body is stationary for part of the wave cycle and can therefore lead to a reduction in power capture. Secondly, as in latching control, it tries to shift the body's velocity to be more in-phase with the wave force to increase the amplitude of the body motion by removing the PTO force for part of the oscillation cycle. As with latching control, the timing of the unlatching represents the control variable and it currently requires the knowledge of the future wave excitation force so it is also an anti-causal strategy [55]. However, unlike latching control there is no requirement for any external force. In a hydraulic PTO the unlatching can be achieved by bypassing the piston at certain moments to make the PTO force zero at these times. These times can

be determined from theory and the power capture can be improved by a factor of two for some wave conditions [56]. Furthermore, results for regular and irregular waves indicate power capture levels at least as high as that of a control strategy for a hydraulic PTO which tries to mimic the behaviour of an optimum viscous damper with the added advantage of requiring a less complex system [57].

Furthermore, [58] shows that a generic optimal control strategy for maximum power extraction involves specific cases of latching and de-clutching in a single wave cycle. However, the duration of each case of latching and de-clutching depends on the specific sea state but it is assumed that the force produced by the PTO is linear and therefore instantly achievable.

2.3.4 PTO Force Control

Varying the force produced by the PTO allows control strategies to be implemented to maximise power capture. One of the ways to do this is to implement a constant reactance tuning method to tune the device according to the incoming wave conditions. Assuming the PTO to be a viscous damper, this is achieved by simply varying the damping coefficient, results indicate the importance of a well tuned device for power capture [45]. Results indicate that for a linear PTO, optimum power capture is greater in regular waves compared to irregular waves of the same energy, as energy is distributed across a range of frequencies [59].

However, the question is how to do this with a hydraulic PTO. The PTO in the Pelamis device controls the moment about each joint to four discrete levels by switching between different actuator chambers using 3:1 area ratio cylinders. Electronically controlled valves control the flow between the cylinders and accumulators, which enables force control to maximise power capture. Simulation work is verified by experimental data for a part and full scale rig with results showing a PTO efficiency of 80% for the primary conversion stage over a range of operating conditions [28]. This would be a similar design to Figure 2-2.

A model of the SEAREV device, which uses a hydraulic PTO is presented in [30]. Non-linear hydraulic component models are used and a maximum system pressure is included to limit the PTO torque. However, power losses such as pressure drops, cylinder friction and motor leakage and friction are neglected. This model presents an induced body stall when the PTO torque is greater than the torque produced by the device. Results indicate that varying two parameters of the hydraulic PTO, (supply pressure to the motor and generator power), has

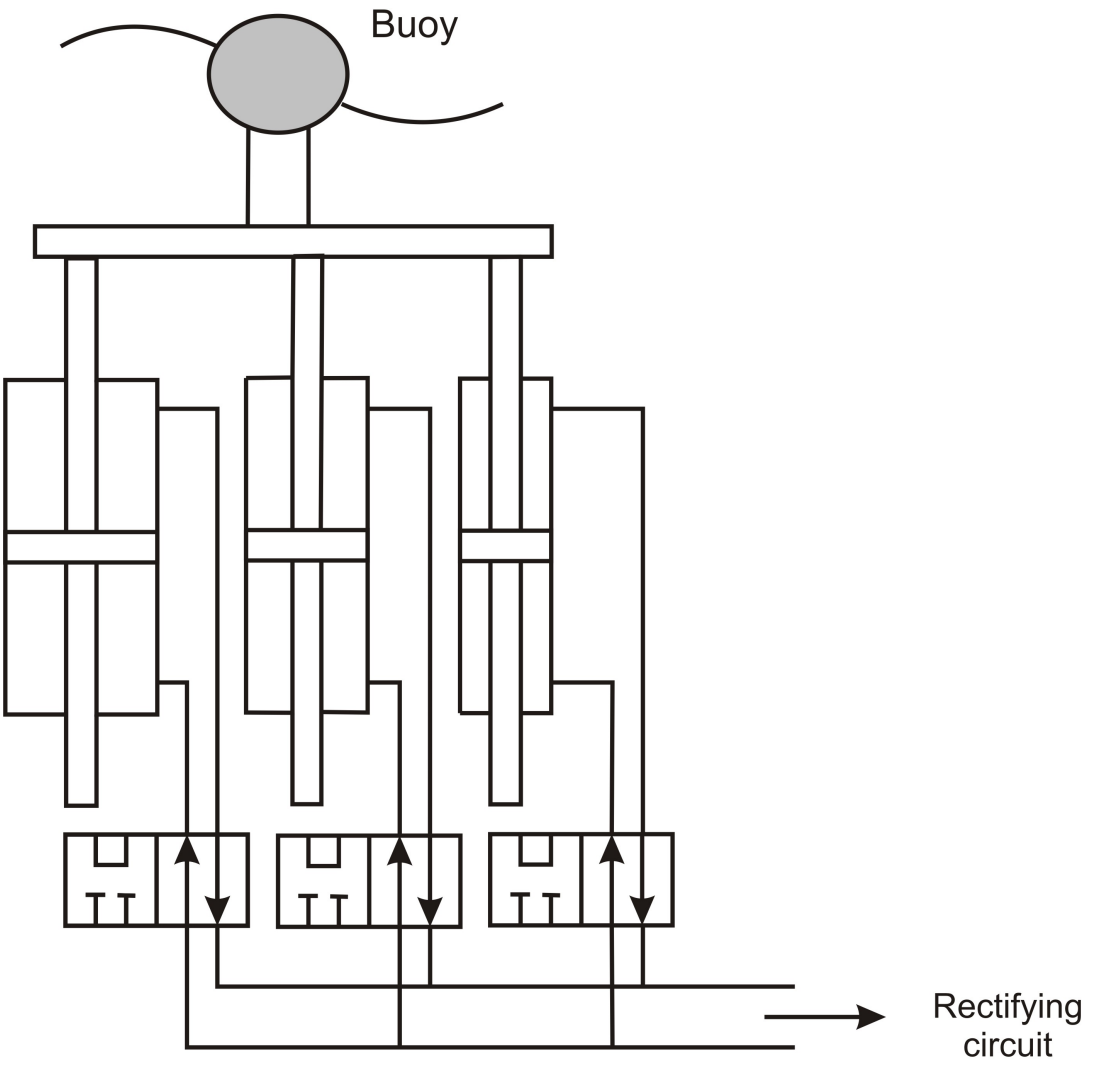

Figure 2-2: *Hydraulic PTO to give discrete level force control*

a large influence on the power generated and these parameters can be optimised for a given sea state. Therefore to increase the bandwidth of the device and increase efficiency it is necessary to control the PTO and tune it to the different sea conditions. Finally, the work shows that a "realistic model can achieve, and sometimes exceed, the performance of the linear damper for all the sea states with a hydraulic PTO" when the configuration is adapted to the sea state [30].

Work looking at a combined hydrodynamic and hydraulic PTO model was presented by Falcão [42]. A model of a heaving buoy connected to a hydraulic PTO with power smoothing accumulation is presented but there are simplifying assumptions in the PTO model, such as infinite accumulator sizes and zero power losses. In this case, there is induced body stall, or a natural latching, when the wave force is insufficient to overcome the piston force so the resistance force is akin to a Coulomb damping force. By controlling this coulomb type damping force, a hydraulic PTO can attain very nearly the same level of power capture as an optimal linear PTO with the PTO parameters only dependent on wave period [42].

Another non-linear model of a hydraulic PTO and oscillating WEC is presented in [60]. It provides a detailed configuration of the hydraulic PTO using the common rectifying circuit and accumulation for power smoothing with a fixed displacement hydraulic motor. However, the only losses included in the PTO model are the pressure losses across the rectifying valves. In contrast this work uses the modulation of the generator torque, which has been proven in wind turbines, to tune the device in regular and irregular waves. Results show that there is an optimal value of torque that corresponds to the dominant wave period that maximises power generation. The work also investigates a phase control strategy which uses two smaller accumulators that can store and release energy by controlling hydraulic valves. The idea is to release energy from the accumulators to generate an increase in acceleration of the WEC so that the velocity of the WEC is more in phase with the wave excitation force. However, results indicate only a minimal increase in electrical power output for an optimally tuned PTO.

A non-linear model of a hydraulic PTO and point absorber is also presented in [54] with sizes provided for the hydraulic components but losses not included. The same Coulomb damping effect is observed and the PTO is tuned by varying the piston area to adjust the PTO force amplitude. Results indicate a possible power gain of 300% from a well tuned device. Furthermore, the work investigates the possible power gains from reactive control with a hydraulic PTO using an

artificial negative spring in parallel to the PTO model. A power increase from 58 kW to 220 kW is obtained but the author acknowledges that the creation of this effect would be very difficult to implement in real devices.

An oscillating wave surge converter is modelled in [61] with two different hydraulic PTO designs considered that include power losses. The first system is a decentralised strategy with each of the four wave energy converters having its own PTO, while the second is a centralised strategy with the four converters driving a single PTO. The different designs are used to compare three different control strategies. The first system implements a velocity-proportional damping where the system pressure is proportional to the piston velocity. This is implemented by removing the accumulation and varying the hydraulic motor displacement and generator torque to achieve the desired system pressure with constant generator speed. The second system can implement two damping strategies, which are a constant pressure system and a volume flow proportional damping strategy that attempts to overcome the possibility of a constant damping force stalling the device in low wave powers. The displacement of the central motor is altered to control the overall pressure so it is proportional to the total flow into the motor. For the wave condition simulated the worst performing strategy was the constant pressure strategy. There was a 14% increase in power generated from the flow proportional strategy and a 42% increase from the velocity proportional damping strategy. Furthermore, due to the accumulation in the centralised strategy there was a reduction in the peak powers so hydraulic components could be sized more efficiently.

Different design concepts for the hydraulic PTO of the Wavebob point absorber device are considered in [62]. A modular approach consisting of two pumping modules and two generation modules can be combined in any desired way to give greater variety in power producing capacity. Two different types of generation module are considered. Firstly, a hydraulic transformer circuit (Figure 1-12) is proposed but it is dismissed due to the need for the primary motor to be rated at maximum input power meaning that overall conversion efficiencies would be low. Alternatively, a rectifying circuit with accumulation (Figure 1-11) is considered with an extra flow path to a second hydraulic motor. The two motors are variable displacement and they are coupled to a single generator. The second motor allows the generator to be driven in low sea states when the wave force is less than the accumulator force. However, the hydraulic model is modelled in an ideal manner with the only power losses due to pressure drops across the check

valves.

A damping force control strategy is proposed with the force proportional to velocity in calm seas and a constant force in normal sea conditions. The desired damping force is achieved by controlling the displacements of the two hydraulic motors. Results are not presented to show the power capture gains of this strategy but there is a relatively smooth power output. However, the displacement of one of the hydraulic motors is constantly ramping up and down so the authors acknowledge that the actual power output would be somewhat lower due to the resulting inefficiencies.

Hansen [63] concentrates on providing force control using a hydraulic PTO in the Wavestar device. The Wavestar device uses a PTO consisting of a symmetrical cylinder which is driven by a float. The flow produced by the cylinder drives an over-centre variable displacement swash plate motor coupled to a generator, which means that the bi-directional cylinder flow is turned into uni-directional high speed rotation to drive the generator, similar to Figure 2-3. The generator is asynchronous with an inverter for the grid connection to enable variable speed control. PTO force is controlled by varying a combination of the motor displacement and generator torque to match the cylinder force reference produced via an algorithm. To improve the accuracy of the model the following losses are included:

- Hydraulic cylinder modelled with a constant efficiency
- Hydraulic motor modelled with a variable efficiency depending on the specific operating conditions
- Boost pump installed to replenish the external leakage loss of the hydraulic motor
- Inverter modelled with a constant efficiency

A number of control strategies were investigated with the best strategy found to be controlling the generator speed to maximise motor displacement. This strategy gives the highest PTO efficiency of 55% to 72% for the range of wave conditions considered, which the authors of the paper consider inadequate. Furthermore, the strategy requires the motor and generator to speed up and down during each wave cycle. This is a challenge with this sort of PTO design as there is no hydraulic power smoothing.

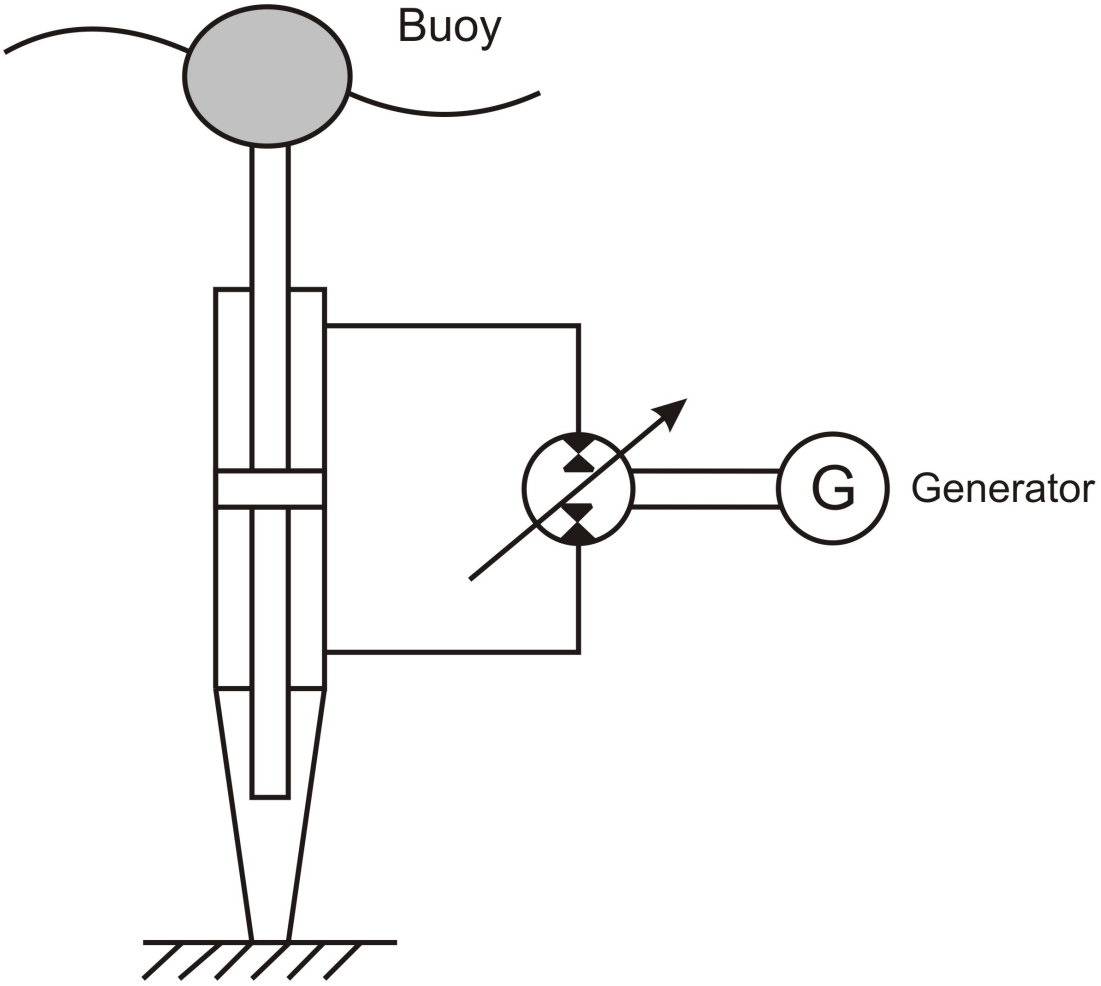

Figure 2-3: *Force control by varying motor displacement and generator torque*

In general, these papers investigate force control strategies which are implemented by tuning the hydraulic PTO. The force produced by a hydraulic PTO can be adjusted by varying either the displacement of the hydraulic motor, the area of the hydraulic piston by switching in or out different cylinder chambers or the torque of the electrical generator. All the results show an increase in power generation that is dependent on wave conditions and the specific control strategy implemented. In the beginning, only very basic hydraulic circuits were investigated with many simplifying assumptions made, but since 2010 these have become more realistic with specific component dimensions and simple loss models included in some studies.

To determine the gains and limitations from theoretical force control strategies and estimate more realistic power levels it is necessary to include losses in the PTO simulation. Losses such as friction, leakage and pressure drops and undesirable characteristics such as compliance, compressibility and inertia mean that the desired force is not accurately achieved using open loop control [31]. For the specific hydraulic PTO design considered in [31] power generated was only about 30% of the ideal value for some wave conditions and even negative power flow was observed in low wave power conditions. PTO efficiency can be increased by sizing certain components correctly depending on the incoming wave conditions with smaller pumps and motors being more preferable at smaller wave heights. However, there is a fundamental problem of designing and sizing a power transmission to perform well at one operating point which then gives low efficiencies at other operating points. This is a major issue for WEC designers as there is an extreme variability in the power available from different waves throughout the year and in different locations.

In response to this problem a Digital Displacement ® motor has been developed by Artemis Intelligent Power with the aim of maintaining a high efficiency over its entire displacement and speed range. When using a Digital Displacement ® motor instead of a standard axial piston hydraulic motor the PTO efficiency increases by 17% irregardless of control strategy [64]. Also, PTOs with a modular system that are capable of switching in different pumping and generating modules depending on wave conditions have been found to improve PTO efficiency due to the more appropriate component sizing [62].

To summarise the literature, there are 3 main PTO models which have been used in investigations to date:

- **Linear PTO model**: This type of model assumes the PTO force to be a

combination of a damping and spring force. Therefore, the PTO force is linearly dependent on the velocity of the device.

- **Non-Linear PTO (Idealised)**: This type of model assumes the PTO force to not be linearly dependent on the velocity of the device. It generally assumes sizes for the hydraulic components of the PTO but the hydraulic PTO is assumed to be 100% efficient.
- **Non-Linear PTO (With Losses)**: This type of model incorporates inefficiencies in the hydraulic PTO components such as pressure drops, torque losses and frictional losses.

A summary of the PTO models used in different citations by authors in the area is provided in Table 2.1.

PTO Model	Citations
Linear	[10] [40] [44] [45] [47] [49] [53] [55] [59] [65] [35] [58]
Non-Linear (Idealised)	[42] [43] [56] [57] [61]
Non-Linear (With Losses)	[30] [31] [54] [60] [62] [63] [64]

Table 2.1: *List of PTO models in citations*

2.4 Wave Estimation

When devices are deployed at sea the wave conditions will be highly irregular but most of the proposed control methods require knowledge of the incoming wave conditions to tune the devices (Figure 2-4). Therefore the control problem can be considered in two stages; the prediction of the wave conditions and tuning the PTO accordingly [65]. In regular waves it is straightforward to determine the wave frequency and height but in irregular waves this estimation is a more difficult task as the wave elevation data is complex and unpredictable. Using a linear PTO, results show that tuning the PTO to a varying estimated wave frequency gives improved power capture compared to fixed PTO parameters in irregular waves. The estimated wave frequency can be calculated using a Discrete Fourier Transform of the surface elevation with a moving average of 20 s. Results show power capture gains of up to 300% when tuning to this frequency in comparison to the site average [10].

This work was continued to investigate different tuning methods. Three passive tuning methods, which are based upon statistical methods, are investigated

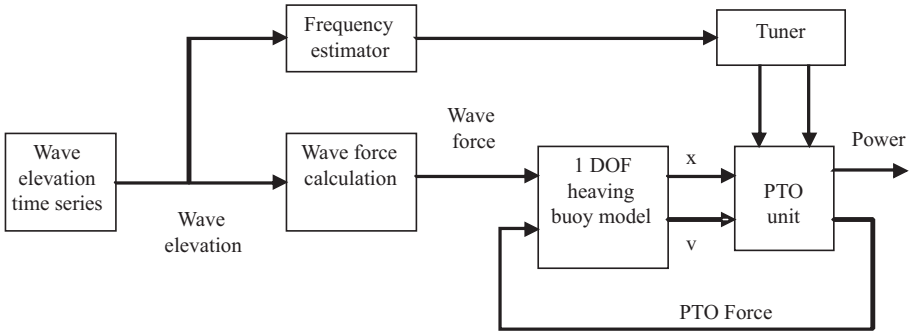

Figure 2-4: *System structure for tuning a device from wave estimation [10]*

with the device being tuned to a mean peak frequency, a site peak frequency and a site energy frequency. Results show that tuning the device to the site peak frequency gives the greatest power capture in all sea states considered [35]. The authors also illustrate that an overestimation of the peak frequency is better than an underestimation due to the asymmetric nature of the power capture. Furthermore, the work investigates three active tuning methods which aim to continuously calculate the wave frequency from the wave elevation data and rapidly adjust the PTO parameters accordingly. The first method uses a sliding Discrete Fourier Transform method to calculate the wave frequency every few wave periods. This method requires future knowledge of the wave elevation data so it would only be practical if the measurement buoy is upwind of the device. The other method does not require any future knowledge of the wave profile and it continuously estimates the wave frequency from successive wave periods using the zero crossing method. Results show the second active tuning method, which uses only the wave period analysis, to give the highest power capture but all the active tuning methods outperform the passive tuning methods [35]. However, this work again assumes a linear PTO with PTO characteristics that can be achieved instantly. This may not be the case for a non-linear hydraulic PTO.

Calculation of the wave frequency can be done from the wave elevation data or the wave excitation force data. It is initially believed to be more advantageous to use the wave excitation force data as the method is trying to ensure the optimal phase condition which requires the phase of the wave excitation force [50]. The work continues to demonstrate that the wave force can be estimated by low-pass filtering the wave elevation data and using the wave frequency from the estimated wave force to tune the PTO improves power capture without any future wave information being required [65]. "Results also indicate that the estimated or measured wave elevation information can practically be used instead of the wave

force information without much compromise on the power capture performance" [65].

2.5 Concluding Remarks

To predict energy production and prove the economic viability of WECs it is necessary to look in more detail at the PTO. From the literature there are a number of factors which have become apparent. Firstly, it is evident that a hydrodynamic modelling technique has been developed, which is based on linear theory. This method is the standard practice for modelling the hydrodynamic action of a point absorber WEC and is therefore a natural starting point for this work. Also, most work investigating the power capture capabilities of WECs has been performed using a linear PTO model. This assumption means that the control methods proposed show a large increase in power capture, but they do not take into account the practical problems with these methods such as force limits, energy losses and energy re-circulation. Recently, work using a simplified hydraulic PTO model has demonstrated their operation and certain issues with electricity generation in real seas. However, most of these models still make simplifying assumptions and do not investigate the effect of component sizing and losses on the behaviour of the overall device. Therefore, it is a natural step to create a combined model of the hydrodynamics and PTO with an accurate hydraulic model including realistic component sizes and losses. This model can be used to better understand the behaviour of a device in different wave conditions and find ways to improve power generation as it will reveal where the power is lost in the PTO. Furthermore, it can be used to determine the effectiveness of different control strategies and their practical limitations of using a hydraulic PTO.

CHAPTER 3

SYSTEM MODELLING

This chapter introduces the techniques used to model the behaviour of the WEC and the power take-off unit (PTO). Firstly, the hydrodynamic modelling approach for the WEC is presented. Linear wave theory is used for the majority of research in this area and is therefore adopted for this work. Subsequently the different modelling approaches for a PTO are presented. Initially, the most basic assumption of a linear PTO, comprising of a damping and spring force, is used and its behaviour described as this is the assumption made for the majority of previous work. Secondly, the design and modelling approach for a realistic hydraulic PTO is explained with component losses not included. This helps to understand the workings of the hydraulic PTO during a wave cycle and to determine if the device is behaving as anticipated. Furthermore it provides a comparison to the linear PTO to determine any significant differences in the behaviour of the two devices. Finally, accurate losses are included in the hydraulic PTO components to determine if this causes any changes in the device's behaviour. These losses include an accurate hydraulic motor model, which gives precise performance data over a wide range of operating conditions. In addition, the loss model provides an indication as to where the major inefficiencies occur in the PTO. Simulink and Simhydraulics are used to implement the models and generate the simulation results in this Chapter.

3.1 Hydrodynamics of a Point Absorber

The following, as derived by Jeffreys [37] and Falnes [38], describes how to model the hydrodynamic forces on a WEC using linear wave theory in the frequency and time domain. It was decided to model a point absorber as this type of device has shown promise as a WEC [66]. Assume the buoy is a vertical cylindrical body, radius a and height $2l$, with an extended hemisphere in its lower end (to reduce viscous effects). If the body was unrestrained it would have six degrees of freedom; three translational: heave, surge and sway; and three rotational: pitch, roll and yaw. However, for simplicity consider only a single degree of freedom with the body oscillating in heave (coordinate x, with $x = 0$ at steady state in the absence of waves), as this is the only direction of motion which can be used by the PTO to generate power. The governing equation of motion for the buoy

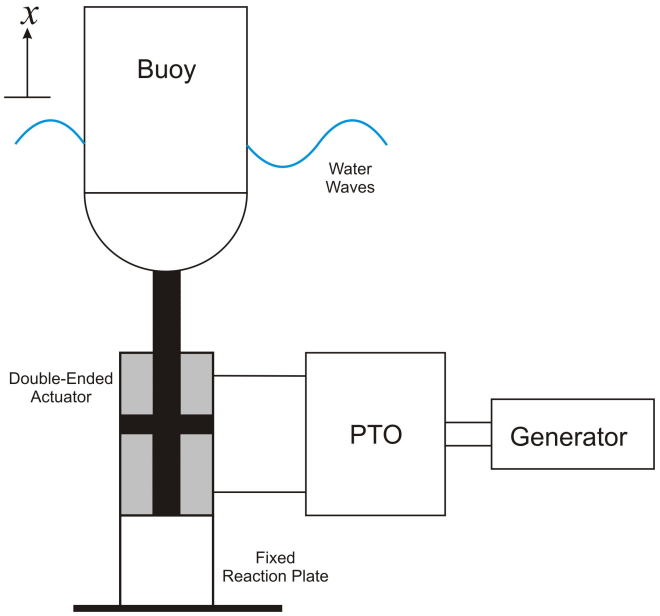

Figure 3-1: *Schematic of the WEC*

is

$$m\ddot{x} = f_h(t) + f_m(t) \tag{3.1}$$

where m is the mass of the buoy, $\ddot{x}$ is the buoy's acceleration, $f_h(t)$ is the total wave force and $f_m(t)$ is the mechanical force created by the PTO and moorings. As linear wave theory is assumed, the wave force can be decomposed as follows

$$f_h(t) = f_e(t) + f_r(t) + f_{hs}(t) \tag{3.2}$$

$f_e(t)$, is the excitation force which is the force produced by an incident wave on an otherwise fixed body. $f_r(t)$ is the radiation force which is produced by an oscillating body creating waves on an otherwise calm sea, and $f_{hs}(t)$ is the hydrostatic buoyancy force. For small heave displacements, which are expected, the hydrostatic force can be linearised so that

$$f_{hs}(t) = -\rho g S x \tag{3.3}$$

where ρ is the water density, g is the acceleration due to gravity and S is the buoy cross sectional area in the x-direction.

3.1.1 Frequency Domain Modelling

Initially a regular wave input will be investigated, i.e. the wave profile is a simple sinusoidal function of time, Figure 3-2. If this is the case then the excitation force is also a harmonic function of time so it can be written

$$f_e(t) = Re(F_e e^{j\omega t}) \tag{3.4}$$

where F_e is the complex excitation force amplitude. The excitation force is a sum of the incident and diffracted wave components. Falnes [38] suggests that if the body is small compared to the incoming wavelength the diffracted term can be neglected and the excitation force is simply equal to the incident wave component, which is known as the 'Froude-Krylov' force. Furthermore since the system is linear and there is only a single degree of freedom, the excitation force amplitude is proportional to the wave amplitude such that

$$|F_e| = \Gamma(\omega)\frac{H}{2} \tag{3.5}$$

where H is the wave height and $\Gamma(\omega)$ is a real and positive excitation force coefficient which is dependent on the body's shape and the wave frequency.

Considering the radiation force, it is assumed that the complex amplitude of the radiation force is in proportion to the complex amplitude of the buoy motion such that

$$F_r = G(j\omega)X(j\omega) \tag{3.6}$$

where

$$f_r(t) = Re(F_r e^{j\omega t}) \tag{3.7}$$

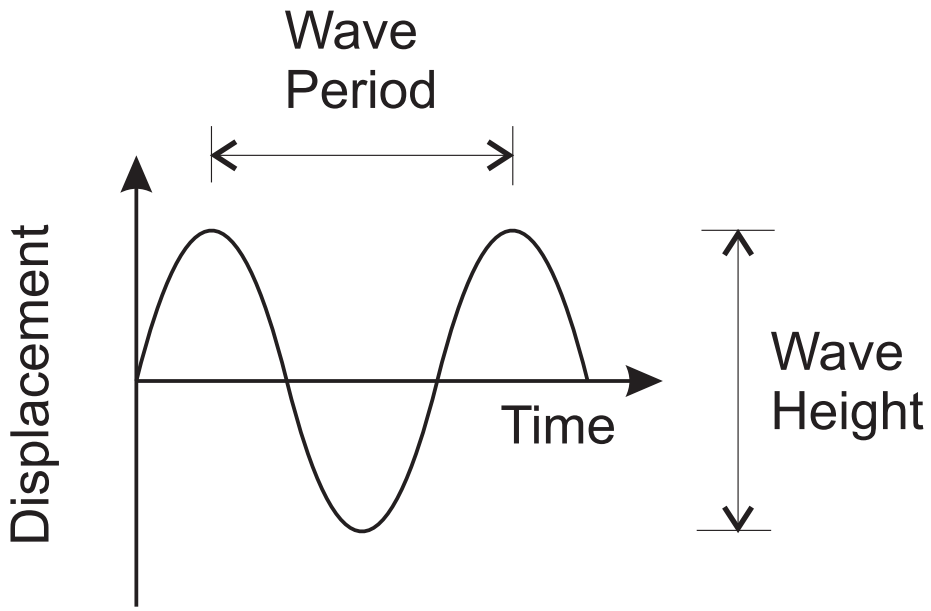

Figure 3-2: *Regular wave profile*

and

$$x(t) = Re(Xe^{j\omega t}) \tag{3.8}$$

The radiation force can be decomposed into components in phase with the buoy's acceleration and velocity [38] [13] so that

$$G(j\omega) = \omega^2 A(\omega) - j\omega B(\omega) \tag{3.9}$$

and

$$f_r(t) = -A(\omega)\ddot{x} - B(\omega)\dot{x} \tag{3.10}$$

The coefficients $A(\omega)$ and $B(\omega)$ are defined as the added mass and radiation damping coefficients respectively and are dependent on the body shape and wave frequency. They can be evaluated analytically for simple geometries or numerically using hydrodynamics packages for all other body shapes [42] [44] [30]. For the body shape that is being assumed, Falnes [38] uses previous work by Hulme [67] on the wave forces acting on a floating hemisphere to derive an expression for the radiation damping for this body shape

$$B(\omega) \approx R_H e^{-2kl} \tag{3.11}$$

where R_H is the radiation damping coefficient for a semi-submerged sphere

$$R_H = \omega\rho(\frac{2\pi}{3})a^3\epsilon \tag{3.12}$$

and ϵ is Havelock's dimensionless damping coefficient computed by Hulme [67]; $\epsilon = \epsilon(ka)$ and k is the wave number ($k = \frac{\omega^2}{g}$) given by the deep water dispersion equation.

Falnes [38] has also shown that there is a relationship between the radiation damping coefficient and the excitation force coefficient for bodies with a vertical axis of symmetry oscillating in heave such that the heave excitation force is

$$F_e \approx F_H e^{-kl} \tag{3.13}$$

where F_H is the heave excitation force for a semi-submerged sphere of radius a. The excitation force coefficient can be calculated from the radiation damping coefficient using

$$\Gamma(\omega) = \left(\frac{2g^3\rho B(\omega)}{\omega^3}\right)^{0.5} \tag{3.14}$$

Therefore by combining equations 3.1, 3.2, 3.3, 3.4 and 3.10, one can obtain an expression for the amplitude of the heaving buoy in regular waves such that

$$(m + A)\ddot{x} + B\dot{x} + \rho gSx = F_e e^{j\omega t} + f_m \tag{3.15}$$

Taking the Laplace transform gives:

$$X(s) = \frac{F_e(s) + F_m(s)}{(m + A)s^2 + Bs + \rho gS} \tag{3.16}$$

3.1.2 Time Domain Modelling

The PTO in devices of this type are highly non-linear when modelled accurately meaning that the frequency domain is not applicable and it is necessary to model the buoy in the time domain. In this case, the hydrostatic and excitation force terms remain the same but the radiation force term is altered. The radiation force in the time domain is given by the inverse Fourier transform of equation 3.6 [37].

$$f_r(t) = \frac{1}{2\pi}\int_0^\infty (\omega^2 A(\omega) - j\omega B(\omega))X(j\omega)e^{j\omega t}d\omega \tag{3.17}$$

This approach was firstly used by Cummins [39] for ship hydrodynamics but has been adopted for use in other body hydrodynamics like WECs. This means that the overall equation of motion in the time domain, as given by Falnes [38], is an integro-differential equation

$$(m + A_\infty)\ddot{x}(t) + \rho g S x(t) + \int_{-\infty}^{t} L(t-\tau)\ddot{x}d\tau = f_e(t) + f_m(x, \dot{x}, t) \tag{3.18}$$

where A_∞ is the limiting value of the added mass term; $A(\omega)$ for $\omega = \infty$ and τ is a dummy time variable. The convolution integral in equation 3.18 represents the memory effect of the radiation force, which means that the force is dependent on the history of the buoy's motion. The excitation force is the same as given in equation 3.5 and the mechanical force acting on the buoy is a function of x and $\dot{x}$ which varies with time. The memory function ($L(t)$) is given by the sine transform of the radiation damping coefficient ($B(\omega)$) and is given by Falnes [38] as

$$L(t) = \frac{2}{\pi}\int_0^\infty \frac{B(\omega)}{\omega}\sin\omega t d\omega \tag{3.19}$$

The memory effect decays with time and can be neglected after a certain period of time depending on the body shape, meaning that the infinite integral in equation 3.18 can be replaced by a finite one. The infinite integral in equation 3.19 can also be replaced by a finite one as an upper limit on the wave frequency can be assumed.

To calculate the memory function from equation 3.19 an upper finite limit of ω=5 rad/s is placed on the integral as there are very few waves above this frequency. Equation 3.19 is solved numerically to produce Figure 3-3, which shows the memory function for this body shape as a function of time. It indicates that the body's motion 2 seconds prior has the largest influence on the current radiation force and that the memory effect decays with time and equals zero after approximately 10 seconds. This implies that the motion of the buoy more than 10 seconds prior no longer effects the current motion of the buoy and can therefore be neglected, meaning that a lower integration limit of -10 s can be placed on equation 3.18.

In the simulation it would be possible to store values of L and $\ddot{x}$ as discrete time-series as the simulation is run and use these values to continuously calculate the radiation force at each discrete time-step. However, this process was found to increase the simulation run time drastically. Therefore in an attempt to re-

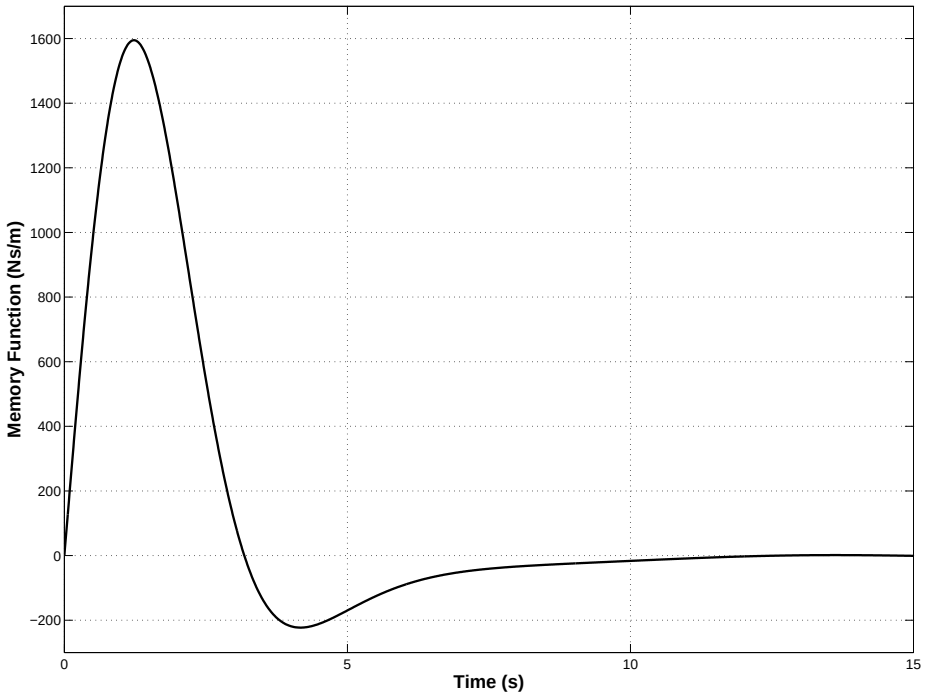

Figure 3-3: *Memory function, L(t)*

duce simulation run-time it was noted that the memory function for this shape, Figure 3-3, is very similar to the impulse response for a second order system. An optimisation algorithm was used to estimate a second order transfer function to produce a similar plot for the impulse response using the 'least squares' fitting method. The resultant transfer function was

$$R(s) = \frac{K\omega_n^2}{s^2 + 2\zeta\omega_n s + \omega_n^2} = \frac{3232}{s^2 + 1.137s + 1.241} \tag{3.20}$$

The comparison between the impulse response from the transfer function and the memory function is shown in Figure 3-4 and indicates that both approaches produce a very similar result. Therefore, in the simulation model a transfer function is used to filter the buoy's acceleration signal instead of the convolution integral. This provides comparable results with the advantage of significantly reducing the simulation run-time.

Table 3.1 presents the key physical parameters of the buoy, which remain constant for all the work, including the added mass ($A(\infty)$) for a body of this shape [68]. These sizes are similar to a range of heaving buoy-type WECs which

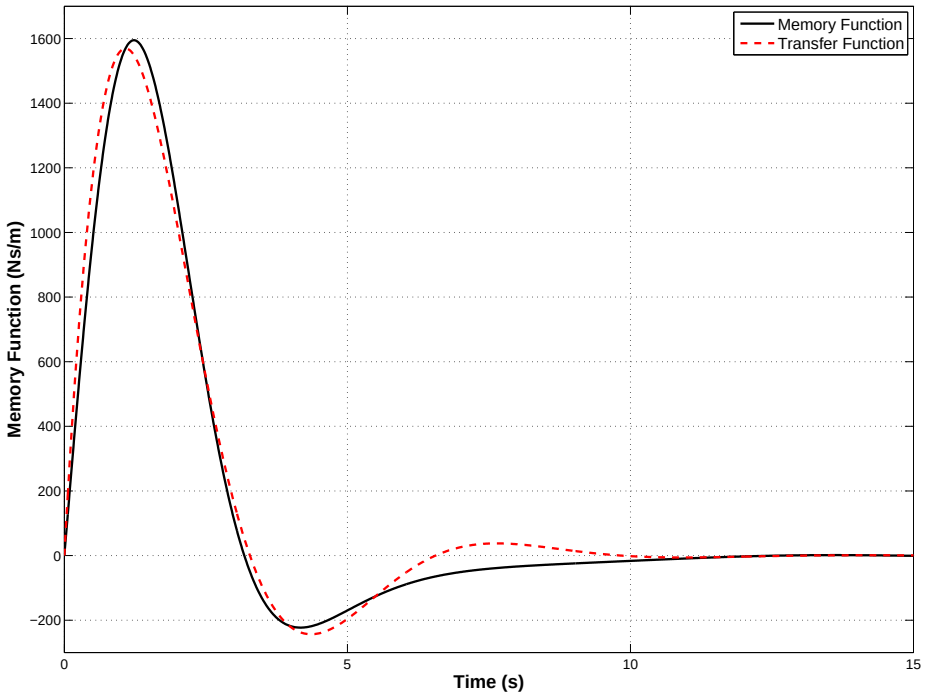

Figure 3-4: *Memory function comparison*

are being investigated. It would be defined as a small, low-draft heaving buoy [66]. Figure 3-5 represents the block diagram of the Simulink model.

Buoy mass (m) + Added mass (A_∞)	53 tonne
Radius (r)	2 m
Height ($2l$)	6 m
Hydrostatic stiffness ($\rho g s$)	126.5 kN/m
Natural frequency (ω_n)	1.54 rad/s

Table 3.1: *Buoy parameters*

3.2 Linear Power Take-Off

As a starting point for work on the PTO, it is necessary to determine the nature of the mechanical forces acting on the WEC (f_m). They comprise of the force applied on the buoy by the PTO and the mooring force. In this work the vertical component of the mooring force is assumed to be zero and initially the PTO force

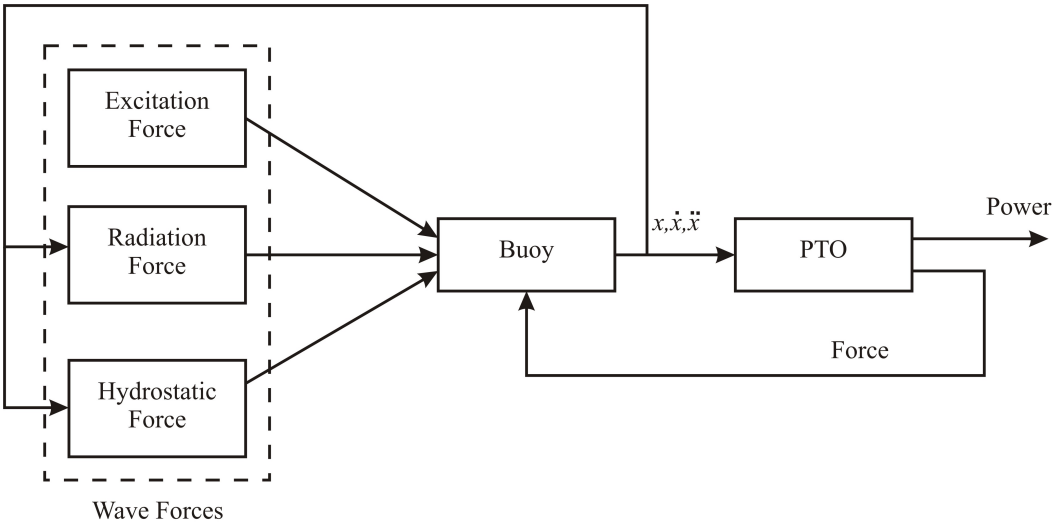

Figure 3-5: *Block Diagram of Simulink Model*

is assumed to be linear so that

$$f_m(t) = -Kx - C\dot{x} \tag{3.21}$$

where K and C are the spring stiffness and damping coefficients respectively. The spring effect $(-Kx)$ may or may not exist depending on the specific PTO while the damping effect $(-C\dot{x})$ is associated with the energy extraction of the PTO. Equation 3.15 now takes the form

$$(m + A)\ddot{x} + (B + C)\dot{x} + (\rho gS + K)x = f_e(t) \tag{3.22}$$

This is the classical approach for modelling the PTO which leads to analysis of the system in the frequency domain [57]. Taking the Laplace transform of equation (3.22) gives the following transfer function

$$\frac{X(s)}{F_e(s)} = \frac{1}{(m + A)s^2 + (B + C)s + (\rho gS + K)} \tag{3.23}$$

Transforming into the frequency domain

$$X(j\omega) = \frac{F_e(j\omega)}{-\omega^2(m + A) + j\omega(B + C) + (\rho gS + K)} \tag{3.24}$$

Equation (3.24) can be re-written in terms of velocity, U, to give

$$U(j\omega) = \frac{F_e(j\omega)}{j\omega(m+A) + (B+C) + (\frac{\rho g S + K}{j\omega})} \tag{3.25}$$

These equations are only valid for regular monochromatic waves and they can be used to predict the conditions for maximum power capture. The instantaneous power capture is given by

$$P_{cap} = C\dot{x}^2 \tag{3.26}$$

The equations can also be used to predict the motion of the buoy in irregular waves by the superposition of results for a number of regular waves with a range of frequencies, phases and heights.

To determine how the linear PTO behaves in regular waves, the model was run for a wave of $H = 2\,m$ and $T = 8\,s$. Figure 3-6 shows that the motion of the buoy lags the motion of the waves and there is an amplitude ratio which is dependent on the damping and spring term of the PTO. The PTO force and power captured are sinusoidal in nature with the values of power being negative for certain periods of the cycle. This means that during these periods the PTO is generating power and therefore acting as a wave generator. This is an example of reactive phase control (Section 2.3.1), and by adjusting the spring term resonance can be achieved for any specific wave frequency. This significantly increases the magnitude of buoy displacement and therefore increases power capture.

A hydraulic PTO capable of the force control required for reactive control would be complex. Therefore it is presumed that a simple hydraulic PTO will be incapable of acting as both a power generator and absorber so for this work the linear PTO is assumed to be incapable of providing a spring term ($K = 0$). Therefore, the PTO can only extract energy from the waves and not generate any power so there are no negative power values, as seen in Figure 3-7. Without the negative spring term the displacement of the buoy and the power captured reduces but the demands of the PTO, in terms of the PTO force requirement and complexity, have also reduced. This can be seen in the 50% reduction in PTO force magnitude in Table 3.2.

K (kN/m)	$\lvert x\rvert$ (m)	$\lvert f_m\rvert$ (kN)	$\bar{P_{cap}}$ (kW)
0	0.73	57.2	16.4
-100	1.11	141.3	38.1

Table 3.2: *Comparison of linear PTOs, with and without reactive control*

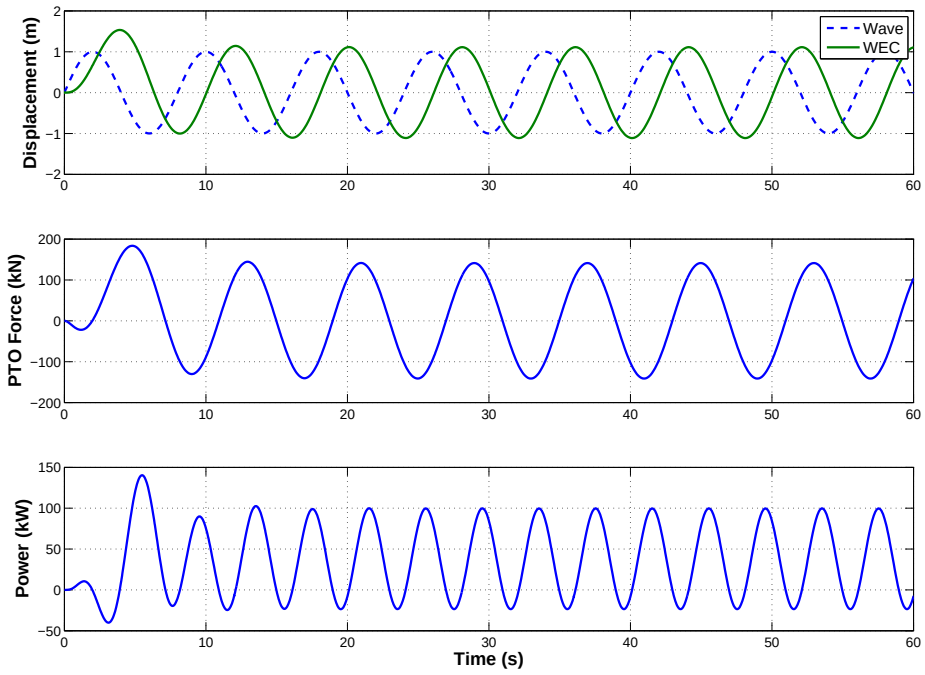

Figure 3-6: *Top: Wave and WEC displacement, Middle: PTO Force, Bottom: PTO Power for linear PTO characteristics C = 100 kNs/m and K = -100 kN/m*

3.3 Hydraulic Power Take-Off

As outlined in Section 1.4, hydraulic PTOs are generally used in WECs due to their advantages for dealing with low frequency, high force wave inputs and their high power density and robustness. There is no standard configuration for a hydraulic PTO, with the design normally consisting of "sets of hydraulic cylinders that pump fluid, via control manifolds, into high pressure accumulators for short term energy storage. Hydraulic motors use the smooth supply of high-pressure fluid from the accumulators to drive grid-connected electric generators" [28]. The main aim of the PTO is to convert the irregular wave input into a smooth electrical power output by decoupling the power capture from the power generation. This is done by using accumulators for energy storage and means that the primary element of power capture can be sized to deal with the maximum power input and the secondary element of power generation can be sized according to the average power capture and can therefore be smaller, cheaper and more efficient.

The hydraulic PTO used in this simulation model is shown in Figure 3-8.

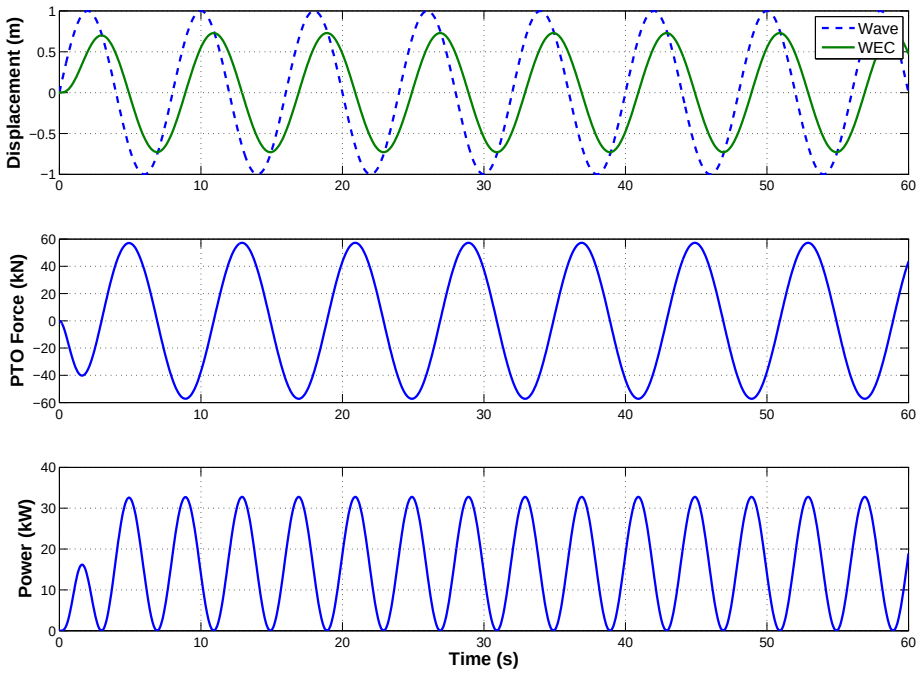

Figure 3-7: *Top: Wave and WEC displacement, Middle: PTO Force, Bottom: PTO Power for linear PTO characteristics $C = 100\,kNs/m$ and $K = 0\,kN/m$*

The simple circuit excludes components such as filters and coolers which would be required in the real hydraulic system but would add unnecessary complexity at this stage. The initial work is to ensure the circuit and the influence of the different components are fully understood before any further investigations are undertaken into the optimisation of the device.

A rigid link between the buoy and the PTO means that the motion of the buoy directly drives the double-acting equal area hydraulic piston working within a fixed cylinder. This motion drives fluid through a set of four check valves to rectify the flow so that fluid always passes through the hydraulic motor in the same direction (independent of the direction of the buoy motion). A high pressure accumulator is placed on the inlet to the hydraulic motor, and a low pressure accumulator on the outlet of the hydraulic motor. The pressure difference between the two accumulators drives a variable displacement motor, which is connected to an electrical generator. The accumulators are included to try and keep an approximately constant pressure differential across the motor so it spins at a roughly constant speed and therefore power is generated at almost a constant rate. The thermodynamic transformations in the accumulators are assumed to

be isentropic, which is reasonable considering the cycle time of the device. In this work, the generator is modelled as a simple rotational damper with varying damping coefficient meaning that the resistive torque imposed by the generator can be altered by varying this damping coefficient. In a real circuit, there will be external leakage from the motor to tank. Therefore to replenish the circuit and avoid cavitation in the cylinder a boost pump is required. This is incorporated with a pressure relief valve to maintain a minimum pressure in the system, which can be adjusted by varying the pressure relief valve setting. In this case the pressure relief valve is set to 10 bar.

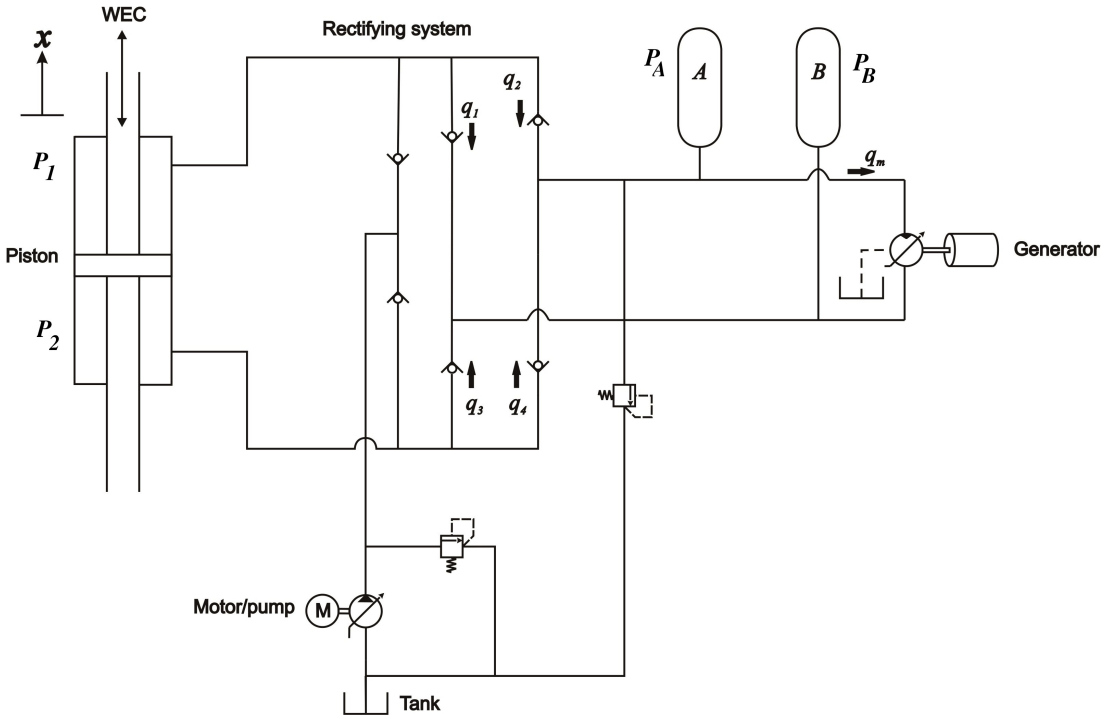

Figure 3-8: *Hydraulic PTO unit circuit diagram*

In reality there will be losses throughout the hydraulic circuit such as friction in the piston, pressure losses in the pipes, leakage in the motor and torque losses due to friction in the motor and generator. These losses will depend on the specific operating conditions in the unit, which are determined by the size of certain components and the constantly changing wave conditions. However, as a starting point to help understand the PTO, it has been simplified so there are no losses in the circuit. Section 3.4 will investigate the PTO with losses. Without losses the following equations hold true for the hydraulic circuit.

PTO force:

$$\Phi = (p_1 - p_2)A_p \tag{3.27}$$

where p_1 and p_2 are the pressures in the piston chambers and A_p is the piston area. Φ is used to represent the PTO force in the hydraulic circuit as it is the symbol commonly used in other work in this area. It corresponds to f_m in the linear PTO.
Mechanical power captured by the PTO:

$$P_{cap} = \Phi\dot{x} \tag{3.28}$$

Cylinder flow balance:
If sign($\dot{x}$) is positive:

$$A_p\dot{x} - q_1 - q_2 = \frac{V_1}{B_o}\frac{dp_1}{dt} \tag{3.29}$$

If sign($\dot{x}$) is negative:

$$A_p\dot{x} - q_3 - q_4 = \frac{V_2}{B_o}\frac{dp_2}{dt} \tag{3.30}$$

where V_i is the volume of oil in piston chamber 'i = 1,2' and B_o is the bulk modulus of the oil.

Check valve flows:

$$q_1 = \left\{ \begin{array}{rcl} 0 & : & p_1 > p_B \\ -K_v\sqrt{p_B - p_1} & : & p_B \geq p_1 \end{array} \right\} \tag{3.31}$$

$$q_2 = \left\{ \begin{array}{rcl} 0 & : & p_A > p_1 \\ K_v\sqrt{p_1 - p_A} & : & p_1 \geq p_A \end{array} \right\} \tag{3.32}$$

$$q_3 = \left\{ \begin{array}{rcl} 0 & : & p_2 > p_B \\ -K_v\sqrt{p_B - p_2} & : & p_B \geq p_2 \end{array} \right\} \tag{3.33}$$

$$q_4 = \left\{ \begin{array}{rcl} 0 & : & p_A > p_2 \\ K_v\sqrt{p_2 - p_A} & : & p_2 \geq p_A \end{array} \right\} \tag{3.34}$$

K_v is the valve coefficient, which is initially chosen to be very large so that the pressure drop across each check valve is negligible.

Rectified flow:

$$q_r = q_2 + q_4 \tag{3.35}$$

Flow to accumulator 'A':

$$q_A = q_r - q_m \tag{3.36}$$

Volume of oil in accumulator 'A':

$$V_A(t) = \int_0^t q_A dt \tag{3.37}$$

Flow to accumulator 'B':

$$q_B = q_m - q_1 - q_3 \tag{3.38}$$

Volume of oil in accumulator 'B':

$$V_B(t) = \int_0^t q_B dt \tag{3.39}$$

Assuming the compression in the accumulators to be isentropic, the pressure in each accumulator is given by:

$$p_A V_A^\gamma = p_o V_o^\gamma \tag{3.40}$$

$$p_B V_B^\gamma = p_o V_o^\gamma \tag{3.41}$$

where p_o is the pre-charge pressure and V_o is the volume of each accumulator and γ is the adiabatic index.

Flow to hydraulic motor:

$$q_m = D_m \omega_m \tag{3.42}$$

where D_m is the motor displacement and ω_m is the motor speed.

Rotational acceleration:

$$\dot{\omega}_m = \frac{D_m(p_A - p_B) - T_g}{J} \tag{3.43}$$

where p_A is the pressure in accumulator 'A', p_B is the pressure in accumulator 'B' and J is the inertia of the generator.

Generator torque:

$$T_g = C_g \omega_m \tag{3.44}$$

where C_g is the damping coefficient of the generator.

Motor torque:

$$T_m = (p_A - p_B) D_m \tag{3.45}$$

Mechanical power generated by the PTO:

$$P_{gen} = T_m \omega_m \tag{3.46}$$

Table 3.3 shows the component parameters in the PTO. These values are not based on any specific design but are a representation of suitable sizing for the buoy size. In this idealised case the effect of the boost pump is negligible and the electrical generator is assumed to be 100% efficient so the electrical power generated can be equated to the mechanical power generated by the PTO. The high pressure accumulator ('A') has a relatively low pre-charge pressure to ensure that it charges even in calm wave conditions.

To determine how the idealised hydraulic PTO behaves compared to the linear PTO, the model was run under the same wave conditions as before with the hydraulic motor at full displacement. As expected, Figure 3-9 indicates that there are some notable differences between the two PTOs. The force from the hydraulic PTO (Φ) resembles a square wave compared to the sinusoidal nature of the linear PTO. The motion of the buoy is not fully sinusoidal with the buoy arresting at its endpoints; this is not very obvious in Figure 3-9 but will be shown in more detail in the next section. In the early stages, the magnitude of Φ increases as the pressure in accumulator 'A' increases from the initial condition to a steady state value. The power captured (P_{cap}) and generated (P_{gen}) also increases as the system pressure increases until a steady state condition is reached. Finally, as Φ increases there is a slight decrease in the magnitude of the displacement of the WEC.

After the initial transients, the system reaches a steady state where P_{cap} varies between zero and a maximum value during each half cycle of the wave but P_{gen} varies only minimally around the average value of P_{cap}. This shows that the hydraulic PTO is providing the desired power smoothing effect meaning that the motor and generator can be sized according to this average value. Although it

Maximum system pressure	350 bar
Equal area piston	
Area	$0.007\,\mathrm{m}^2$
Stroke Limit	$\pm 2.5\,\mathrm{m}$
HP Gas accumulator 'A'	
Pre-charge Pressure	30 bar
Volume	200 L
γ	1.4
LP Gas accumulator 'B'	
Pre-charge Pressure	10 bar
Volume	200 L
γ	1.4
Variable Displacement Motor	
Capacity	180 cc/rev
Generator	
Damping coefficient	$2.5\,\mathrm{Nm/(rad/s)}$
Inertia	$2\,\mathrm{kgm}^2$
Boost Pump	
Capacity	50 cc/rev
Relief valve pressure	10 bar
Oil Properties	
Viscosity	50 cSt
Density	$850\,\mathrm{kg/m}^3$

Table 3.3: *PTO component values*

was presumed that the PTO would be incapable of generating power it can be seen that P_{cap} is slightly negative for a small part of the cycle, which is due to the inertia of the buoy and the compressibility of the oil. To fully understand the action of the PTO during a cycle of the buoy motion, it is necessary to look in more detail at the workings of the hydraulic circuit.

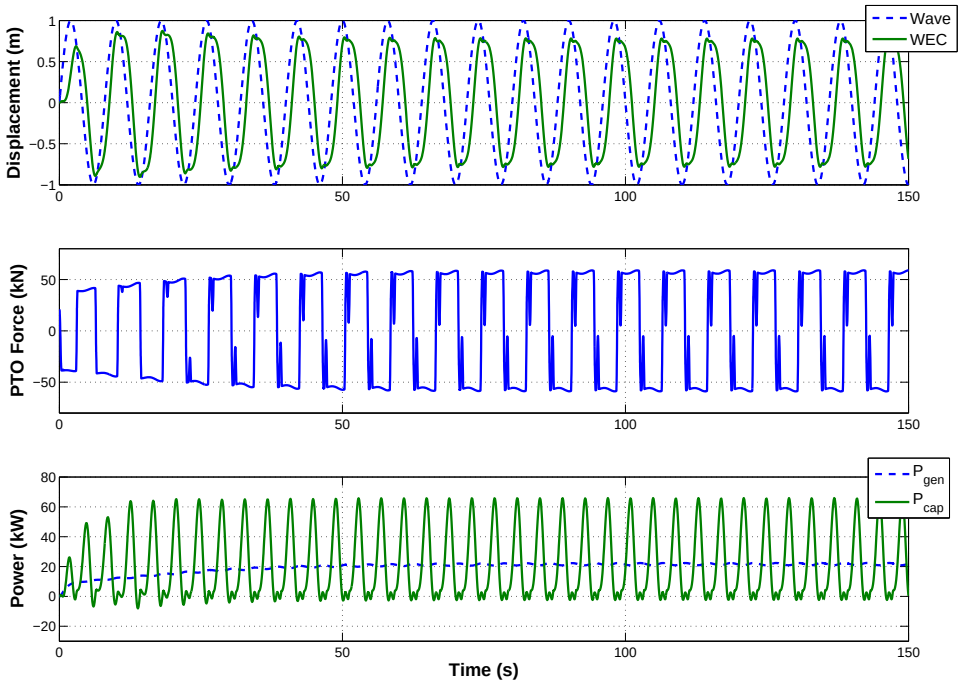

Figure 3-9: *Top: Wave and WEC displacement, Middle: PTO force, Bottom: PTO captured and generated power*

3.3.1 Wave Cycle Behaviour

This section describes how the hydraulic PTO behaves during one cycle of the buoy's motion after the initial transients. This will give a better understanding of the action of the PTO and it may also help determine possible ways in which the PTO can be optimised.

The following points, with the help of Figures 3-10 - 3-13, will explain the sequence of events which is occurring during the cycle for $T = 8\,\text{s}$ after steady state has been reached:

- At time $= 390.5\,\text{s}$ the piston approaches its endpoint and the pressure in the piston chamber (p_2) falls below the accumulator pressure (p_A) so the check

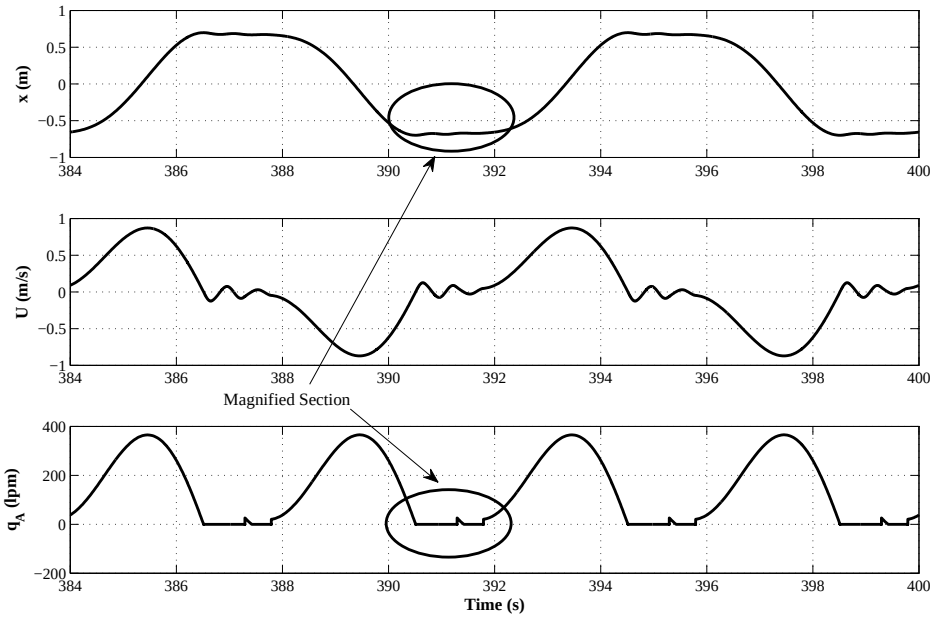

Figure 3-10: *Top: Piston displacement, Middle: Piston velocity, Bottom: Rectified flow*

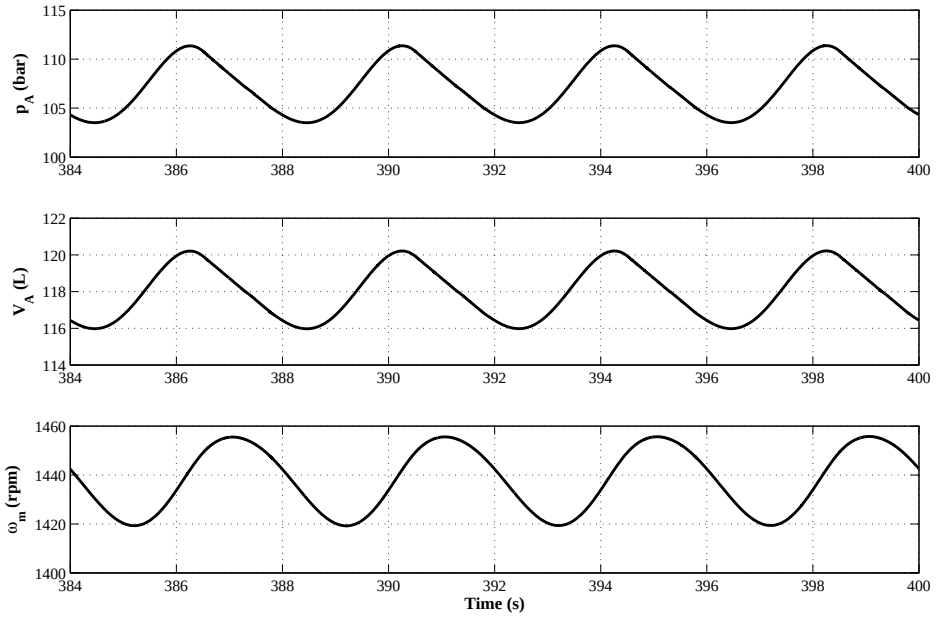

Figure 3-11: *Top: Accumulator 'A' pressure, Middle: Accumulator 'A' volume, Bottom: Motor speed*

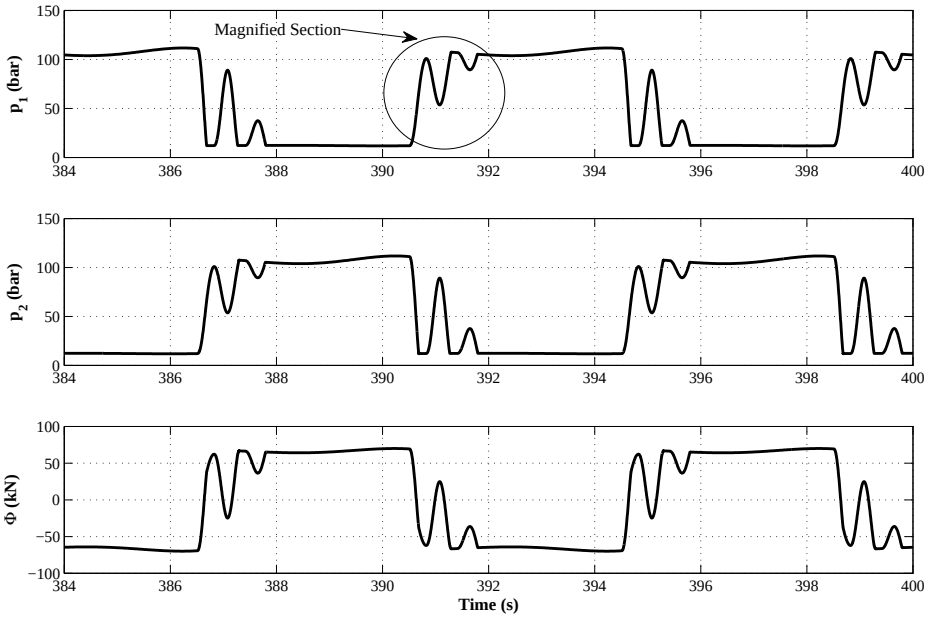

Figure 3-12: *Top and Middle: Piston chamber pressures, Bottom: Piston force*

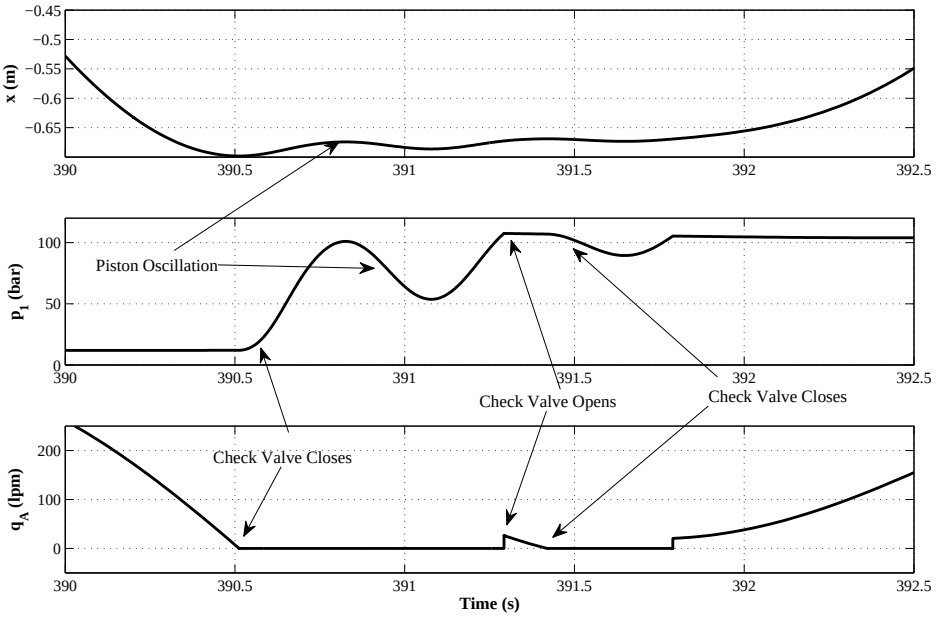

Figure 3-13: *Magnified section of; Top: Piston displacement, Middle: Piston Chamber pressure, Bottom: Rectified flow*

valve closes and there is zero rectified flow.

- At this point the piston changes its direction of motion so the high pressure piston chamber becomes the low pressure chamber and visa versa (p_1 and p_2).

- When the piston is at its endpoints the wave force is insufficient to overcome the piston force so it stalls for approximately two seconds (time = 390.5 - 392 s). However, due to the inertia of the buoy there are still small piston oscillations during this period, see Figure 3-13.

- When the check valves are closed this forms two columns of oil in each piston chamber and joining pipeline. As the piston oscillates during this period it compresses one column of oil and increases the pressure (p_2) whilst the other column of oil has a reduction in pressure (p_1). This oscillation causes the chamber pressure and piston force oscillations which can be seen in Figure 3-12 at time = 391 s.

- The wave force is trying to move the buoy and as it increases, the pressure in one of the chambers (p_1) increases sufficiently to open the check valve. This causes a small spike in the rectified flow, which can be seen in Figure 3-13 at time = 391.5 s.

- When the check valve opens p_1 reduces and the check valve closes again resulting in zero rectified flow. This occurs because the wave force is still insufficient to overcome the piston force and maintain p_1 higher than p_A to keep the check valve open.

- At time = 392 s the wave force becomes greater than the piston force and p_1 increases to overcome p_A. The check valve opens and the piston is now moving freely which creates rectified flow.

- As the piston velocity increases the flow increases until the maximum at time = 393.5 s. At the point of maximum piston velocity and flow, the wave force becomes less than the piston force again and the piston velocity decreases meaning that the flow begins to reduce.

- Figure 3-11 indicates that flow from the piston causes the pressure and volume of oil in the accumulator to increase after a short delay.

- The motor speed also increases with the accumulator pressure after a short delay.
- As p_A increases, p_1 decreases slightly. At time = 394.5 s, p_A becomes greater than p_1 and the check valve closes.
- When the check valves are closed and there is zero flow from the piston, the motor tries to maintain a constant speed by drawing oil from the accumulator. Therefore the accumulator volume and pressure fall during this period causing the motor speed to reduce as well.
- The accumulator then re-charges when there is maximum flow from the piston as there is more flow than is required by the motor during this time.
- This repeating cycle causes the oscillations in the motor speed, accumulator pressure and accumulator volume around an average value.

Figure 3-10 shows more clearly that the previous assumption of sinusoidal motion made for the case of the linear PTO does not hold true when an idealised hydraulic PTO is introduced. It can be seen that the piston is arrested at its endpoints and remains almost stationary for approximately two seconds until the wave force exceeds the piston force. This induced body stall is also noted by Falcão [43] [42]. It is clear from the behaviour of the idealised hydraulic PTO that the system does not capture energy in the same sinusoidal manner as a linear PTO. Due to the large accumulators the pressure drop across the motor remains nearly constant. Therefore the actuator experiences a virtually constant amplitude force resembling a square wave so the behaviour is more like that of a Coulomb damper.

3.4 Hydraulic PTO Including Losses

The next stage of the work is to model the hydraulic PTO more realistically by introducing losses to determine more accurately what magnitude of power can be generated by the PTO. It is also necessary to establish if the behaviour of the PTO changes when losses are included and what are the main components that are the source of the power losses (P_{los}). The losses now included in the hydraulic PTO are:

- Friction in the cylinder

- Friction in the pipework
- Pressure loss across the check valves
- Internal flow leakage in the motor
- Viscous and coulomb friction torque losses in the motor
- Boost pump power

The cylinder friction, F_{fr}, simulates the friction between both piston and piston rod and the cylinder body and is the sum of the coulomb and viscous components. It is calculated using:

$$F_{fr} = f_c sign(\dot{x}) + f_v \dot{x} \tag{3.47}$$

where f_c is the coulomb friction and f_v is the viscous friction coefficient. The pressure losses (Δp) in the pipework are calculated for a fully developed flow (q) using D'Arcy's equation:

$$\Delta p = 4f \frac{L}{d} \frac{\rho_o U_f^2}{2} \tag{3.48}$$

where f is the pipe friction factor, L is the pipe length, d is the pipe diameter, ρ_o is the oil density and U_f is the mean fluid velocity. The pressure drop (Δp) across the check valve is obtained from the orifice equation for turbulent flow:

$$q_i = K_v \sqrt{\Delta p} \tag{3.49}$$

3.4.1 Hydraulic Motor Model

A variable displacement hydraulic piston motor was used, with a capacity of 180 cc/rev, in the model. This motor was chosen as it was a suitable size for the PTO in a wide variety of operating conditions. Furthermore, there was available experimental data for the motor so an accurate model could be created. An accurate model is required as the variable wave conditions, which a WEC will encounter depending on location and time of year, will result in the motor operating under a variety of pressures, speeds and part displacements. Ivantysynova [69] states that "the reliable prediction of losses of fluid power systems by system simulation requires a very high accuracy of steady state models of all components, but especially of displacement machines in the whole parameter range." It is therefore imperative to determine what efficiencies are expected from the

motor under all these conditions so power generation can be predicted accurately and the entire PTO can be optimised effectively. The motor losses have been approximated using the Wilson model [70] with three dimensionless coefficients: the slip coefficient (C_s), the viscous friction coefficient (C_v) and the coulomb friction coefficient (C_f). The motor torque (T_m), flow rate (q_m) and motor efficiency (η_m) are thus given by:

$$T_m = (1 - C_f)D_m(p_A - p_B) - C_v D_m \mu \omega_m \tag{3.50}$$

$$q_m - \frac{C_s D_m (p_A - p_B)}{\mu} = D_m \omega_m \tag{3.51}$$

$$\eta_m = \frac{T_m \omega_m}{Q_m (p_A - p_B)} \tag{3.52}$$

where μ is the dynamic viscosity of the oil. If the dimensionless coefficients are constants the model does not give a good match to the experimental data for a range of operating conditions. McCandish and Dorey [71] have previously shown that there can be significant differences between real performance data and the results predicted by the classic Wilson model over a wide range of operating conditions. Therefore, to improve the accuracy of the model a variable coefficient linear model was implemented where C_s and C_v are functions of speed [71, 72]. This is a modification to [71] where C_f is a function of speed but this form of the model gave a better agreement to the experimental results. For 100% capacity, the coefficients are given by the following:

$$C_{s_\omega} = 1.14 \times 10^{-8} + (1.53 \times 10^{-8} - 1.14 \times 10^{-8}) \left(\frac{\omega_m - 500}{2500 - 500} \right) \tag{3.53}$$

$$C_{v_\omega} = 1.98 \times 10^{5} + (3.12 \times 10^{5} - 1.98 \times 10^{5}) \left(\frac{\omega_m - 500}{2500 - 500} \right) \tag{3.54}$$

where ω_m is the motor speed in rpm (revolutions per minute).

As this is a variable capacity motor the losses are also a function of displacement. Therefore, the high and low speed coefficients of the linear model in Equations 3.53 and 3.54 vary with displacement. The model was further adapted to include a non-linear component, which is a function of displacement, to calculate the correct coefficients at each displacement. Figures 3-14 to 3-17 reveal that

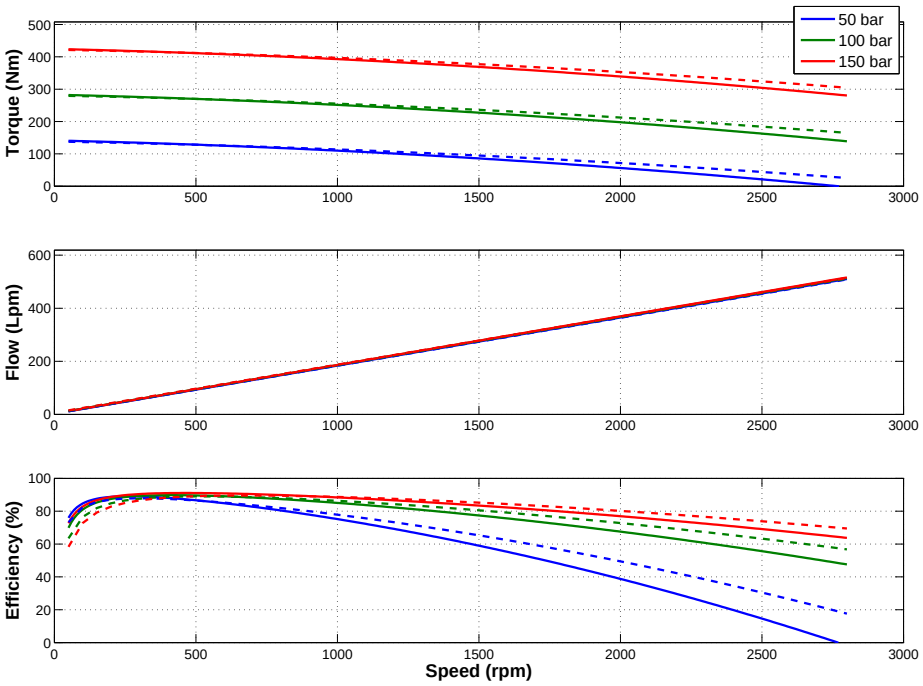

Figure 3-14: *Motor Performance Curves for 100% displacement; Solid line is simulation model, dotted line is experimental data*

the final model shows a good overall correlation to the experimental data over the full range of operating conditions. For the range of displacements the model predicts near identical motor speeds to the experimental data at all flow rates. At full displacement it is noted that the torque and efficiency of the model is lower at high speeds compared to the experimental data. However, these results were still found to be acceptable because such high speeds at full displacement are not generally expected with standard wave conditions and to increase the accuracy of the model any further would significantly increase simulation complexity and run time.

The generator and grid connection losses have not been incorporated at this stage as the main focus of the research is on the optimisation of the hydraulic transmission. Therefore, as previously, the power generated will be equated to the mechanical power produced by the PTO. Table 3.4 shows the parameters of all the other components required to calculate the losses.

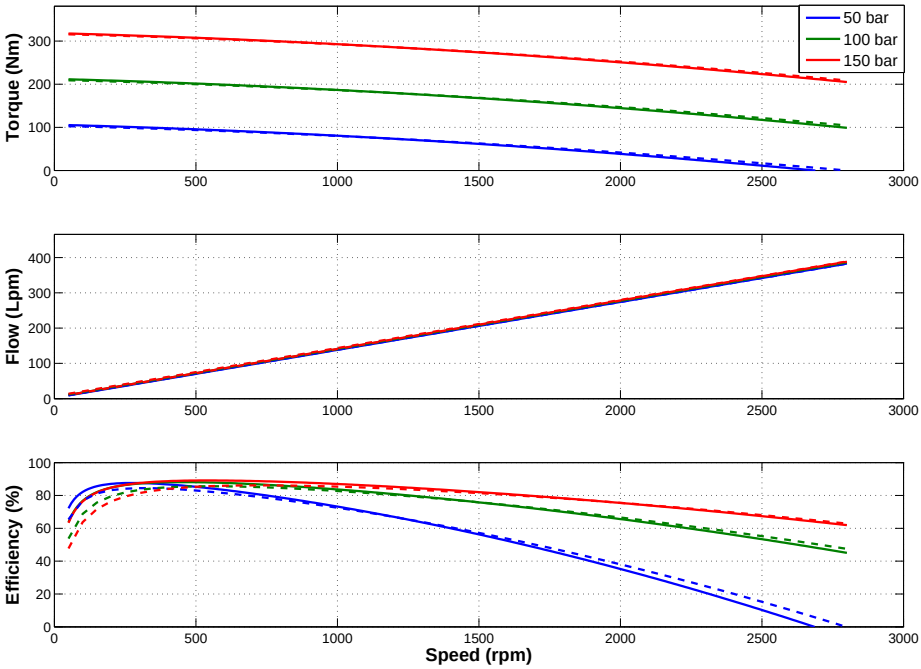

Figure 3-15: *Motor Performance Curves for 75% displacement*

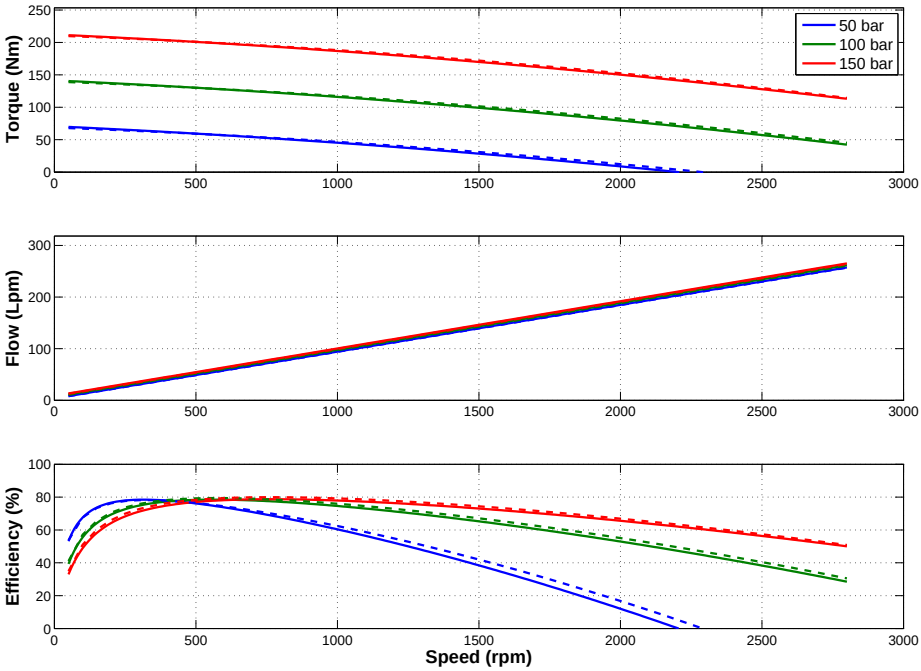

Figure 3-16: *Motor Performance Curves for 50% displacement*

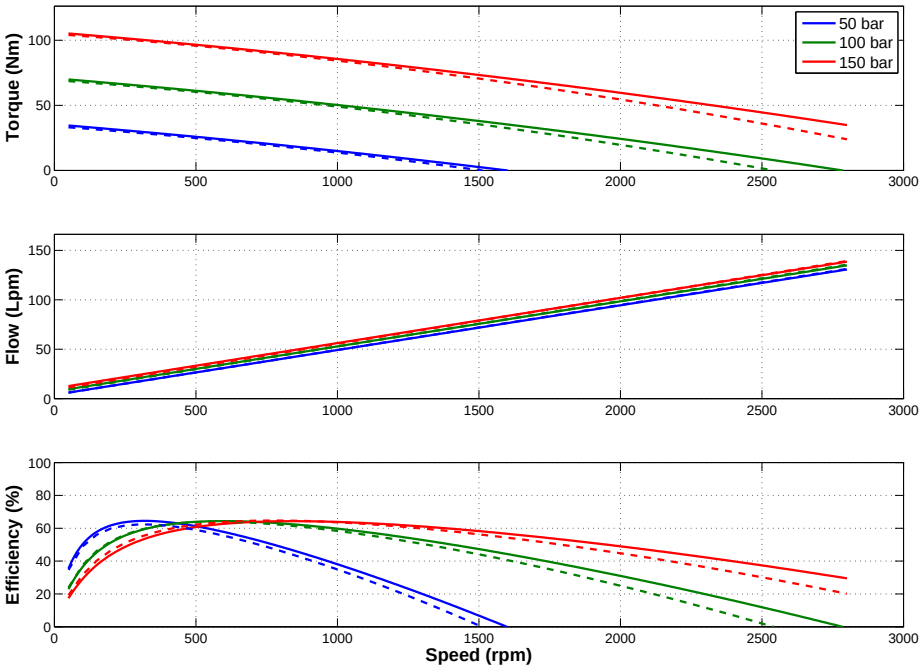

Figure 3-17: *Motor Performance Curves for 25% displacement*

Cylinder	
Coulomb friction (f_c)	3500 N
Viscous friction coefficient (f_v)	100 N/(m/s)
Variable Displacement Motor	
C_f	0.014
Check Valve	
Valve constant (K_v)	8.5×10^{-6}
Cracking Pressure	0.3 bar
Pipework	
Diameter (d)	50 mm
Total Length (l)	10 m

Table 3.4: *PTO unit component loss parameters*

3.4.2 Wave Cycle Behaviour

The model was run with the same wave conditions and PTO component sizes to discover how the PTO with losses behaves during a wave cycle. Comparing Figures 3-18 and 3-9, the motion of the WEC is very similar but the magnitude of the oscillation is slightly reduced. A similar increase in PTO force and power is observed as the system pressure increases until a steady state is reached. The magnitude and shape of the PTO force are also very similar with the PTO still exhibiting a Coulomb damping nature. The biggest difference, as expected, is the reduction in the magnitude of P_{gen} but there is also a slight reduction in the magnitude of P_{cap}. In terms of cycle behaviour the two models behave in the same manner except there is no check valve opening and closing when the buoy is arrested, as noticed with the idealised model in Figure 3-13. This means that the number of duty cycles for the check valves reduces.

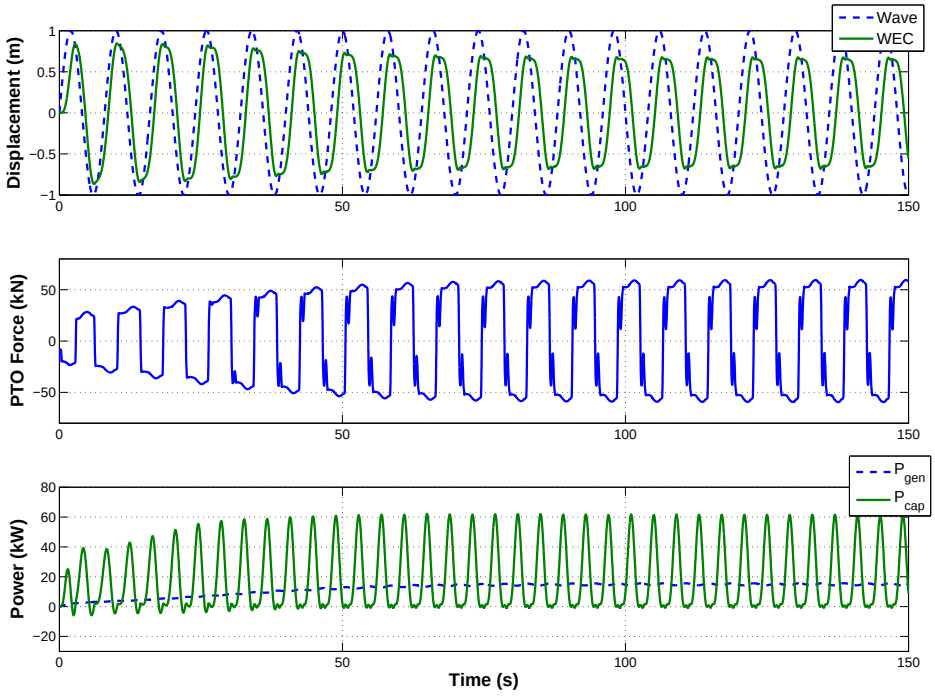

Figure 3-18: *Top: Wave and WEC displacement, Middle: PTO force, Bottom: PTO captured and generated power for the PTO loss model*

3.4.3 Power Take-Off Efficiency

Equation 3.56 presents the PTO efficiency (η_{pto}) as the ratio of P_{gen} to P_{cap}. There is also the ratio of the P_{cap} to the incident wave power (P_{wave}), which is defined as the buoy capture efficiency (η_{cap}) and given by equation 3.57. These two terms are combined to give the overall WEC efficiency (η_{wec}), which relates P_{wave} to P_{gen} (equation 3.58). Equation 3.55 gives the wave power for a regular monochromatic wave [11].

$$P_{wave} = \frac{a\rho g^2 T H^2}{16\pi} \tag{3.55}$$

$$\eta_{pto} = \frac{P_{gen}}{P_{cap}} \tag{3.56}$$

$$\eta_{cap} = \frac{P_{cap}}{P_{wave}} \tag{3.57}$$

$$\eta_{wec} = \frac{P_{gen}}{P_{wave}} = \eta_{pto}\eta_{cap} \tag{3.58}$$

Table 3.5 shows the resulting powers and efficiencies for the two hydraulic PTO models.

Idealised PTO	Power (kW)
Wave	125.7
Captured/Generated	21.9
Loss PTO	**Power (kW)**
Captured	20.4
Generated	14.8
PTO Losses	5.6
	Efficiency (%)
η_{cap}	16.1
η_{pto}	72.5
η_{wec}	11.7

Table 3.5: *Average Powers and Efficiencies for $H = 2\,m$ and $T = 8\,s$*

The first point to note is the difference in P_{cap} for the two models. With

Component	Power (kW)	Efficiency (%)
Cylinder	1.7	91.7
Check valves (Rectifier)	1.3	93.0
Pipework	0.1	98.2
Motor	2.4	85.9
Boost Pump	0.1	n/a

Table 3.6: *Average Power losses in the hydraulic circuit*

PTO losses included the average P_{cap} is lower compared to the idealised PTO, indicating that the inclusion of PTO losses causes the WEC to behave slightly differently. This is demonstrated in the reduced oscillation magnitude in Figure 3-18. Furthermore, Table 3.5 shows that even for a small wave height of 2 m there is still a significant power loss of 5.6 kW in the PTO giving $\eta_{pto} \approx 72\%$.

Table 3.6 indicates that the motor is the main contributor to power loss. The efficiency of hydraulic motors depends on many parameters such as speed, pressure difference and fraction of displacement, as discussed previously (Section 3.4.1). Therefore, the motor efficiency will depend on those parameters which will vary depending on the differing wave conditions. The next biggest losses are from the cylinder and check valves of the rectifying unit. The viscous component of the cylinder friction will increase with buoy velocity and the pressure drop across the check valve is similar to a viscous friction effect as it will increase when piston velocity and flows increase at larger wave heights. To minimise this pressure drop, the flow rate in the circuit could be reduced by using a smaller piston area. However, this approach must be matched by the requirement to choose a piston area which is large enough so not to violate the maximum system pressure in large waves. The current piston area gives a good balance between the two requirements so will be used for future investigation. The losses associated with the hydraulic pipes and the boost pump are small in comparison. The power consumed by the boost pump is the power required to replenish the circuit with the external leakage flow from the hydraulic motor at the minimum pressure of 10 bar. This leakage flow will increase with reduced motor displacement and as motor speed increases at larger wave heights. However, the power consumed is still likely to be negligible when compared to the losses from the cylinder, check valves and hydraulic motor.

Figure 3-19 shows η_{pto} over a range of wave heights for four different wave periods. It indicates that η_{pto} reduces slightly with wave height and is generally lower for higher wave periods. This is due to a number of reasons. Firstly, the

cylinder friction is Coulomb dominant so the overall loss from the cylinder does not increase greatly with wave height. Secondly, motor efficiency only reduces slightly as motor speed increases with flow and wave height. It is more dependent on motor displacement and will therefore reduce more substantially if the motor is run at part displacement. As expected the pressure drop across the check valves increases exponentially with wave height, which produces the slightly reduced η_{pto}. The losses associated with the pipework and boost pump show a slight increase but still remain negligible.

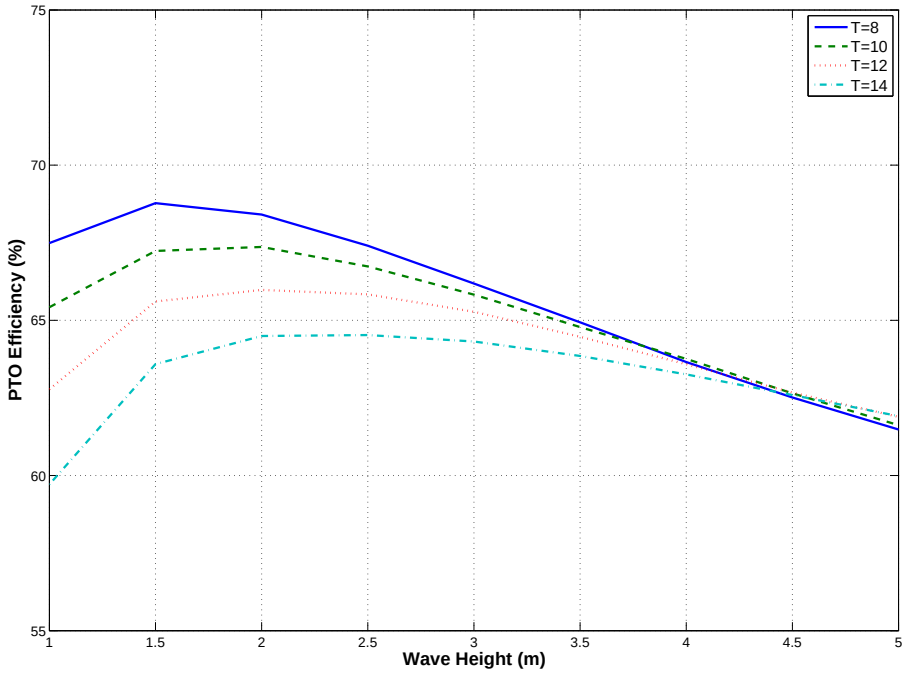

Figure 3-19: *PTO efficiency against wave height for four different wave periods*

3.5 Concluding Remarks

This chapter detailed the different modelling approaches for the WEC and the PTO. Firstly, the hydrodynamics of the buoy were presented using linear wave theory for a frequency domain and time domain analysis. The time domain analysis was slightly modified from the classical approach to use a transfer function to filter the buoy acceleration to represent the radiation force in order to reduce simulation time.

A simple linear PTO model of a linear spring and damper was presented. The model was shown to give large power capture when the PTO could act as a power generator and absorber, which is achieved by having a large negative spring force to achieve resonance. However, it is assumed that a hydraulic PTO could not produce this negative spring force without a complex design so it was removed for future work.

An appropriately sized hydraulic PTO was then modelled with no losses included initially. A thorough explanation and investigation of the action of the PTO during a wave cycle was presented. Results indicate that the sinusoidal motion of the WEC and viscous damping effect associated with a linear PTO is now replaced by an induced body stall and Coulomb damping effect from the hydraulic PTO. Accurate loss models were then added to the hydraulic components of the PTO to provide a more accurate representation of the overall device. With hydraulic losses included the action of the WEC and PTO remains generally the same. There is a small reduction in captured power and, as expected, a larger reduction in generated power with the hydraulic motor being the biggest source of power loss. The PTO efficiency was found to show only a slight decrease with wave height but this will be investigated further.

CHAPTER 4

MAXIMISING POWER GENERATION IN REGULAR WAVES

This chapter investigates the methods used to tune the overall device by altering specific parameters of the PTO. Initially, the tuning of a linear PTO is investigated by analysing the system in the frequency domain and adjusting the viscous damping coefficient. Comparisons are then made to a hydraulic PTO and ways to tune the WEC are investigated, initially with an idealised hydraulic PTO and then with a hydraulic PTO including losses. The gains in power generation are presented and possible control methods discussed.

4.1 Linear PTO Tuning

First consider a linear PTO, which consists of a viscous damper, as explained in Section 3.2. The frequency domain expressions derived previously in Section 3.2 can be used to theoretically determine the criteria for maximum power capture. Consider the wave excitation force to buoy displacement transfer function:

$$\frac{X(s)}{F_e(s)} = \frac{1}{(m+A)s^2 + (B+C)s + (\rho g S)} \tag{4.1}$$

Transforming into the frequency domain:

$$X(j\omega) = \frac{F_e(j\omega)}{-\omega^2(m+A) + j\omega(B+C) + \rho g S} \tag{4.2}$$

Equation 4.2 can be re-written in terms of velocity, U, to give

$$U(j\omega) = \frac{F_e(j\omega)}{j\omega(m+A) + (B+C) + \frac{\rho g S}{j\omega}} \tag{4.3}$$

The time averaged power captured by the PTO ($\bar{P_{cap}}$) is given by

$$\bar{P_{cap}} = \frac{1}{2} C |U(j\omega)|^2 \tag{4.4}$$

Substituting for $U(j\omega)$ using equation 4.3

$$\bar{P_{cap}} = \frac{\frac{C}{2}|F_e(\omega)|^2}{(B+C)^2 + \left(\omega(m+A) - \frac{\rho g S}{\omega}\right)^2} \tag{4.5}$$

There is an optimum condition to maximise $\bar{P_{cap}}$, which can be found from equation 4.5. The optimum PTO damping rate (C_{opt}) can be obtained from $\frac{\partial \bar{P}}{\partial C} = 0$. This gives

$$C_{opt} = \sqrt{\left(B^2 + \left(\omega(m+A) - \frac{\rho g S}{\omega}\right)^2\right)} \tag{4.6}$$

Considering a wave period range of 8 - 14 s, as most ocean waves are in this range, Figure 4-1 shows that C_{opt} varies approximately linearly with the wave period (T) in this range. Equation 4.6 indicates that C_{opt} is independent of wave height meaning that a PTO of this type could be tuned to an incoming wave by knowledge of only the wave frequency.

There is also an optimum buoy velocity amplitude (U_{opt}) to maximise $\bar{P_{cap}}$ which is obtained by re-arranging equations 3.25 and 4.3 and using C_{opt} (equation 4.6). This gives

$$U_{opt} = \frac{\Gamma(\omega)\frac{H}{2}}{\sqrt{(C_{opt}+B)^2 + \left(\omega(m+A) - \frac{\rho g S}{\omega}\right)^2}} \tag{4.7}$$

Figure 4-1 shows that the relationship between U_{opt} and T is non-linear but equation 4.7 indicates that there is a linear relationship between U_{opt} and H.

The force produced by the PTO is a product of the damping rate and the buoy velocity, so the optimum PTO force amplitude (Φ_{opt}) is:

$$\Phi_{opt} = C_{opt} U_{opt} \tag{4.8}$$

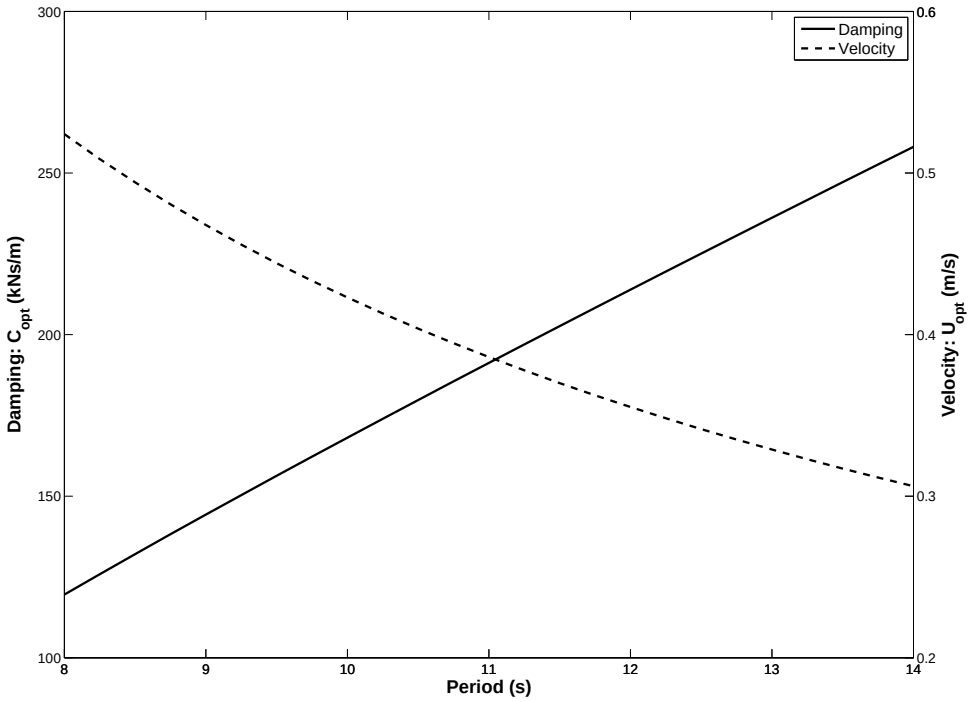

Figure 4-1: *Optimum damping coefficient and buoy velocity amplitude vs wave period for* $H = 2\,m$

Furthermore, the maximum average power captured ($\bar{P}_{max}$) can be found by combining equations 4.6 and 4.5 to give

$$\bar{P}_{max} = \frac{|F_e(\omega)|^2}{4\sqrt{B + \left(B^2 + \left(\omega(m+A) - \frac{(\rho g S)}{\omega}\right)^2\right)}} = \frac{\left(\Gamma(\omega)\frac{H}{2}\right)^2}{4(B + C_{opt})} \tag{4.9}$$

Figure 4-2 reveals that, as expected, Φ_{opt} does not vary linearly with T. However,

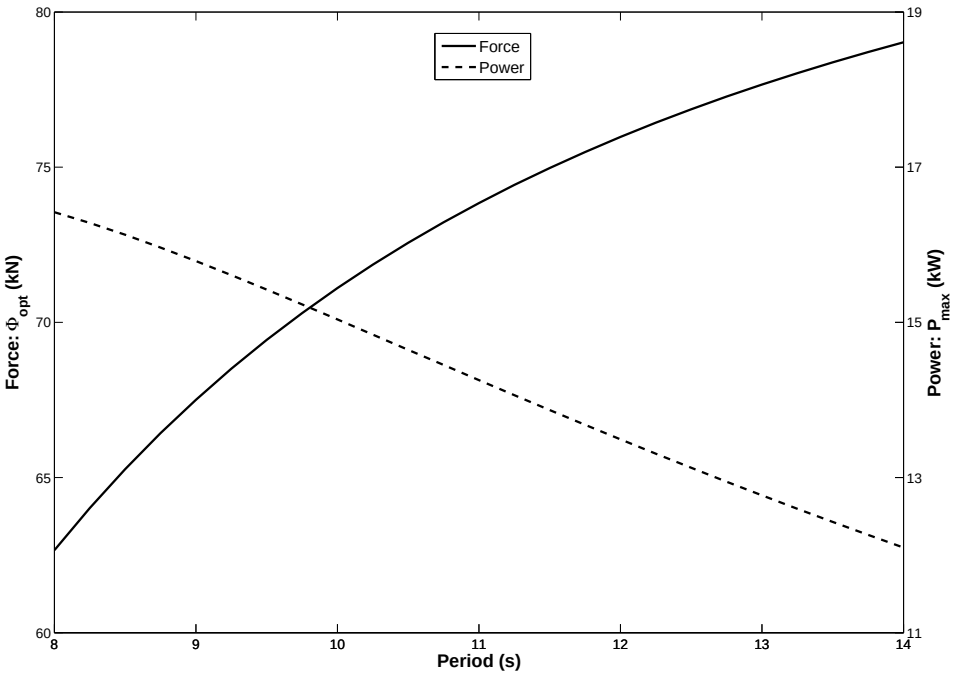

Figure 4-2: *Optimum PTO force amplitude and maximum power generated vs wave period for $H = 2\,m$*

as U_{opt} is in proportion to wave height, Φ_{opt} is also in proportion to wave height. Figure 4-2 also reveals that $\bar{P}_{max}$ reduces with T in an approximately linear manner due to the reduced U_{opt} at larger wave periods. Equation 4.9 states that $\bar{P}_{max}$ is in proportion to the square of the wave height, indicating the greater importance of wave height over frequency in terms of power generation. The values presented in Figures 4-1 and 4-2 are for a wave height of 2 m.

4.2 Idealised Hydraulic PTO Tuning

The frequency domain analysis has proven that if a PTO behaves like a linear viscous damper an optimum damping condition to maximise power capture can be derived, which depends on wave frequency but not height. Furthermore, this damping condition corresponds to an optimum force amplitude that the PTO produces. Subsequently, even though it is evident that a hydraulic PTO does not capture energy in the same manner as a linear PTO (Section 3.3), it is still reasonable to assume that a similar optimum condition to maximise power capture might be found by altering the PTO damping. Varying the PTO damping will alter the pressure in the accumulators, hence changing the force experienced by the actuator and therefore adjusting the power captured by the WEC.

Referring the generator characteristic to the piston, the following PTO damping term (α) can be formulated with the same units as a viscous damper:

$$\alpha = \left(\frac{A_p}{D_m}\right)^2 C_g \tag{4.10}$$

Equation 4.10 indicates that to change α any of the three components can be varied in size; the piston area (A_p), the motor displacement (D_m) or the damping coefficient of the generator (C_g).

A_p can not be constantly varying but it is possible to include multiple actuators of different areas to effectively adjust the cylinder area on which the system pressure acts by switching between different combinations of actuators. For example, Schlemmer et al. [62] investigate using multiple pump modules with variable cylinder areas in order to achieve force control. Babarit et al. [57] also indicate that force control could be achieved by using several hydraulic cylinders or by using multiple accumulators of different pressure levels. This force control strategy is an attempt to mimic the continuous sinusoidal force that a viscous damper would produce with multiple discrete control levels achieved by quick switching between a combination of different actuators or accumulators. Ricci et al. [60] show that generator torque can be varied to optimise PTO performance in regular waves.

4.2.1 Results

When regular monochromatic waves are used as the input to the system, a pseudo steady state condition is reached where the angular velocity and torque produced

by the motor oscillates about an average value, as shown in Figure 3-11. The amplitude of this oscillation is dependent on the size of the accumulators but in this work only the average value will be presented. To determine if the generated power (P_{gen}) can be maximised by varying any of the three components in equation 4.10, simulations were run with a regular monochromatic wave of $H = 2\,\mathrm{m}$ and $T = 10\,\mathrm{s}$. Each of the three components were varied independently, to give the same values of α, to show the effect on P_{gen} in Figure 4-3.

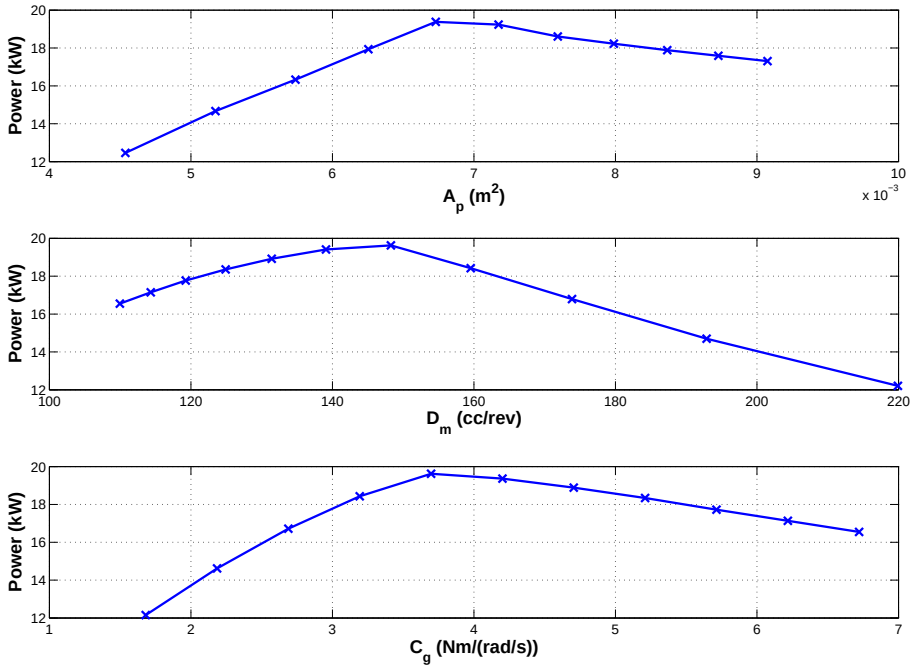

Figure 4-3: *Power generated vs Top: piston area, Middle: motor displacement and Bottom: generator damping, for $H = 2\,m$ and $T = 10\,s$*

Figure 4-4 reveals that P_{gen} can be maximised by varying α. If α is too high the WEC is over damped and remains stationary for too long. Likewise, if α is too small the WEC is under damped and the motion is not resisted enough. Furthermore, Figure 4-4 indicates that there is no difference, in terms of P_{gen}, between varying D_m or C_g. Varying A_p gives a negligible difference in the magnitude of P_{gen} compared to varying the other two components.

Therefore, in terms of P_{gen}, it does not matter which of the three components is varied. Figure 4-4 also shows the optimum value of α for this wave condition. This suggests that the PTO can be tuned by varying any of the three components to alter α. However, for the purpose of this work only D_m will be varied at this

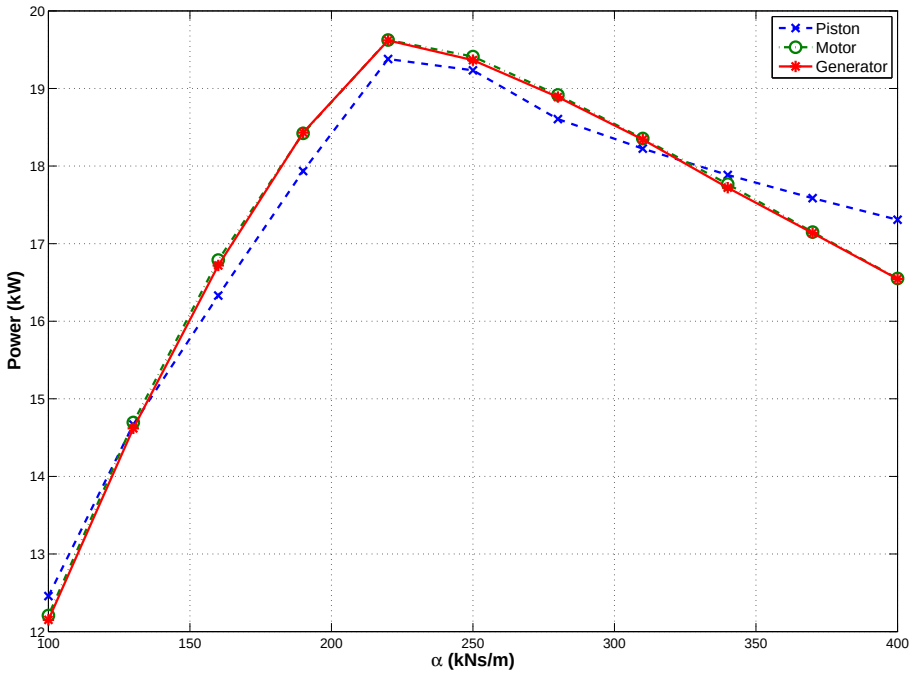

Figure 4-4: *Power generated vs PTO damping for the three components for $H = 2\,m$ and $T = 10\,s$*

stage because in practice it is the easiest of the three components to vary. This means that the variation of D_m is being expressed in the form of α.

4.2.2 Variable Wave Properties

To determine if the optimal value of PTO damping (α_{opt}) differs with T, simulations were run with $H = 2\,\text{m}$ for 4 different wave periods. Assuming $A_p = 0.007\,\text{m}^2$ and a minimum value of $\alpha = 100\,\text{kNs/m}$ corresponding to $D_m = 180.3\,\text{cc/rev}$, this gives $C_g = 1.75\,\text{Nm/(rad/s)}$. These parameters are used to produce the following results.

Figure 4-5 reveals that α_{opt} increases with T and furthermore, P_{gen} reduces as T increases in this range. These are the same trends as for a linear PTO and the results found for a hydraulic PTO in [42].

The power of the incident wave is proportional to the square of the wave height [11] so if the system is fully linear, this relationship will also hold true for P_{gen}. Simulations were run to for $T = 10\,\text{s}$ with 3 different wave amplitudes to produce Figure 4-6. It clearly shows that P_{gen} normalised by the square of the wave

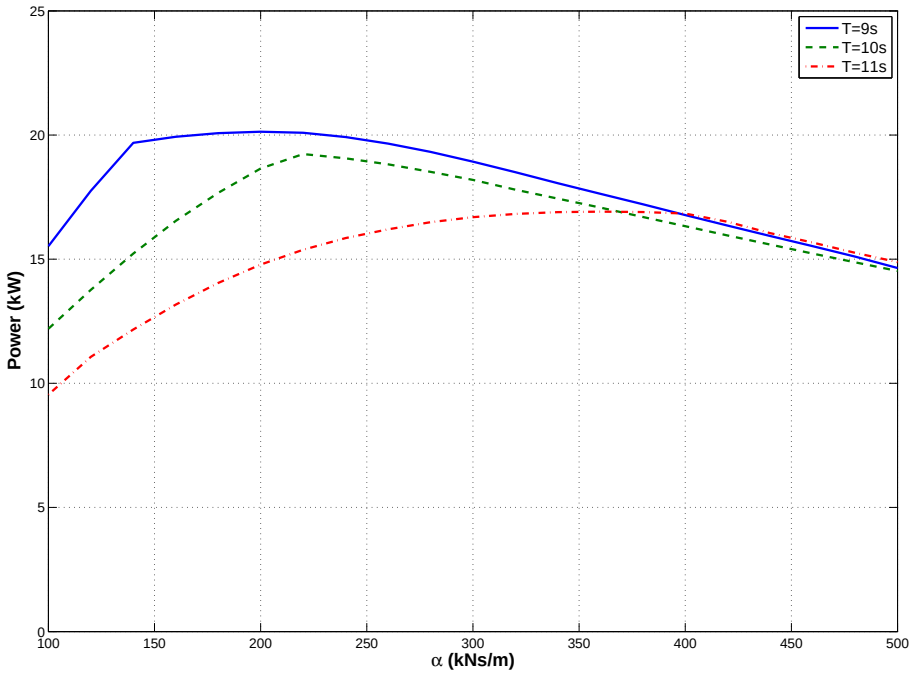

Figure 4-5: *Power generated vs PTO damping for varying wave periods for $H = 2\,m$*

amplitude reduces at larger wave heights, which indicates that, as expected, the system is non-linear. However, in terms of tuning, Figure 4-6 reveals a minimal variation in α_{opt} with wave height.

The two trends revealed in Figures 4-5 and 4-6 are that α_{opt} is highly dependent on T but shows negligible variation with wave height. These are the same trends as found by Falcão [42] and Ricci [60] and it follows the theory for a linear PTO. However, it remains to be seen if the values of optimum damping are the same for the two PTO models. Determining if C_{opt} and α_{opt} differ will reveal if the theory to tune a linear PTO can be applied with confidence to a hydraulic PTO.

Figures 4-7 to 4-9 present the values of α_{opt}, P_{gen} and Φ_{opt}, for a wave period range of 8 - 14 s, for the idealised hydraulic PTO and linear PTO models. These results were produced using an optimisation algorithm at each wave period. Figure 4-7 shows that C_{opt} and the trend for α_{opt} both show a linear relationship to T but the magnitude of the values is markedly different, which demonstrates the difference between the two PTO models.

Figure 4-8 indicates that P_{gen}, for the idealised hydraulic PTO, reduces with T but it is higher, for the majority of this wave period range at this wave height,

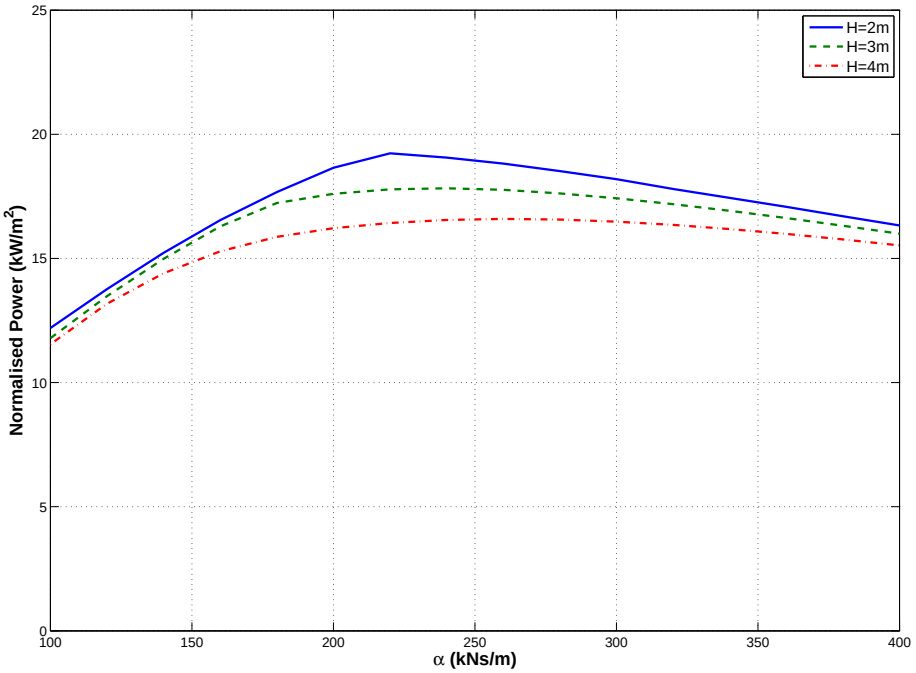

Figure 4-6: *Power generated vs PTO damping for varying wave heights at* $T = 10\,s$

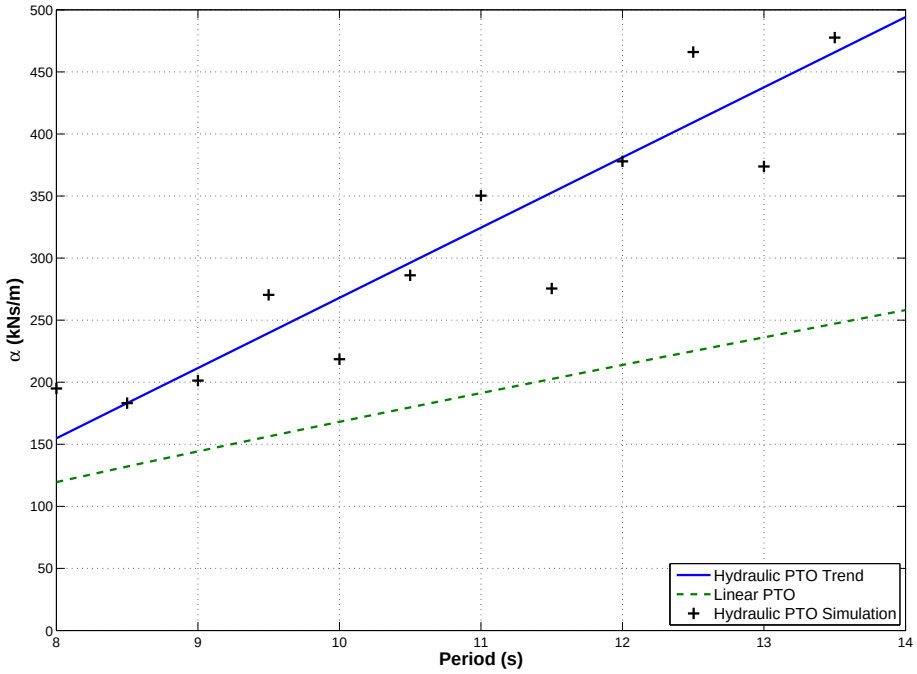

Figure 4-7: *Optimum PTO damping vs wave period for* $H = 2\,m$

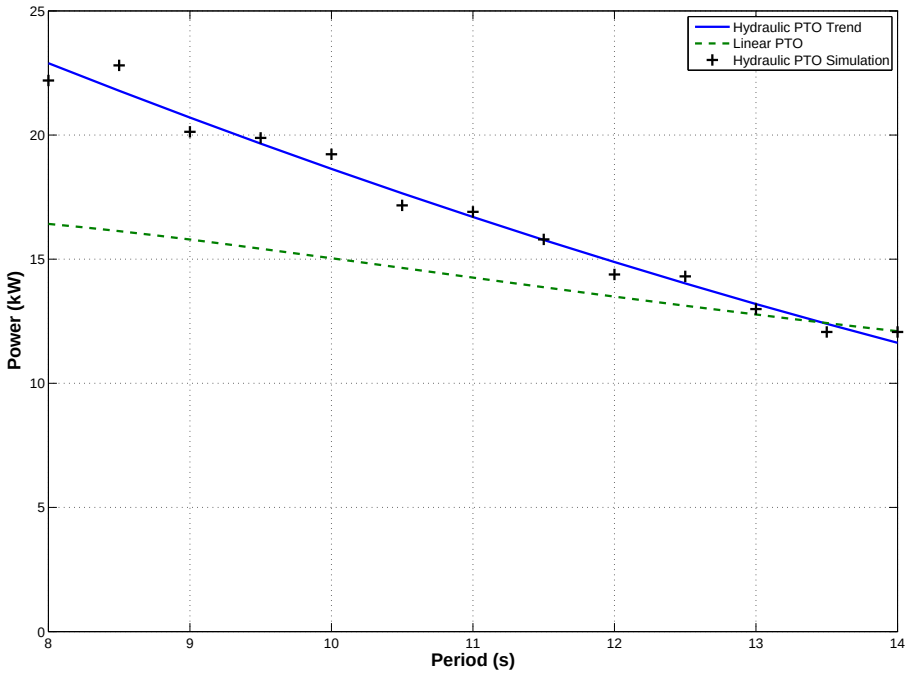

Figure 4-8: *Maximum power generated vs wave period for $H = 2\,m$*

compared to the linear PTO. This is encouraging as it could be assumed that an optimal linear PTO would give a larger P_{gen} over the full range of wave conditions. Furthermore, it suggests that the force control strategy to mimic the behaviour of a viscous damper is sub-optimal. These results contradict Falcão [42], who stated that a highly non-linear PTO could not attain the same power levels as an optimally controlled linear one. However, the results support Josset [30] who showed that a realistic PTO model can be adapted to produce power levels which sometimes exceed the performance of a linear PTO.

The additional P_{gen}, compared to the linear PTO, decreases as T increases. As T increases the wave excitation force increases, which causes a pressure increase in the accumulator 'A'. This, in turn, increases the PTO force and means that the WEC stalls for longer at its endpoints so the piston displacement and velocity is reduced. This causes a lower flow from the piston over one cycle and therefore a reduction in P_{gen} is observed.

The final comparison to consider is optimum PTO force amplitude (Φ_{opt}). Figure 4-9 reveals that the trend of Φ_{opt} for the idealised hydraulic PTO shows a strong correlation to the values derived for a linear PTO over this range of wave periods. This implies that Φ_{opt} may be constant and it is irrespective of the type

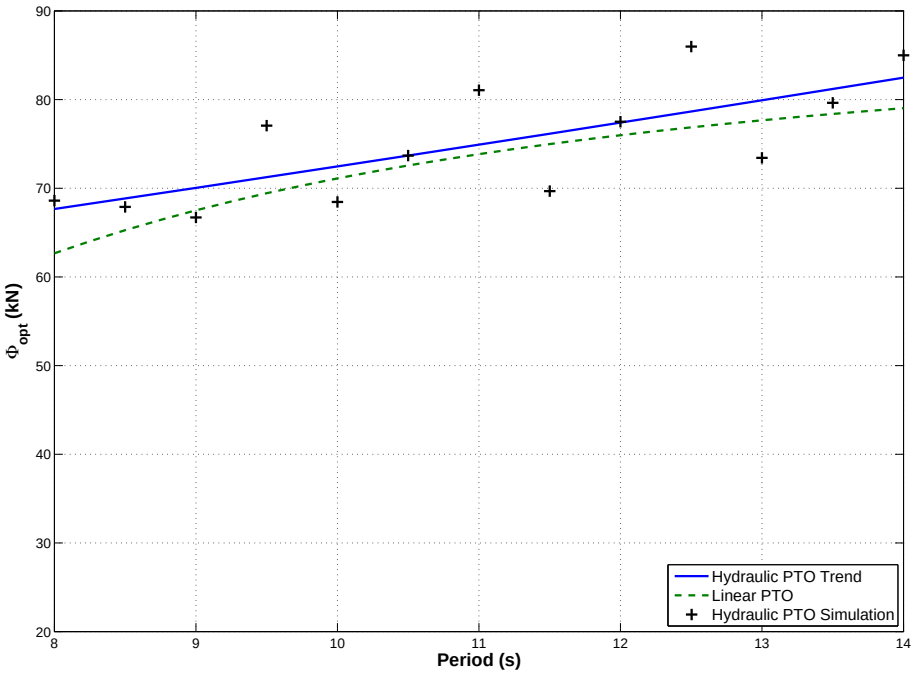

Figure 4-9: *Optimum PTO force amplitude vs wave period for $H = 2\,m$*

of PTO employed.

4.3 Hydraulic PTO With Losses Tuning

Previously it has been demonstrated that the behaviour of a hydraulic PTO containing losses is very similar to the behaviour of an idealised hydraulic PTO (Section 3.4). It is therefore logical to determine if both models can be tuned in the same manner. Simulations were run for the same wave conditions with D_m again being varied to alter α to compare all three PTO models; linear PTO, idealised hydraulic PTO and hydraulic PTO with losses.

Figure 4-10 indicates that the hydraulic PTO with losses can also be tuned by varying α. When compared to Figure 4-5, for the idealised hydraulic PTO, the maximum P_{gen} has reduced as expected but α_{opt} has remained approximately the same for each T. The power gains from using α_{opt} are appreciable. For example, if α is double the optimal value, P_{gen} is reduced by approximately 20% for each T. This emphasises the importance of using the correct D_m as a small discrepancy in D_m is squared in terms of α and this results in an appreciable reduction in P_{gen}.

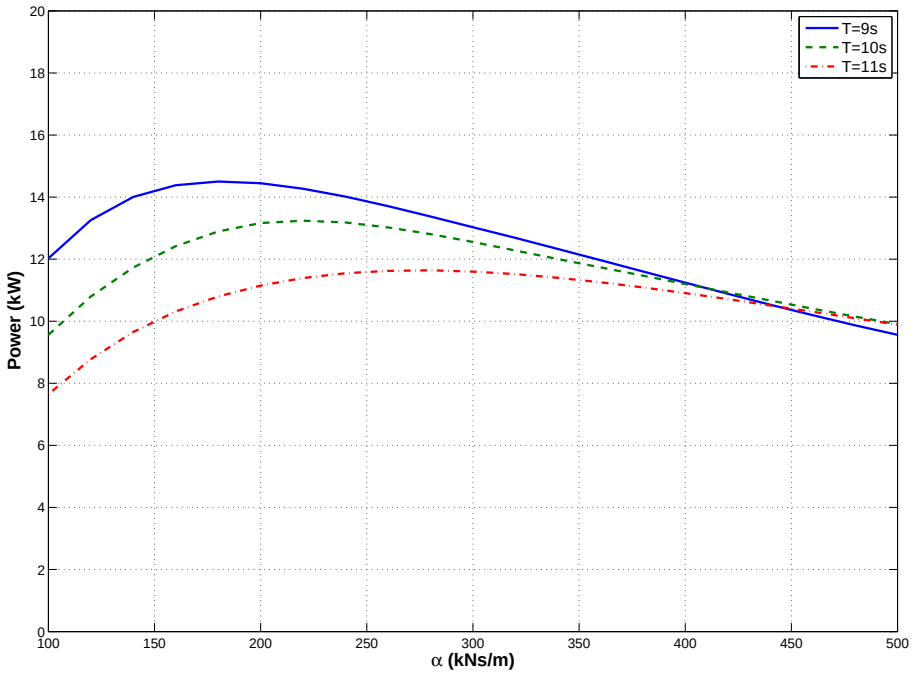

Figure 4-10: *PTO with losses: Power generated vs PTO damping for varying wave periods for $H = 2\,m$*

Figure 4-11 represents the equivalent result to Figure 4-6. As for the idealised hydraulic PTO, the normalised captured power (P_{cap}) reduces with wave height indicating a reduced power capture efficiency (η_{cap}). The normalised P_{cap} is marginally lower for the PTO model with losses indicating that the losses have a slight effect on the overall behaviour of the device. As expected, there is also a significant drop between the normalised P_{cap} and P_{gen} due to the PTO losses. In relation to tuning, Figure 4-11 reveals that α_{opt} has only a negligible difference whether optimising for P_{cap} or P_{gen} so α_{opt} corresponds to the maximum η_{cap}. Like previously, α_{opt} does not vary with wave height and the values of α_{opt} are similar to Figure 4-6. It is interesting to note from Figure 4-11 that PTO efficiency (η_{pto}) is relatively constant for all wave heights and values of α.

Figures 4-12 to 4-14 compare the values of α_{opt}, P_{gen} and Φ_{opt} for the three PTO models. Figure 4-12 reveals a linear trend between α_{opt} and T for the PTO with losses but the values have reduced significantly compared to the idealised PTO. This result indicates the importance of including accurate loss models to represent the hydraulic PTO because even though both models seem to behave in a similar manner (Section 3.4.2), it can be seen that they are optimised by

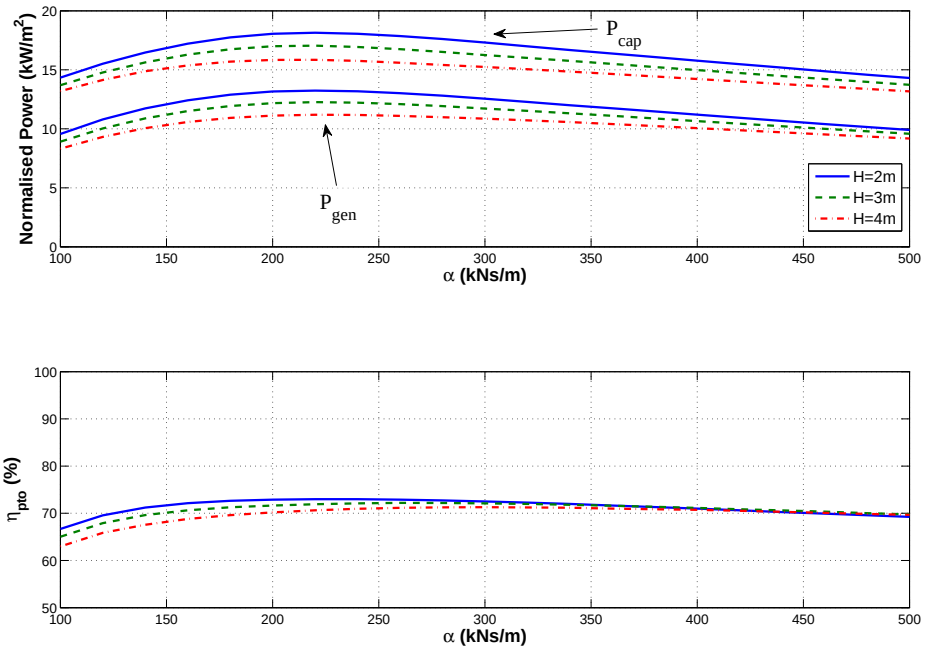

Figure 4-11: *PTO with losses. Top: Normalised power generated and power captured vs PTO damping. Bottom: PTO efficiency vs PTO damping for varying wave heights at $T = 10\,s$*

different values of α for the same wave conditions.

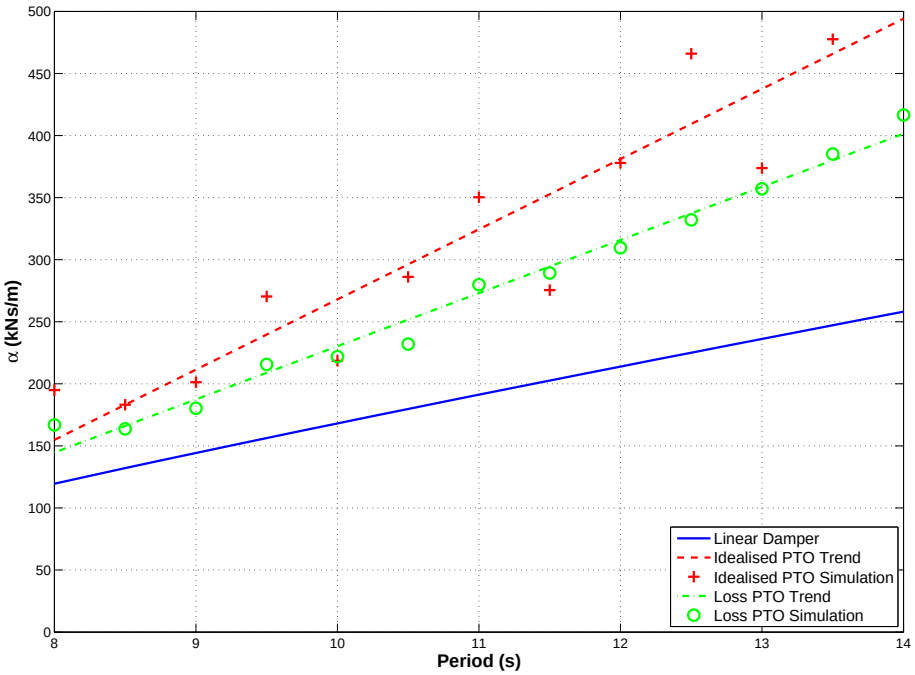

Figure 4-12: *Optimum PTO damping vs wave period for $H = 2\,m$*

One of the main reasons to include losses in the PTO model is to discover the reduction in P_{gen}. Figure 4-13 shows that, in this range of wave periods, P_{gen} reduces significantly with T for the PTO with losses. This is a similar linear trend to the idealised PTO with both models having a greater reduction in power than for the linear PTO. It is noted that the PTO with losses shows a lower maximum P_{gen} than the linear PTO over the full range of wave periods for this wave height. The maximum values of P_{cap} are comparable to the idealised PTO model so the PTO is still capturing more power than the linear PTO model with the reduction in P_{gen} only due to the losses included.

For this wave height, $\eta_{pto} = 70\text{-}73\%$ for the optimal case. As T increases, there is an increase in α_{opt}, which corresponds to a decrease in part motor displacement (x_m) and an overall reduction in motor efficiency (η_m) (Section 3.4.1). However, as T increases there is a reduction in piston velocity that corresponds to a lower flow and motor speed, which increases η_m. Therefore, these two conditions combine to maintain a relatively constant η_{pto}.

Results have revealed that α_{opt} is different for the three PTO models. However, Figure 4-14 indicates that Φ_{opt} remains similar. The only difference is that

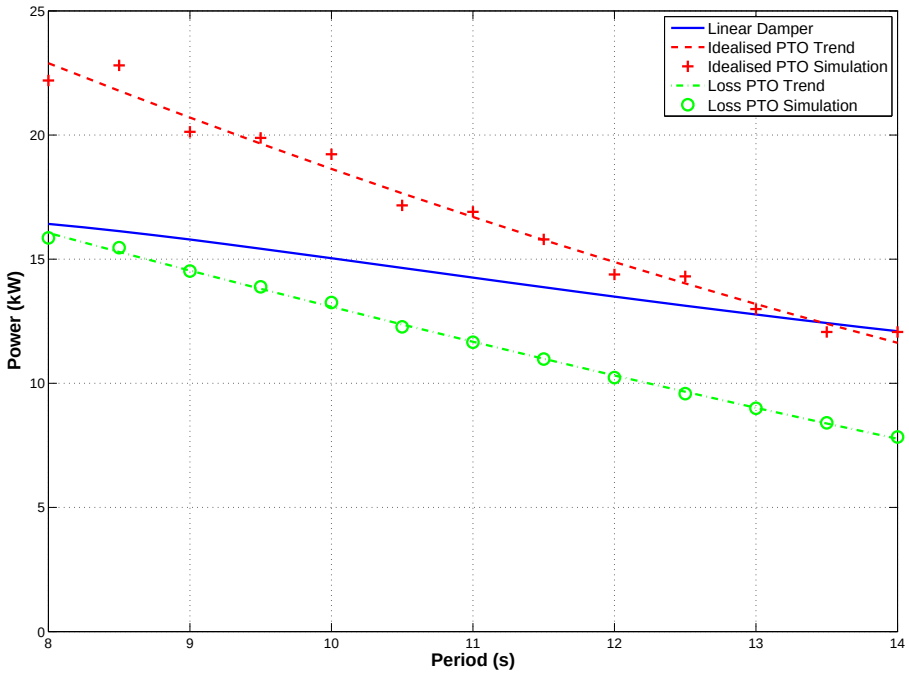

Figure 4-13: *Maximum power generated vs wave period for $H = 2\,m$*

the PTO with losses does not show the same increase in Φ_{opt} with T as the other two models. This result reiterates that, irrespective of how the PTO behaves, there is an optimum PTO force amplitude that the PTO must produce to maximise P_{gen}, which is dependent on wave conditions.

The results indicate the the PTO with losses can be tuned in the same manner as an idealised hydraulic PTO but it requires different values of α to produce a similar Φ_{opt} and maximum P_{cap}. Furthermore, the results suggest that a force control strategy device could be introducing to maximise power generation with the desired PTO force, calculated from the theory for a linear PTO, achieved by varying the motor displacement to alter the PTO damping.

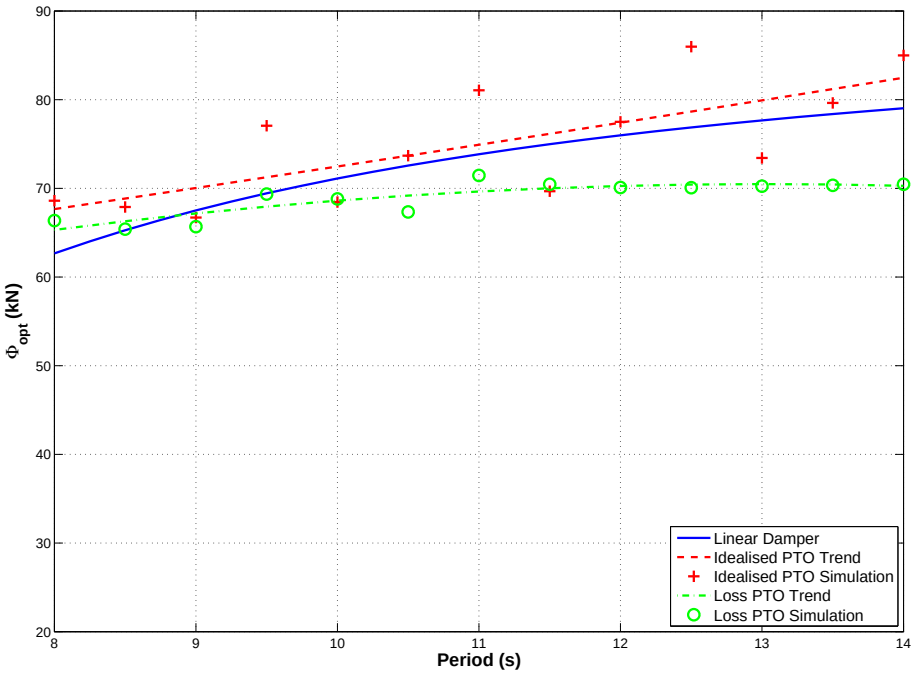

Figure 4-14: *Optimum PTO force amplitude vs wave period for* $H = 2\,m$

4.4 Concluding Remarks

This chapter investigated the ways to maximise power capture and generation in the different PTO models in regular waves. Firstly, a linear PTO was analysed in the frequency domain to determine its optimal parameters. Values of optimal damping, PTO force amplitude and maximum power capture were obtained theoretically and it was shown that a linear PTO could be tuned with knowledge of only the wave frequency.

A damping term for the hydraulic PTO was derived from the relationship between the piston area, motor displacement and generator damping so a hydraulic PTO model could be compared to the linear PTO model. It is not important which of the three components is varied as the overall device behaves the same if this PTO damping remains constant. Results confirm that power generation can be maximised by varying the PTO damping and that optimal values for both the idealised and loss model are approximately linearly dependent on wave period but not dependent on wave height. However, the optimal values for all three models are significantly different, indicating the importance of an accurate hydraulic PTO model in tuning the overall device.

For all three cases there is a reduction in power generation with wave period. For the idealised hydraulic PTO, power generation is higher in comparison to the linear PTO which is evidence of the power gain from the induced stall of the WEC caused by the Coulomb type resisting force of the hydraulic PTO. The power generation from the loss PTO is lower, as expected, but results give an accurate prediction of the power levels which a device of this nature could produce.

Even though all three PTO models are shown to be optimally tuned by different values of damping the optimum PTO force amplitude for all three show a closer correlation. This indicates that any PTO, irrespective of its behaviour, must produce a specific force amplitude to maximise power capture and generation. Consequently, a force control strategy could be implemented in a device of this nature with the theoretical force calculated from knowledge of the incoming wave period and height.

For the remainder of the work only the model of the hydraulic PTO with losses will be used as it provides more accurate results in terms of optimal damping and power generation and it will provide more realistic results when investigating irregular wave inputs and different control strategies.

CHAPTER 5

MAXIMISING POWER GENERATION IN IRREGULAR WAVES

Real seas are not regular, so it is imperative to predict how WECs will behave in irregular, non monochromatic wave conditions. Performing simulations using an irregular wave input will help to predict realistic levels of power generation and how the PTO will operate in real sea conditions. It will also indicate whether the tuning trends found for regular waves remain valid in realistic sea conditions. Work is also presented on a motor speed control strategy to maintain the maximum flow of electrical power to the grid, assuming the use a doubly fed induction generator (DFIG). Finally, the sizing of key components in the PTO is considered in an attempt to maximise PTO efficiency and generated power.

5.1 Wave Spectra and Irregular Wave Profiles

Sea waves are random in nature but they can be analysed by assuming they consist of an infinite number of waves with different frequencies and directions. Wave spectra are created by decomposing an irregular wave profile into a number of component sinusoidal waves. The distribution of energy of these wavelets can be plotted against frequency to give the frequency spectrum [73]. These spectra are used to represent and compare different sea states.

The characteristics of the frequency spectra of sea waves is now well established and formulae have been developed by researchers such as Bretschneider, Pierson-Moskowitz, Hasselmann and Mitsuyasu, to produce spectra [73]. Wave

spectra formulae are mainly defined by two quantities, the peak wave period (T_p) and the significant wave height (H_s). The significant wave height is the average of the wave heights of the third largest waves and the peak period is the wave period corresponding to the most energetic waves in the spectrum. There is also a JONSWAP spectrum which is based on wave data from the North Sea that includes a value to control the sharpness of the spectral peak because the North Sea does not represent a fully developed wind wave [74].

These spectra can be used to produce irregular wave profiles. Defining the significant wave height and peak period enables a spectrum to be created using a chosen formula. In this work the Pierson-Moskowitz spectrum will be used (equation 5.1) [75]. From the spectrum a finite number of sinusoidal waves can be created. Each individual wave component is created, using equation 5.2, with its own amplitude and frequency characterised by the spectrum. Each sinusoidal wave is assigned with a random phase and the time series is generated as a sum of the individual components using equation 5.3.

$$S_n(\omega) = 5\pi^4 \frac{H_s^2}{T_p^4} \frac{1}{\omega^5} exp\left[-\frac{20\pi^4}{T_p^4}\frac{1}{\omega^4}\right] \tag{5.1}$$

$$\eta_i(t) = \sqrt{2S_n(\omega_i)\Delta\omega}\sin(\omega_i t) \tag{5.2}$$

$$\eta(t) = \sum_{i=1}^{n} \sqrt{2S_n(\omega_i)\Delta\omega}\sin(\omega_i t + \varphi_{rand,i}) \tag{5.3}$$

ω_i is the frequency, $\varphi_{rand,i}$ is the random phase component of each wave and $\Delta\omega$ is the frequency band calculated from:

$$\Delta\omega = \frac{\omega_{max}}{n} \tag{5.4}$$

where ω_{max} is the maximum frequency of the spectrum and n is the number of wave components. ω_{max}= 8π and n= 1280 will be used in the following work.

Assuming linear wave theory means that the excitation force is generated as a sum of the individual excitation wave force components. The excitation force of each component is calculated using the wave amplitude and the excitation wave force coefficient ($\Gamma(\omega_i)$) for each frequency, (equation 3.14), such that

$$f_{e_i}(t) = \Gamma(\omega_i)\sqrt{2S_n(\omega_i)\Delta\omega}\sin(\omega_i t) \tag{5.5}$$

and

$$f_e(t) = \sum_{i=1}^{n} \Gamma(\omega_i)\sqrt{2S_n(\omega_i)\Delta\omega}\sin(\omega_i t + \varphi_{rand,i}) \tag{5.6}$$

Figure 5-1 presents an example of a Pierson-Moskowitz spectrum and the corresponding wave elevation and force profile that is generated for $H_s = 3\,\mathrm{m}$ and $T_p = 10\,\mathrm{s}$.

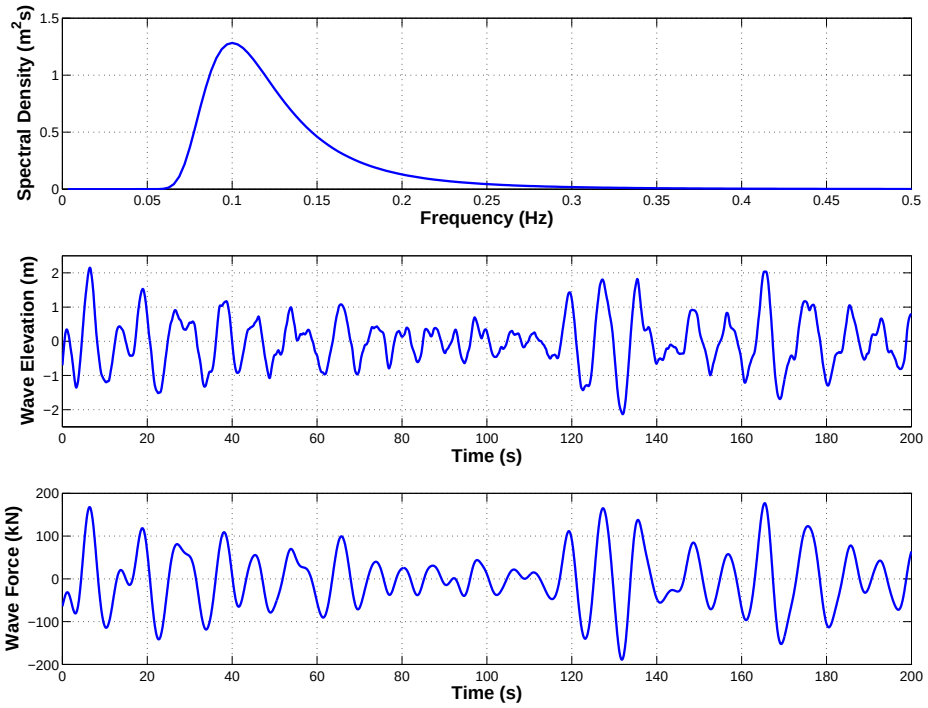

Figure 5-1: *Top: Pierson Moskowitz Spectrum for $H_s = 3\,m$ and $T_p = 10\,s$, Middle: Wave surface elevation, Bottom: Wave Force*

This is the random-phase method that has been used in previous work to represent irregular waves with good approximation [43]. There is another method which uses filtered white noise to represent a random sea profile. The filter is designed according to a specific spectrum as described in [76]. There is also the capability of using data collected from test sites, which will be investigated in Chapter 6. At this stage the random phase method will be used.

5.2 WEC Behaviour

Initially, it is beneficial to get an understanding of how the WEC and PTO will behave in a random sea. Using the wave profile from Figure 5-1, the simulation model was run for 200 s with full motor displacement to produce Figures 5-2 and 5-3.

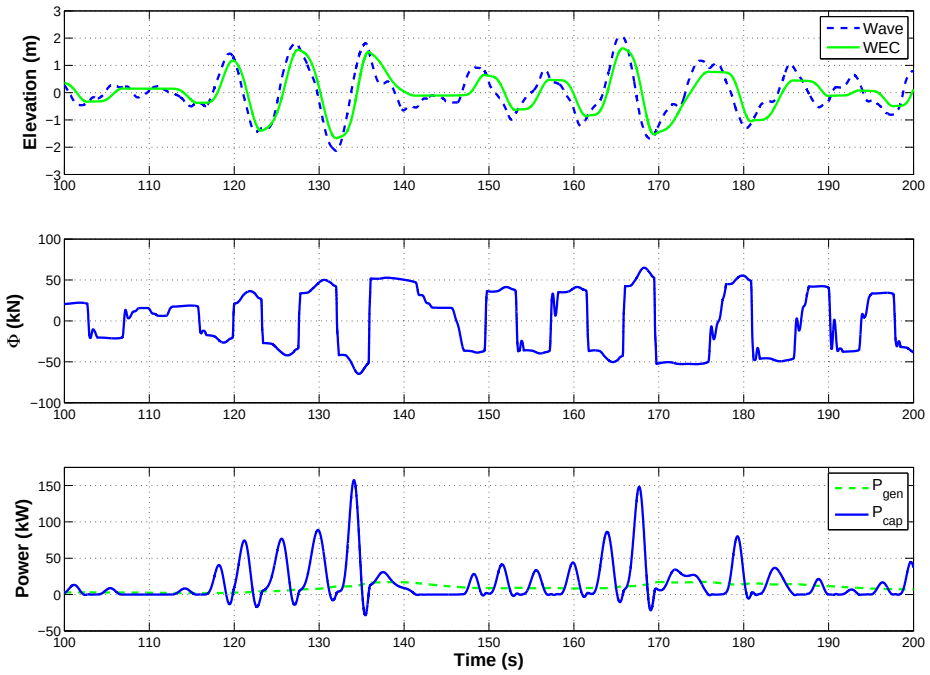

Figure 5-2: *Top: Wave and WEC displacement. Middle: PTO force. Bottom: Power captured and generated. (H_s=3 m and T_p=10 s)*

The first noticeable characteristic is that the induced body stall is more pronounced (e.g. 140 - 147 s). The WEC remains stationary during periods of small incident waves because the wave excitation force is less than the force produced by the PTO. Furthermore, a number of consecutive large incident waves causes large WEC displacements, which increases system pressure and PTO force (e.g. 115 - 135 s). This emphasises the stall as upcoming waves, which may have been large enough to overcome the PTO force before are not large enough now. The PTO force still exhibits a square wave form but its magnitude is variable due to the constantly varying system pressure. Also, the frequency of the square wave is variable as the duration of the body stall is constantly changing.

The power smoothing effect of the accumulators is exhibited with the com-

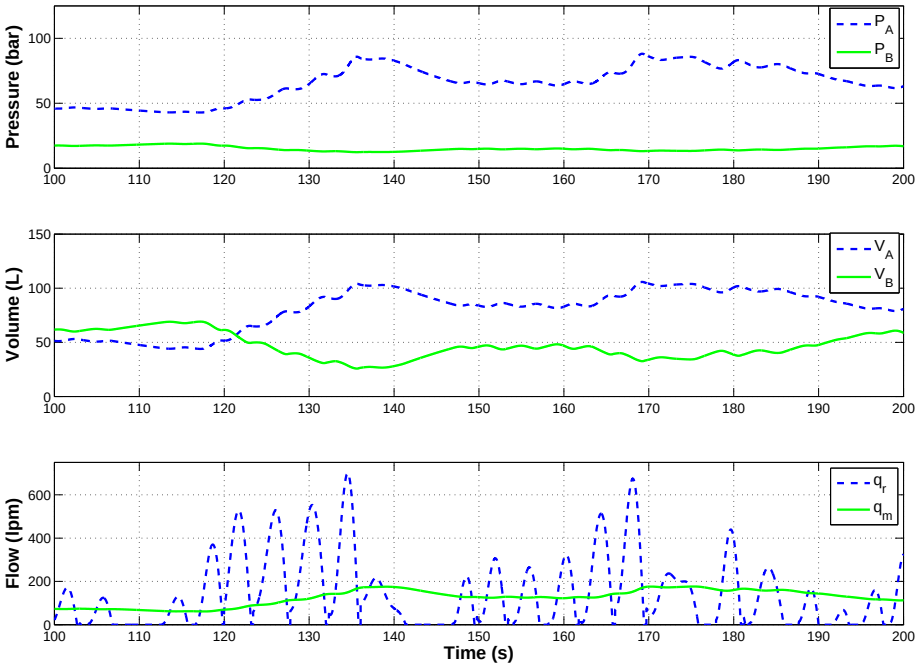

Figure 5-3: *Top: High and Low Pressure line. Middle: Accumulator Volume. Bottom: Flow from rectifier and flow to motor. (H_s=3 m and T_p=10 s)*

parisons between P_{cap} and P_{gen} and the rectified flow (q_r) and the flow to the motor (q_m). P_{cap} has a maximum value of approximately 150 kW compared to 18 kW for P_{gen} which reinforces the importance of power smoothing in detaching the power capture element of the PTO from the power generating element. It means that the hydraulic motor can be sized accordingly to be more efficient.

Although the accumulators are very large (200 L), the pseudo-steady state which is reached with regular waves does not exist in irregular waves. Therefore, it is necessary to examine the energy storage in the accumulators. The constantly varying pressure and volumes in both accumulators are dependent on the incoming wave conditions. P_A and V_A increase from the initial values of 41 bar and 40 L respectively. There is also an increase in V_B but P_B remains approximately constant at 14 bar, just above the pressure relief valve setting of the boost pump.

This means that some of the power captured by the PTO is stored in the accumulators as hydraulic energy instead of being turned into mechanical power that is generated by the motor. It is necessary to determine the additional hydraulic energy which is stored in the accumulators ($E_{A,B}$) and include this in the total power generated. It is understood that this energy is still subject to the

inefficiencies of the motor but it is assumed that all of this hydraulic energy is transferred into mechanical power. Equations 5.7 - 5.11 show how the energy (E_m) and power (P_m) generated by the motor and the energy stored in the accumulators ($E_{A,B}$) is calculated and used to give P_{gen}. Table 5.1 displays the corresponding values for this simulation.

$$E_A(t) = P_A(t)V_A(t) - P_A(0)V_A(0) \tag{5.7}$$

$$E_B(t) = P_B(t)V_B(t) - P_B(0)V_B(0) \tag{5.8}$$

$$E_m(t) = \int_0^t T_m\omega_m dt \tag{5.9}$$

$$P_m(t) = \frac{1}{t}\int_0^t T_m\omega_m dt \tag{5.10}$$

$$P_{gen} = \frac{E_A + E_B + E_M}{t} \tag{5.11}$$

Component	Energy (kJ)
E_m	1679
E_A	345
E_B	43
	Power (kW)
P_{cap}	14.1
P_m	8.4
P_{gen}	10.3
η_{pto}	73.1%

Table 5.1: *Energy distribution in the PTO and Average Power Values for a 200 s simulation. (H_s=3 m and T_p=10 s)*

Table 5.1 reveals that E_B is negligible and E_A is approximately 20% of E_m, which means that the PTO efficiency value (η_{pto}) is slightly higher than in reality.

The wave profile which is generated from using the random-phase method is periodic over a time frame (Δt) which is dependent on the resolution (minimum frequency (ω_{min})) of the spectrum. Therefore to negate the energy storage in the accumulators affecting η_{pto}, the simulation model is run for a total of 640 s, which equates to two full wave cycles. The second full cycle of data will then be extracted and examined so that $E_{A,B} \approx 0$ and $P_{gen} \approx P_m$, which will produce a

more realistic value of η_{pto}.

$$\Delta t = \frac{1}{\omega_{min}} = \frac{2\pi}{8\pi/1280} = 320\,s \tag{5.12}$$

Although not the case in these simulations, note that in more energetic seas, the system pressure may reach the maximum system pressure of 350 bar. This is more likely when a group of large waves occur in succession. This introduces another inefficiency in the PTO as hydraulic energy is wasted as it passes through the pressure relief valve to tank. However, this is is required for safety purposes and to reduce the risk of component failure. It is expected that this loss will be minimal due to the rare wave conditions which cause these pressures.

5.3 PTO Tuning

To maximise the power generated in irregular waves a similar condition of optimum PTO damping (α_{opt}) might exist as with regular waves. It is expected that α_{opt} will stall the device for an optimum average duration and this value will be dependent on T_p of the incoming waves. It is expected that maximum power levels will be less in irregular waves compared to regular waves of the same energy [59] as the device will only be optimally tuned to the wave frequency corresponding to the highest energy.

It is not known how α_{opt} will vary with H_s. In regular waves α_{opt} shows no variation with wave height, see Figure 4-11. Figure 5-4 indicates that this relationship still holds true for irregular waves. However, there are some noticeable differences between the two figures. With irregular waves there is a negligible reduction in normalised power with H_s, compared to the more marked reduction in regular waves, but the normalised power is approximately 40% of the normalised power in regular waves. As with regular waves, α_{opt} is the same whether optimising for P_{gen} or P_{cap} but the value (175 kNs/m) is lower compared to regular waves (225 kNs/m). However, as with regular waves, η_{pto} remains approximately constant for all values of α.

This result shows that, as with regular waves, the PTO can be tuned according to the wave profile by varying α in order to maximise power generation. The next step is to run simulations through the optimisation algorithm to determine if the values of α_{opt} show a relationship to T_p as in regular waves. Figure 5-5 indicates a linear relationship between T_p and the trend for α_{opt} in irregular waves but there

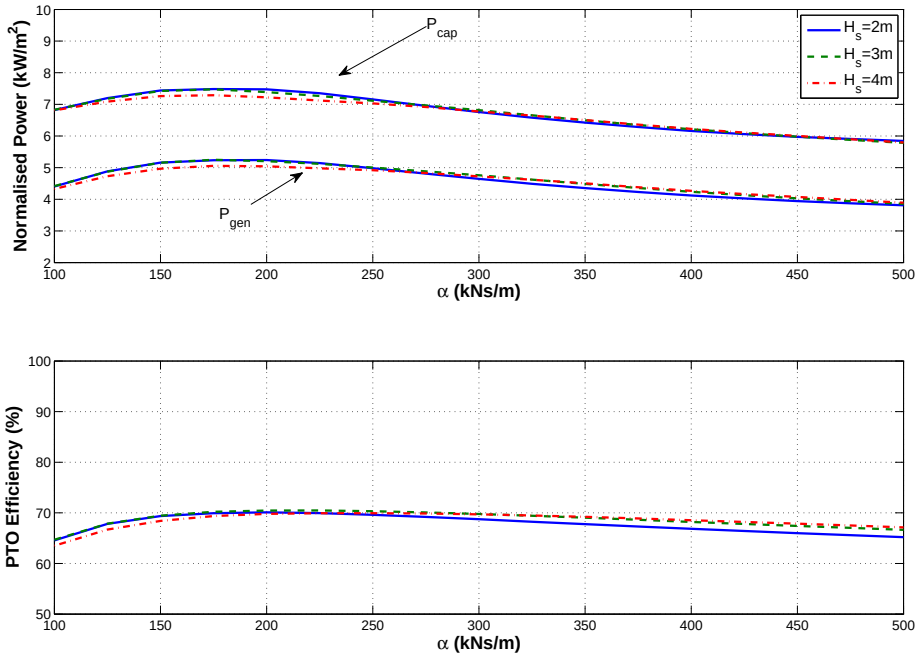

Figure 5-4: *Normalised power and PTO efficiency vs PTO damping for varying significant wave heights and T_p=10 s*

is a larger deviation around this trend line compared to the regular wave results (Figure 4-12), due to the random nature of the waves.

Again there are some clear differences between the two Figures. The magnitude of α_{opt} for the linear PTO has reduced but the gradient is approximately the same as for regular waves. However, for the hydraulic PTO the magnitude of α_{opt} is similar for lower T_p values but the gradient of the line is reduced so the values at higher T_p values are lower in comparison. In general though, there is a marked difference in the results for the two PTO models in the regular and irregular wave conditions.

In terms of power generation, Figure 5-6 reveals that P_{gen} does not reduce as markedly with T_p as in regular waves. Due to the mixture of wave frequencies in each wave profile, there is not the pronounced power reduction as T_p increases. P_{cap} is higher for the hydraulic PTO than for the linear PTO for the majority of T_p values. This again implies that a device should not necessarily try to mimic the behaviour of a linear PTO to maximise power capture. P_{gen} is lower due to the inefficiencies of the PTO but the trend for P_{gen} and P_{cap} is almost identical which indicates a near constant PTO efficiency ($\eta_{pto} \approx 70\%$) for this range of T_p

values at this H_s.

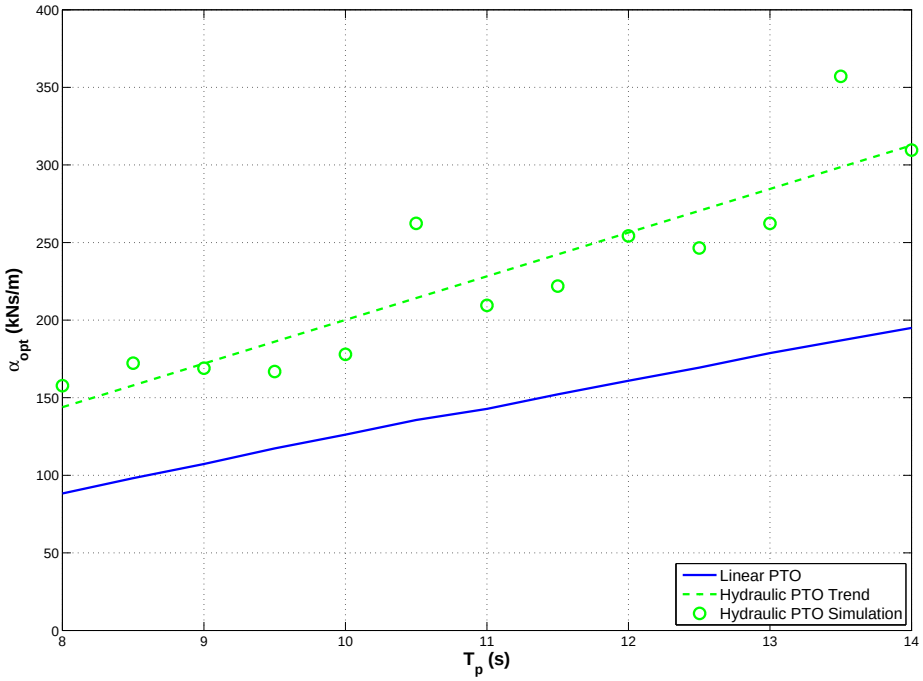

Figure 5-5: *Optimum PTO damping vs peak wave period*

Figure 5-7 compares an optimally tuned hydraulic and linear PTO in the time domain for the same wave profile to determine the similarities between the two PTO models. With the linear PTO, the buoy does not exhibit stall. On the contrary, with the hydraulic PTO, the buoy is stationary for some parts of the wave profile. However, for large motions the displacements of the two models are in phase and of similar magnitude. It is also interesting to note that these large movements cause larger peaks in P_{cap} with the hydraulic PTO, due to the larger value of PTO damping and larger velocity.

5.4 Motor Speed Control

Until now, it has been assumed that all the mechanical power produced by the hydraulic motor is converted into electrical power. No consideration has been given to how the PTO will be connected to the electrical grid and what type of generator will be used in the PTO. Wind turbines face the same challenge of variable speed operation and they generally use a DFIG because they offer variable

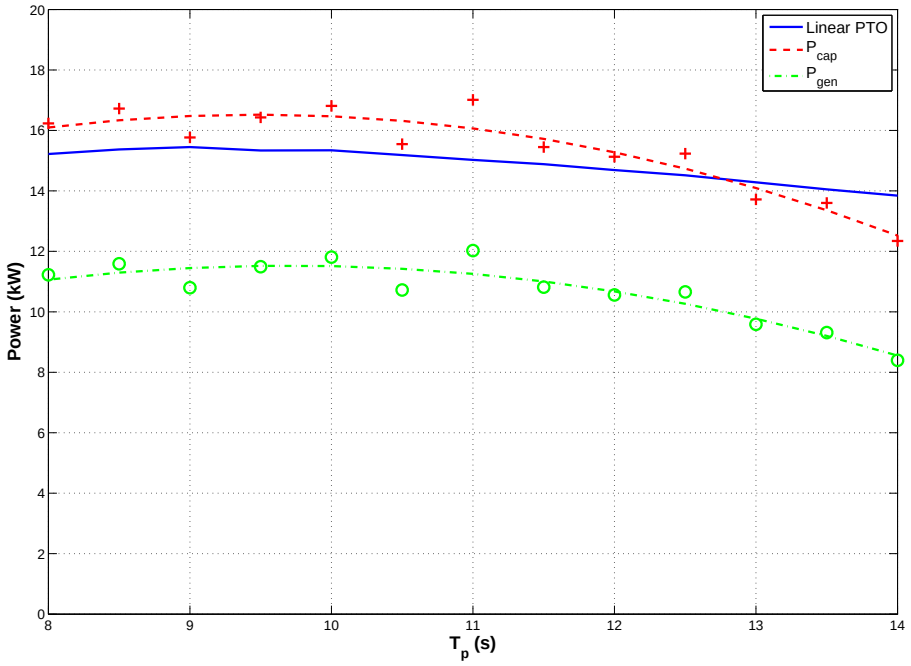

Figure 5-6: *Maximum power generated vs peak wave period for $H_s = 3m$*

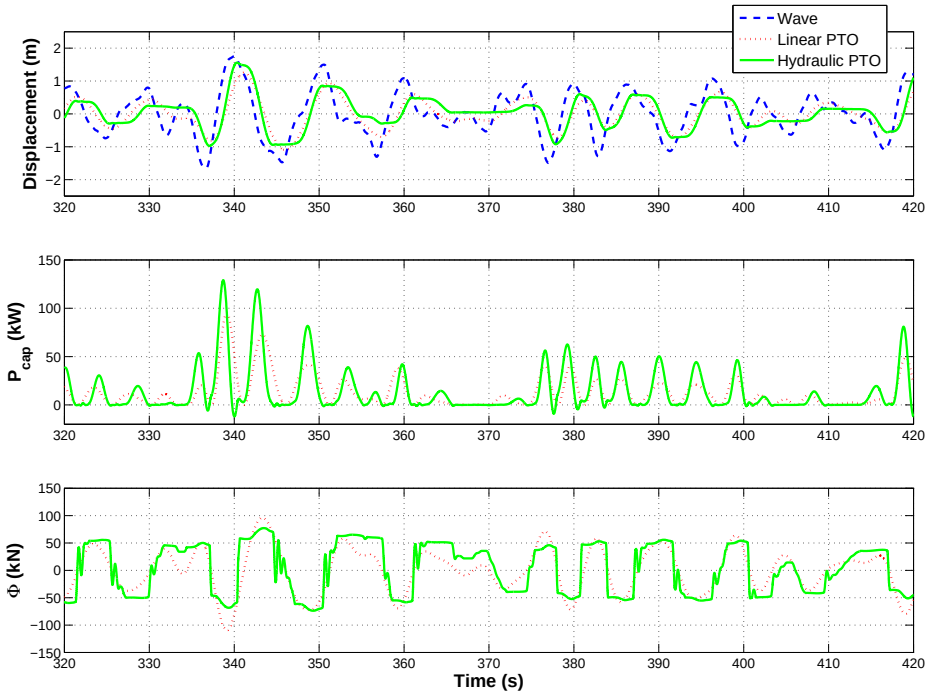

Figure 5-7: *Comparison of the behaviour of an optimally tuned linear and hydraulic PTO in irregular waves. Top: WEC and Wave Displacement, Middle: Power Capture, Bottom: PTO Force. (H_s=3 m and T_p=10 s)*

speed generation in an efficient manner by using a power electronic converter [77]. They have an operational range of about ±30% around the synchronous speed of 1500 rpm so it is assumed that if the hydraulic motor speed is outside of this range no power can be transmitted (P_{trans}) to the grid and the generated power is wasted. A generator efficiency of 100% is still assumed. Two further terms are introduced to analyse this effect; the transmission efficiency (η_{trans}) which is given by equation 5.13 and the total PTO efficiency (η_{tot}) which is given by equation 5.14.

$$\eta_{trans} = \frac{P_{trans}}{P_{gen}} \tag{5.13}$$

$$\eta_{tot} = \eta_{pto}\eta_{trans} \tag{5.14}$$

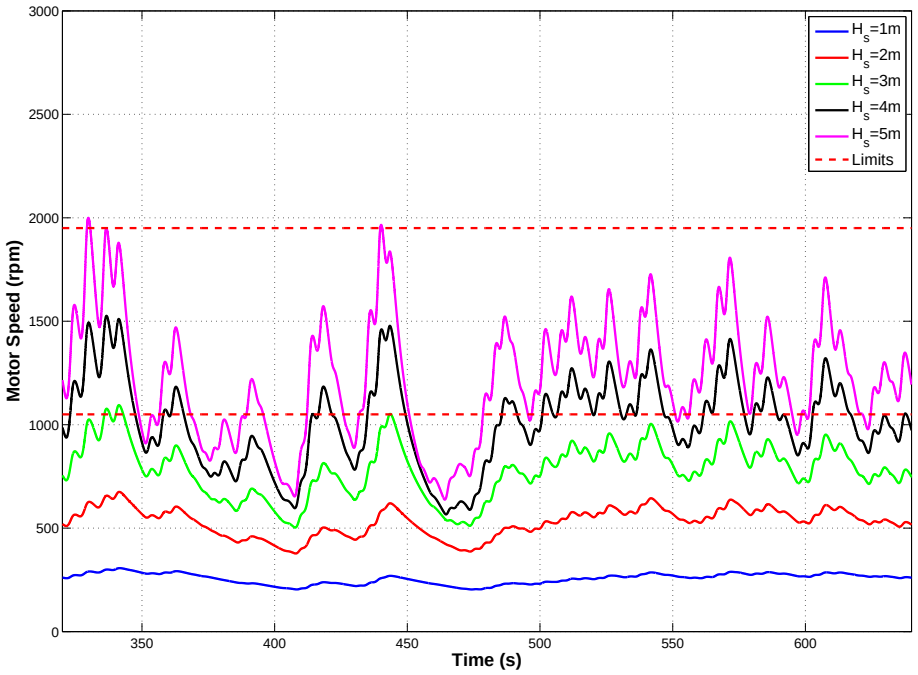

Figure 5-8: *Hydraulic Motor speed vs time for different significant wave heights for an optimally tuned PTO. ($T_p = 11$ s)*

Figure 5-8 displays the motor speed for an optimally tuned PTO in five different significant wave heights of the same wave spectrum. H_s is varied by multiplying the wave amplitude by the appropriate scalar. Figure 5-8 and Table 5.2 illustrate that the magnitude of the motor speed increases with H_s. They also

H_s (m)	Power (kW)		η_{trans}(%)	Speed (rpm)	
	P_{gen}	P_{trans}		$\bar{\omega_m}$	ω_{var}
1	1.25	0	0	256.3	103.2
2	5.43	0	0	530.4	298.0
3	12.03	0.37	3.1	783.3	592.3
4	20.43	11.97	58.6	1012.5	960.1
5	30.42	25.59	84.1	1227.6	1362.5

Table 5.2: *Table showing effects of significant wave height on generated power, transmitted power, average motor speed and speed variation. ($T_p = 11$ s)*

reveal that although the accumulators are large, this does not provide sufficient power smoothing to produce a constant motor speed and the speed variation (ω_{var}) is amplified in larger waves. This means that the motor speed is not always within the operational limits (1050 - 1950 rpm) of the DFIG so, at each H_s, only a certain percentage of P_{gen} can be transmitted to the grid.

For H_s <3 m the motor speed does not reach the lower speed limit so all of P_{gen} is wasted. For $H_s = 3$ m the motor speed only reaches the lower speed limit for a few seconds of the wave cycle so P_{trans} is negligible. However, for H_s >3 m the motor speed is within the limits for a significant portion of the wave cycle so P_{trans} reaches meaningful levels. Results show that the highest η_{trans} of 84% is for $H_s = 5$ m but even for this wave height the average motor speed ($\bar{\omega_m}$) is still less than 1500 rpm.

It would obviously be desirable for $\eta_{trans} = 100\%$, so no power generated by the PTO is wasted. To do this it is necessary to maintain the hydraulic motor speed within the generator speed limits at all times in all wave conditions. To control the motor speed the fraction of motor displacement (x_m) must be adjusted. A PI controller is used to adjust x_m according to the error in speed from the synchronous value with $0.1 < x_m < 1.0$. The transfer function of the PI controller is:

$$G(s) = K_p + \frac{K_i}{s} \tag{5.15}$$

K_p	K_i
0.05	0.01

Table 5.3: *Gain values of the PI controller*

This change in x_m will not be instantaneous as the swash plate of the hydraulic piston motor will have fundamental dynamics. It is assumed that these dynamics

can be modelled as a first order transfer function ($R(s)$) with a time constant, $\tau = 0.1\,\text{s}$, such that

$$R(s) = \frac{K}{1+\tau s} = \frac{1}{1+0.1s} \tag{5.16}$$

To ensure P_{cap} remains at its maximum, $\alpha_{opt}(T_p)$ must be maintained whilst controlling the motor speed. To maintain α_{opt} it is necessary to continually adjust the piston area or generator load at the same rate as x_m. Adjusting the generator load is the only feasible option so it must be varied alongside x_m to maintain α_{opt}.

$$C_g = \alpha_{opt}(T_p)\left(\frac{x_m D_m}{A_p}\right)^2 \tag{5.17}$$

Therefore, in the simulation model the signal to alter the generator load is passed through the same transfer function ($R(s)$) to ensure both signals are in phase. The block diagram of this control strategy is shown in Figure 5-9. This would be possible in practice as the dynamics of both would be investigated and the appropriate signal filtered to ensure they both remained in phase.

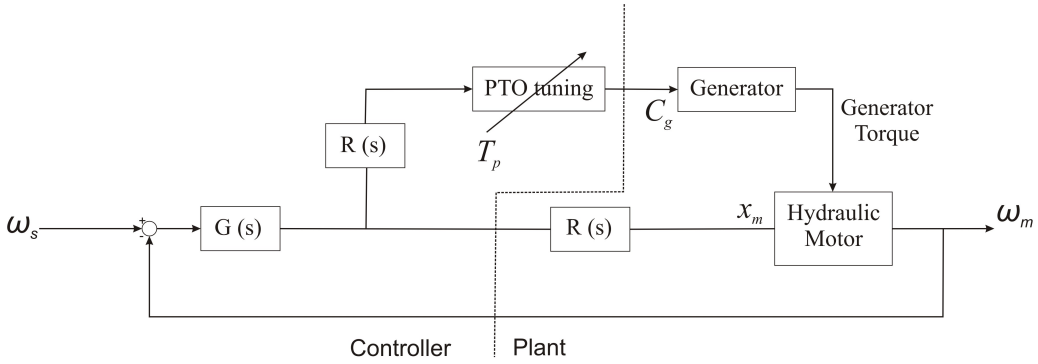

Figure 5-9: *Control Strategy Block Diagram*

Figure 5-10 reveals the advantages of implementing a speed control strategy because the hydraulic motor speed remains approximately constant at the synchronous speed for the full wave cycle, so $\eta_{trans} = 100\%$. Without speed control the motor speed is highly variable and is rarely within the operational limits, so $\eta_{trans} = 3.1\%$. Because α is constant for both cases, P_{cap} is similar but P_{gen} is 40% lower with the speed control strategy due to the large reduction in motor efficiency (η_m), shown in Figure 5-11. To maintain the required motor speed, x_m is constantly varying but on average ($\bar{x_m}$) it is at a relatively low value for this wave profile. $\bar{x_m} = 0.47$ and x_m even reduces to the minimum value for parts of the wave profile. η_m exhibits a strong correlation to x_m (Section 3.4.1), and

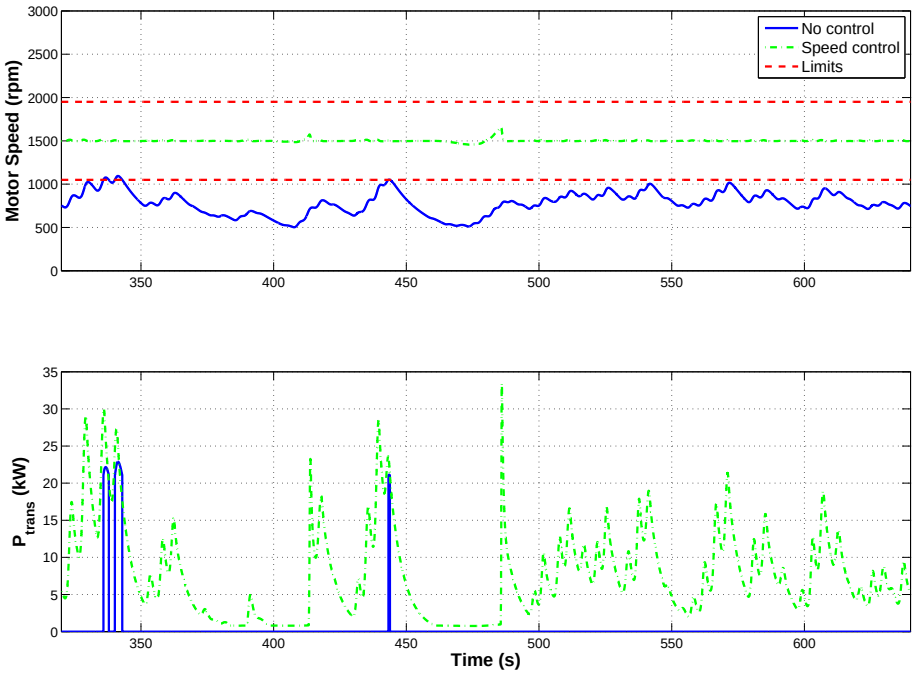

Figure 5-10: *Motor speed and transmitted power with and without speed control. (H_s=3 m and T_p=11 s)*

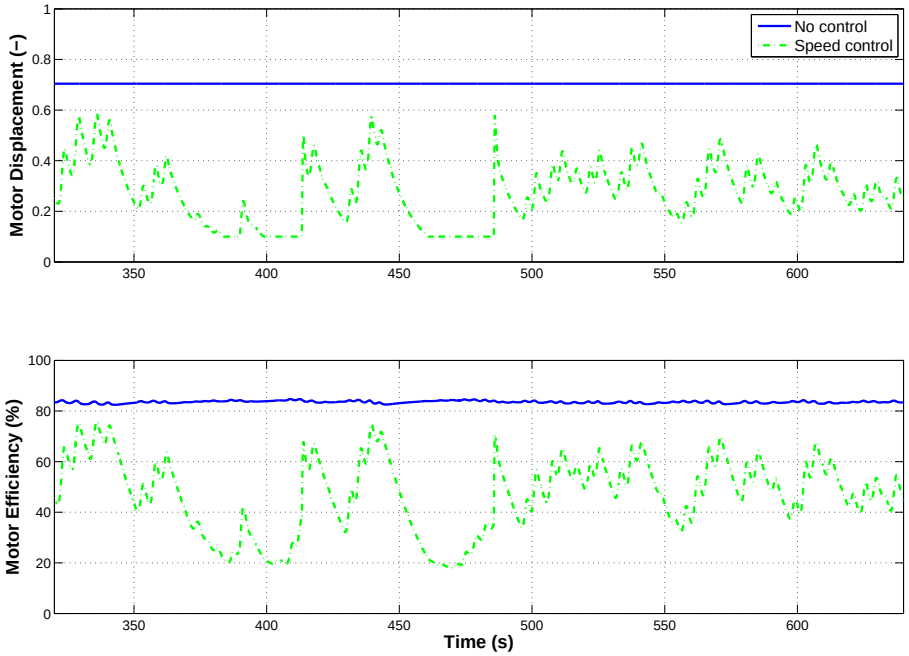

Figure 5-11: *Fraction of motor displacement and motor efficiency with speed control. (H_s=3 m and T_p=11 s)*

together with the increased motor speed, this causes a significant reduction in η_m, and therefore in η_{pto}.

5.5 Control Strategy Evaluation

The result for the single wave profile shows a large improvement in P_{trans} from implementing a motor control strategy. However, to fully evaluate the improvements, it is necessary to consider a number of sea states. The four sea states shown in Figure 5-12, created from the parameters in Table 5.4 are used because they represent a range of wave conditions which the WEC could encounter. For each sea state α_{opt} is given by the trend line from Figure 5-5.

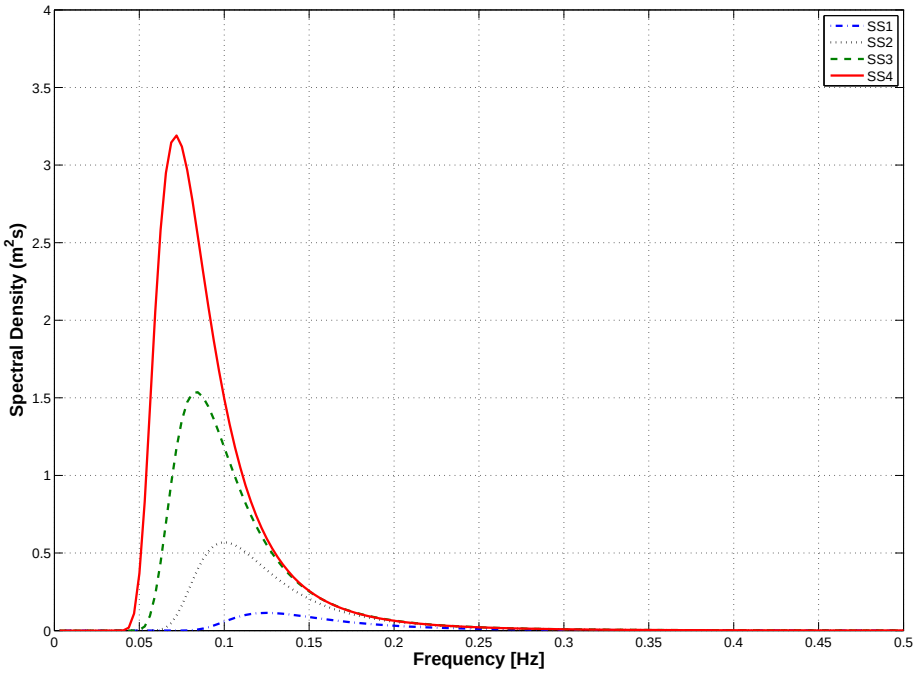

Figure 5-12: *Wave Spectrums for the four sea states being investigated*

Sea State (SS)	H_s (m)	T_p (s)	P_{wave} (kW)	α_{opt} (kNs/m)
1	1.0	8.0	13.5	145
2	2.0	10.0	67.3	200
3	3.0	12.0	181.7	255
4	4.0	14.0	376.9	310

Table 5.4: *Parameters of the four sea states*

For these four sea states, three strategies will be compared:

1. **No PTO tuning and no speed control**- Constant, maximum motor capacity (x_m=1) and generator load (C_g). ($\alpha = 100\,\text{kNs/m}$)
2. **PTO tuning and no speed control**- Motor displacement adjusted to give optimum PTO damping for each SS with generator load at maximum value. Both values constant for the simulation. ($\alpha = \alpha_{opt}$)
3. **PTO tuning and closed loop speed control**- Motor displacement and generator load continually adjusted to maintain optimum PTO damping and provide speed control. ($\alpha = \alpha_{opt}$)

SS	Power (kW)			Efficiency (%)		
	P_{cap}	P_{gen}	P_{trans}	η_{pto}	η_{trans}	η_{tot}
1	1.74	1.01	0	58.2	0	0
2	6.44	4.14	0	64.3	0	0
3	12.75	8.21	0	64.4	0	0
4	18.94	12.01	2.26	63.4	18.85	12.0

Table 5.5: *Control Strategy 1*

SS	Power (kW)			Efficiency (%)		
	P_{cap}	P_{gen}	P_{trans}	η_{pto}	η_{trans}	η_{tot}
1	1.68	1.04	0	61.7	0	0
2	7.54	5.28	0	70.0	0	0
3	15.13	10.56	0	69.8	0	0
4	23.19	16.07	5.26	69.3	32.8	22.7

Table 5.6: *Control Strategy 2*

SS	Power (kW)			Efficiency (%)		
	P_{cap}	P_{gen}	P_{trans}	η_{pto}	η_{trans}	η_{tot}
1	1.06	0.12	0	11.5	0	0
2	5.26	0.89	0.78	17.0	87.4	14.8
3	14.40	6.50	6.50	45.2	100	45.2
4	23.07	12.89	12.89	55.9	100	55.9

Table 5.7: *Control Strategy 3*

The results for the four sea states comparing the 3 strategies are presented in Tables 5.5, 5.6 and 5.7. The power from SS1 is negligible so results for this sea state will not be discussed.

P_{cap} is higher for all sea states with strategy 2 than strategy 1 because the PTO is tuned for α_{opt} with strategy 2, instead of the constant α for strategy 1. P_{gen} is also higher for each SS because of the higher P_{cap} and the higher η_{pto}. However, both strategies give $P_{trans}=0$ for SS2 and SS3 and only a small transmitted power for SS4. Furthermore, these values only represent 19% and 33% of the generated power for the two strategies respectively.

P_{trans} is higher for all the sea states with strategy 3, which shows the gains in transmitted power from the motor speed control. However, it is interesting to note that P_{cap} and P_{gen} is lower for strategy 3 than strategy 2, especially for SS2. With strategy 3, $\bar{x_m}$ is much lower than for strategy 2, which results in a lower η_m (Table 5.8). This is emphasised in the lower wave power of SS2 because $\bar{x_m}=0.1$, the minimum value, for the entire simulation. The resulting low η_m has an effect on the behaviour of the WEC by effectively altering α and therefore reducing P_{cap}. This shows that α_{opt} is effected by η_{pto}, which further emphasises the importance of a realistic PTO model to correctly tune these devices.

For strategy 3, η_m and η_{pto} is lower for each SS. The lower P_{cap} and η_{pto} combine to give a significant reduction in P_{gen}. However, in more energetic sea states, SS3 and SS4, x_m and η_m are higher so α is less effected and P_{cap} and P_{gen} is more equivalent to strategy 2.

SS	Strategy 1		Strategy 2		Strategy 3	
	x_m	$\eta_m(\%)$	x_m	$\eta_m(\%)$	$\bar{x_m}$	$\eta_m(\%)$
1	1.0	83.8	0.85	85.1	0.1	14.3
2	1.0	83.4	0.72	83.6	0.1	19.0
3	1.0	82.8	0.64	81.7	0.23	51.0
4	1.0	82.1	0.58	79.7	0.28	63.4

Table 5.8: *Motor characteristics for the 3 control strategies*

To maximise P_{trans}, it is necessary to combine the behaviours of strategies 2 and 3. It is imperative to maintain η_{trans} at 100% by implementing the motor control strategy. However, it is also important to maximise P_{cap} and η_{pto} by increasing η_m for all sea states by using a smaller hydraulic motor to ensure a higher $\bar{x_m}$. This may result in a small reduction in η_{trans} for more powerful sea states as the hydraulic motor speed may rise above the upper limit for certain periods but it is expected to increase η_{trans} in less powerful sea states. Overall though, it is expected to improve performance by increasing P_{cap} and η_{pto} to give a higher P_{trans}.

5.6 Modified PTO Design

In order to size the hydraulic motor appropriately, information on the wave power at the specific site at which the device will be deployed is required. Using data provided by The European Marine Energy Centre (EMEC), which will be discussed further in Chapter 6, an average wave power can be approximated. The motor has been downsized by a factor of 3 and replaced with a motor capacity of 60 cc/rev to ensure $\bar{x_m} \approx 0.8$ for the average wave power. The efficiency curve for this motor is assumed to be the same as for the previous motor. The gains of the PI controller (k_p and k_i) have been adjusted accordingly to ensure they have the same effect on this smaller motor. In order to maintain $\alpha_{min} = 100\,\text{kNs/m}$, the generator characteristic has been reduced so its maximum value is $C_g = 0.19\,\text{Nm/(rad/s)}$.

K_p	K_i
0.45	0.09

Table 5.9: *Gain values of the PI controller*

Piston area (m^2)	Motor Capacity (cc/rev)	Generator Load (Nm/(rad/s))
0.007	60	0.19

Table 5.10: *Modified PTO parameters*

SS	Power (kW)			Efficiency (%)		
	P_{cap}	P_{gen}	P_{trans}	η_{pto}	η_{trans}	η_{tot}
1	1.70	0.81	0	47.8	0	0
2	7.14	3.52	3.12	49.4	88.4	43.6
3	14.35	6.79	4.28	47.3	63.1	29.8
4	21.52	9.68	3.04	45.0	31.3	14.1

Table 5.11: *Modified PTO Design- Control Strategy 1*

The results for the four sea states comparing the 3 strategies with the modified PTO design are presented in Tables 5.11, 5.12 and 5.13. The power associated with SS1 is negligible so the results for this sea state will not be discussed again.

Compared to the initial PTO design, there is an increase in P_{cap} but a reduction in P_{gen} for each SS with control strategy 1. The reduction in motor capacity increases the motor speed, which reduces η_m and effectively alters α. This increases P_{cap} by approximately 10% for each SS but it also reduces η_{pto} by

SS	Power (kW)			Efficiency (%)		
	P_{cap}	P_{gen}	P_{trans}	η_{pto}	η_{trans}	η_{tot}
1	1.63	0.85	0	51.8	0	0
2	7.45	4.14	3.44	55.6	83.0	46.1
3	14.62	7.97	3.21	54.5	40.3	21.9
4	23.14	11.74	2.27	50.7	19.3	9.8

Table 5.12: *Modified PTO Design- Control Strategy 2*

SS	Power (kW)			Efficiency (%)		
	P_{cap}	P_{gen}	P_{trans}	η_{pto}	η_{trans}	η_{tot}
1	0.63	0.02	0.01	3.5	55.1	1.9
2	7.30	4.15	4.15	56.9	100	56.9
3	15.15	9.80	9.80	64.7	100	64.6
4	23.34	15.76	10.94	67.5	69.4	46.9

Table 5.13: *Modified PTO Design- Control Strategy 3*

SS	Strategy 1		Strategy 2		Strategy 3	
	$\bar{x_m}$	$\eta_m(\%)$	$\bar{x_m}$	$\eta_m(\%)$	$\bar{x_m}$	$\eta_m(\%)$
1	1.0	66.3	0.85	69.6	0.1	4.3
2	1.0	61.0	0.72	64.7	0.56	65.2
3	1.0	57.9	0.64	62.1	0.84	74.3
4	1.0	54.8	0.58	59.3	0.89	76.9

Table 5.14: *Motor characteristics for the 3 control strategies with the modified PTO design*

approximately 15%. Together this means a small reduction in P_{gen}. However, because of the higher motor speed, this means an increase in η_{trans} so overall P_{trans} is larger with the modified PTO design.

For control strategy 2, P_{cap} is similar to before because α_{opt} is the same but there is a 20% reduction approximately in P_{gen} due to the increased motor speed that reduces η_m. Due to the higher motor speed, there is an increase in η_{trans} which results in a higher P_{trans}, except for SS4. For the modified PTO, strategy 2 gives a higher P_{gen} than strategy 1 but there is only a small difference in P_{trans} between the two strategies so the advantages of strategy 2 are only minor. Figure 5-13 reveals that the motor speed for strategy 1 and 2 is very similar throughout the cycle (SS3) with strategy 2 generally being slightly higher. This means that overall P_{trans} is higher for strategy 1 because the motor speed is within the limits for a slightly longer period of time. However, when both motor speeds are within the limits the magntiude of P_{trans} is higher for strategy 2 because η_m is higher (Figure 5-14).

With the modified PTO, control strategy 3 again performs the best. It gives a similar P_{cap} to strategy 2 but it gives a larger P_{gen}, especially for SS3 and SS4, due to a higher η_m from the increased x_m. Furthermore, due to the speed control, η_{trans} is higher for each SS. These combined effects result in a much larger P_{trans} for each SS using control strategy 3. The advantages are clear to see for SS3 in Figures 5-13 and 5-14. It gives the largest overall P_{trans} for the majority of the cycle because the motor speed is always within the limits and the motor efficiency is generally higher so the magnitude of P_{trans} is also predominantly higher.

For both PTO designs, control strategy 3 gives the highest P_{trans} for all sea states. Table 5.15 provides a summary of the results for this strategy for both PTO designs and it reveals the benefits of the smaller hydraulic motor and generator load in the modified PTO.

With the modified PTO, there is an increase in P_{cap} for each SS compared to the initial PTO, especially for SS2. This indicates a better tuned PTO and an increase in power capture efficiency. P_{gen} is also higher for each SS due to the higher η_m from the increased $\bar{x_m}$. Figure 5-15 displays these improvements. It shows that for the both PTOs, the motor speed does not remain constant in SS3 because the motor capacity is either too large for the initial PTO or too small for the modified PTO, to maintain the synchronous speed for certain flows. However, the motor speed remains within the operational limits for both PTOs during these periods so importantly no power is lost. However, P_{trans} is higher

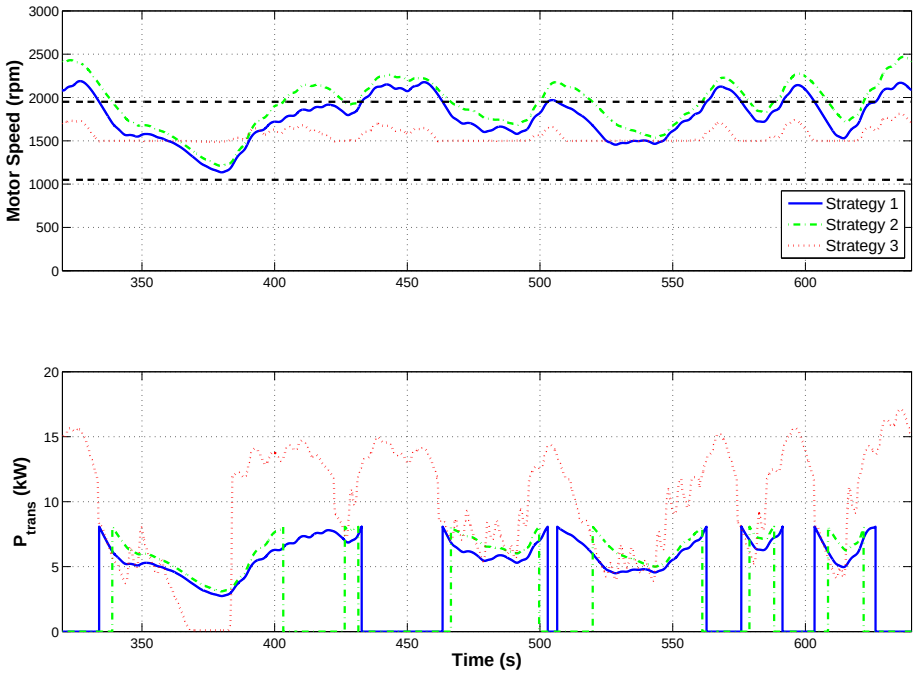

Figure 5-13: *Motor speed and transmitted power for the 3 control strategies in SS3 with the modified PTO design*

for the modified PTO mainly because of the increased η_m, shown in Figure 5-16.

All these combined improvements mean a significant increase in P_{trans} for SS2 (430%) and SS3 (50%). For SS4 there is a small reduction (15%) in P_{trans} due to the reduced η_{trans} but this loss is limited by the increase in η_{pto}. In larger waves the smaller capacity motor can not continually maintain the motor speed within the required range so the upper limit is exceeded for a short period of time. Overall though, it is predicted that SS4 will be less frequent than SS2 and SS3, so when all sea conditions are considered, the modified PTO will provide significant gains in transmitted power.

These results show that the motor efficiency has a big effect on the transmitted power. If motor control is implemented, the full range of motor displacement is utilised in all sea states to maintain the generator synchronous speed. The motor efficiency for this model, exhibits a strong correlation to part displacement so it would be desirable to maintain a constant, high motor efficiency for all displacements. Therefore, ideas such as generating modules with smaller motors that can be switched in and out depending on the incoming wave power have been mentioned [62] but no results have been presented. Likewise, Digital

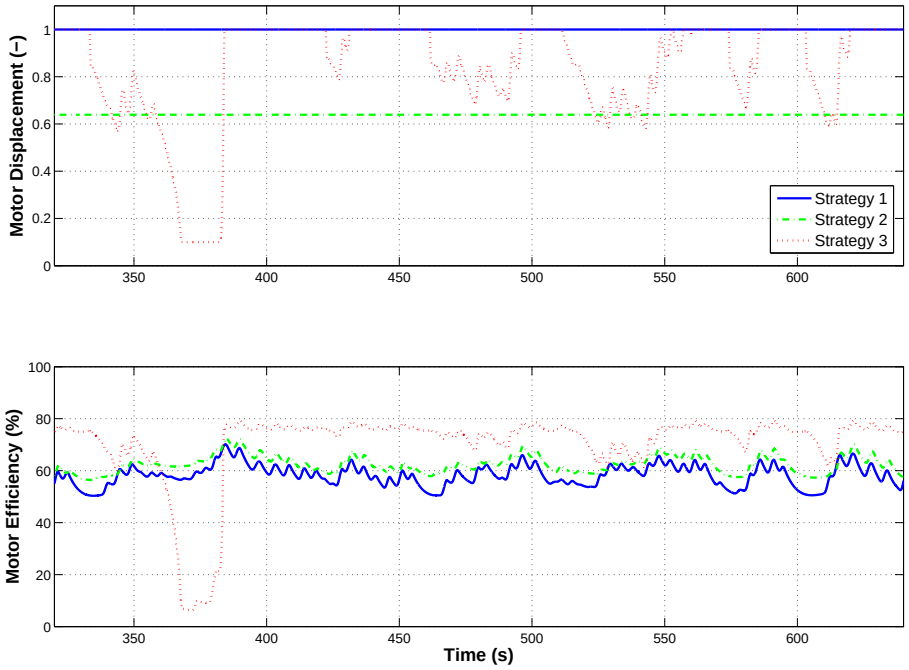

Figure 5-14: *Fraction of motor displacement and motor efficiency for the 3 control strategies in SS3 with the modified PTO design*

Displacement ® pumps and motors have been developed to increase efficiency, especially at part load, so they are a possible solution to this problem because they would allow a larger motor to be implemented whilst not compromising the motor efficiency at part load [64]. Moreover, a combination of the two could give the best overall solution.

Finally, it is worth noting that even with this control strategy, optimal PTO tuning and a more efficient PTO design, the power levels are still relatively low for a device of this size and the generator losses have not been included.

SS	P_{wave}	Initial PTO			Modified PTO		
		P_{cap}	P_{trans}	$\eta_{tot}(\%)$	P_{cap}	P_{trans}	$\eta_{tot}(\%)$
2	67.3	5.26	0.78	14.8	7.30	4.15	56.9
3	181.7	14.40	6.50	45.2	15.15	9.80	64.6
4	376.9	23.07	12.89	55.9	23.34	10.94	46.9

Table 5.15: *PTO comparison with control strategy 3*

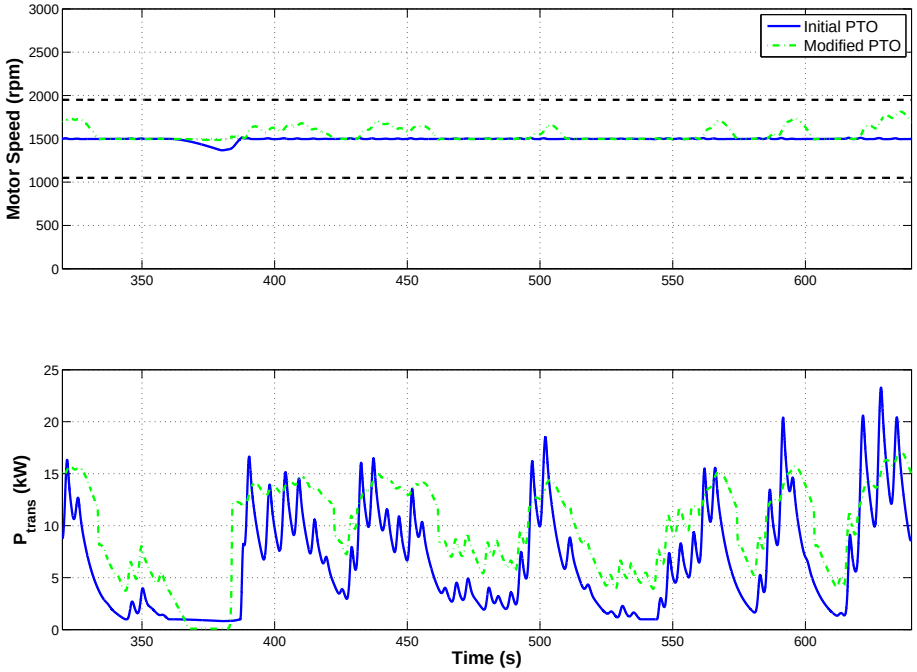

Figure 5-15: *Motor speed and transmitted power for initial and modified PTO design in SS3*

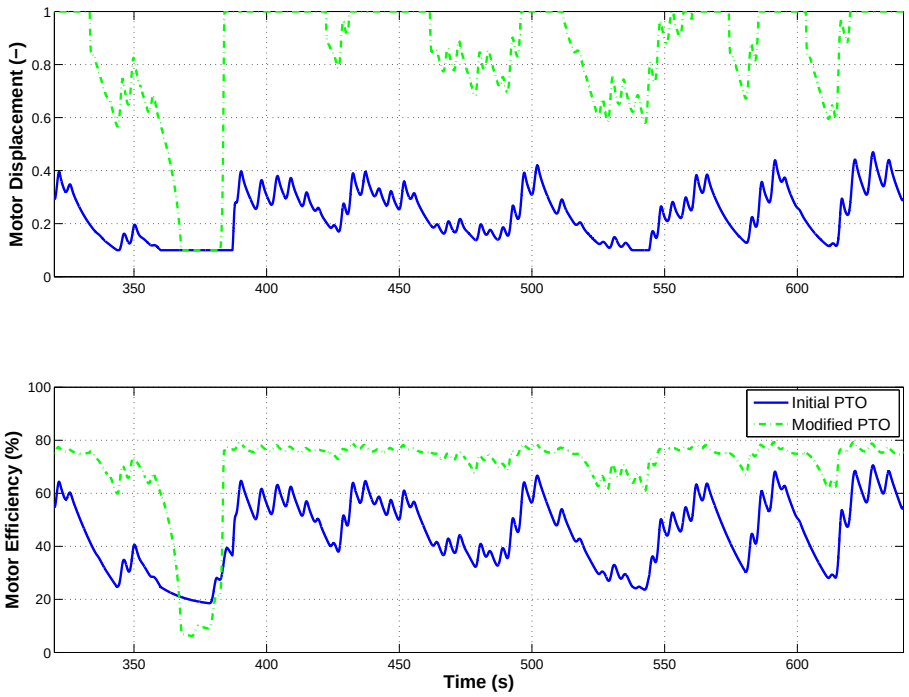

Figure 5-16: *Fraction of motor displacement and motor efficiency for initial and modified PTO design in SS3*

5.7 Concluding Remarks

Firstly this chapter introduced wave spectra; how they are created and their defining parameters. Using the Pierson-Moskowitz spectrum, the random phase method was applied to create the wave elevation and excitation force profile to represent an irregular wave. Using this input the behaviour of the device was examined. As expected no pseudo steady state is reached and the behaviour of the device is very changeable. Induced body stall occurs but the period of stall is constantly varying. The power smoothing effect of the accumulators is more appreciable because the magnitude of the captured power is constantly varying. This causes the pressure and volume of the accumulators to continuously vary in an attempt to maintain a relatively constant motor speed.

In terms of tuning, a linear trend between optimum PTO damping and peak wave period is observed but values differ from those for a regular wave input and they are significantly different to those for a linear PTO. The power captured by the hydraulic PTO is generally slightly greater than for the linear PTO but both values are low in comparison to regular waves of the same wave height.

Consideration was then given to how the mechanical power generated by the PTO would be transmitted into electrical energy. It is assumed that a doubly fed induction generator (DFIG) is used, as in wind turbines, because of its capacity to deal with a variable speed input. It was assumed that power is transmitted if the speed of the hydraulic motor is within the range of $\pm$ 30% of the generator synchronous speed. It was clear that a PI controller is needed to maintain the motor speed within these limits by altering the fraction of motor displacement, and that the generator load must also be altered at the same rate to maintain optimum PTO damping and ensure maximum power capture.

The transmitted power gains from speed control are obvious but due to the low flows and large hydraulic motor, the fraction of motor displacement is very low for all of the sea states investigated. This causes a low motor efficiency, a low PTO efficiency and a reduction in power capture, which all amounts to a reduction in generated power. Therefore, in an attempt to increase PTO efficiency and improve generated power a smaller hydraulic motor and generator load was introduced to improve the overall efficiency of the device. This was found to be a success as it increased the transmitted power for the most prevailing sea states by increasing the capture, PTO and transmission efficiency. There was a slight decrease in the transmitted power for the largest sea state but this sea state is

expected to be less frequent so overall there will be significant power gains for the device. Therefore, for the remainder of the simulation work, the modified PTO design and closed loop speed control will be implemented.

CHAPTER 6

WAVE DATA AND REAL TIME PTO TUNING

This chapter investigates real wave data from the European Marine Energy Centre (EMEC) based in Orkney, Scotland. It presents techniques to analyse the wave energy resource at a particular site by using statistics that are calculated from the raw data. The results are presented and compared for two different months of data. A method to calculate the wave excitation force from the raw wave displacement is presented and this is then used as the input to the simulation model. This provides a prediction of how the WEC will behave and the power which can be generated in real wave conditions.

PTO tuning is then investigated using the real data and compared to the results found previously in Chapter 5. Real time tuning methods are analysed to determine the best method to maximise power generation by updating the PTO damping. Active and passive methods are examined which tune the PTO to a wave frequency calculated from different lengths of wave data.

6.1 Wave Data Analysis

Real waves are random and unpredictable in nature. However, there are key quantities which can be calculated from the data to analyse and compare different sea states. They are defined as non-spectral data because they are not functions of frequency but they involve the integrated properties of the frequency spectrum. These key quantities are calculated from the frequency moments of the variance spectrum (m_a) [78]. The frequency spectrum (S_n) is given by the Fast Fourier Transform (FFT) of the wave displacement. Figure 6-1 shows that

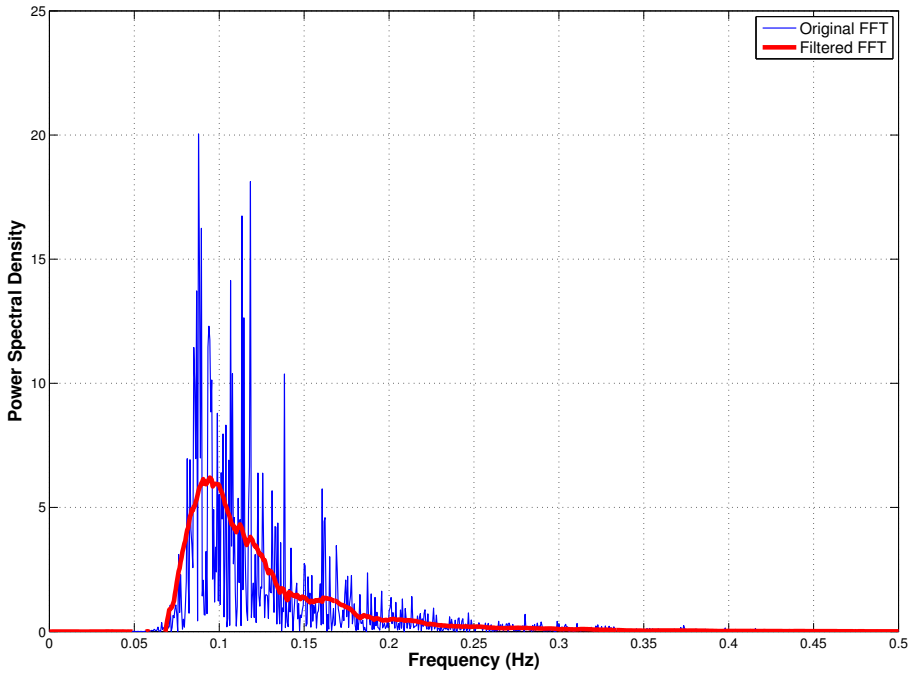

Figure 6-1: *Frequency spectrum showing the unfiltered FFT and filtered FFT*

the FFT produces a noisy spectrum which is difficult to interpret. To produce a smoother spectrum a Savitzky-Golay filter is used because it preserves features of the distribution which other filters tend to remove [79]. A third order polynomial filter is used with a frame size of 81 as these parameters produce a smoother spectrum shape which is similar to a Pierson Moskowitz spectrum, as shown in Figure 6-1.

The moments of the variance spectrum (m_a) for a=-1,0,1,2, are calculated from:

$$m_a = \sum_{i=1}^{N} S_{n_i} \omega_i^a \Delta\omega = \int_0^{\omega_N} S_n \omega^a d\omega \tag{6.1}$$

The significant wave height (H_s) and the peak period (T_p) are also key parameters which were mentioned in Chapter 5.

H_s is given by:

$$H_s = 4\sqrt{m_0} \tag{6.2}$$

and T_p is given by:

$$T_p = \frac{1}{f_p} \tag{6.3}$$

where f_p is the frequency in Hz corresponding to maximum S_n.

The energy period (T_e) is given by:

$$T_e = \frac{m_{-1}}{m_0} \tag{6.4}$$

The total wave power flux (P_{flux}) of the spectrum is the scalar sum over the frequency range:

$$P_{flux} = \frac{1}{2a} \sum_{i=1}^{N} P_{wave_i} \tag{6.5}$$

It is an indicator of the power available per metre width of the incoming wave crest (kW/m) [66]. P_{wave} is the incident wave power of each wave component as given by equation 3.55.

6.2 EMEC Data Analysis

By using wave spectra and the random phase method to create a wave elevation and excitation force profile (Chapter 5) meant that the signals were repeating in nature and had one dominant peak frequency. However, real waves are non repeating and their frequency spectrum may have more than one dominant peak and so not correlate well to a Pierson-Moskowitz spectrum. Therefore, it is necessary to use wave data collected from test sites to determine if the trends and methods which have been found previously are applicable to real waves.

EMEC has a number of data collection buoys in different locations around their site in Orkney. Data for the months of April and October 2011 were obtained for one of the locations (Billia Croo Buoy E). The data is for the wave heave displacement and it is packaged into 30 minute files with a sampling frequency of 1.28 Hz. The two months of data were chosen due to their low percentage of errors but only files which included zero error values are used in this work (Table 6.1).

The wave parameters, defined in Section 6.1, were calculated for each individual file and the results for both months are compared in Figures 6-2 to 6-5. They reveal that the average power available in April was lower than October.

Month	Total Files	Error Files
April	1440	51
October	1488	7

Table 6.1: *EMEC Wave Files for April and October 2011*

October had more occurrences of the lowest level of wave power (<30 kW/m) but there were also more large wave powers (>100 kW/m), which indicates more variable weather. The average values of terms relating to wave period are lower for October but the variance is lower in April. In particular, there are more short period waves in October. This may indicate a changing of the dominant wave frequency through the year in this location but this can not be confirmed without analysing years of full data. Further wave parameters and results are given in Appendix A.

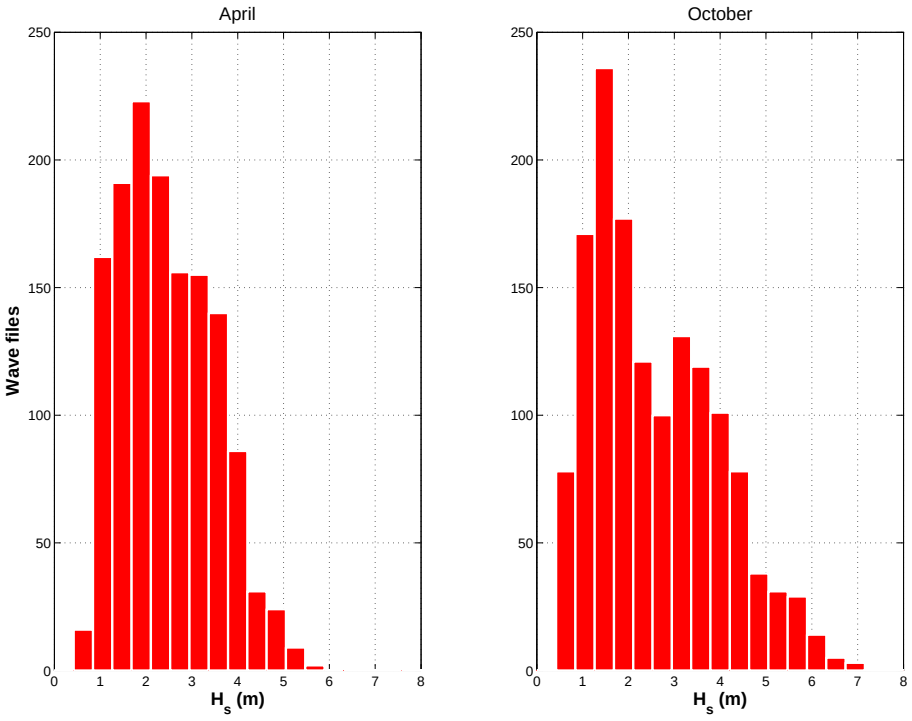

Figure 6-2: *Frequency histogram showing the significant wave height in April and October*

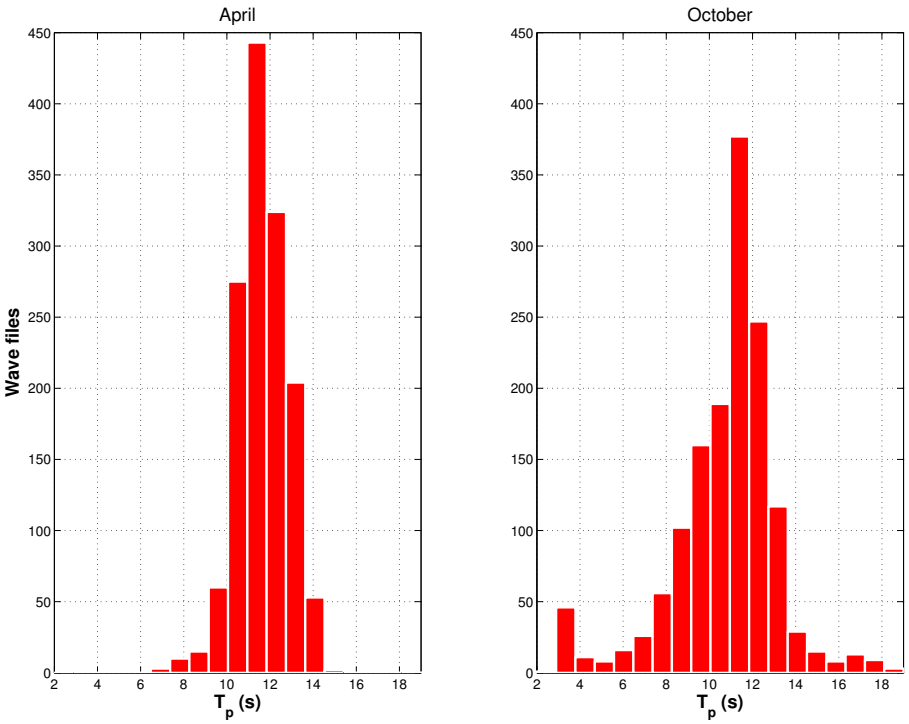

Figure 6-3: *Frequency histogram showing the peak period in April and October (from filtered spectrum)*

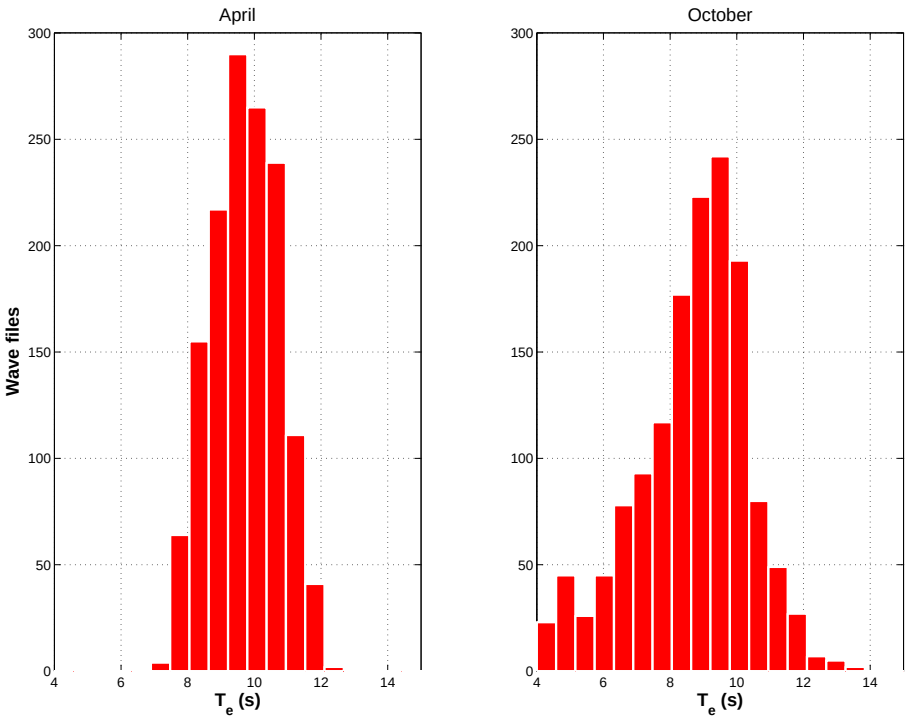

Figure 6-4: *Frequency histogram showing the energy period in April and October*

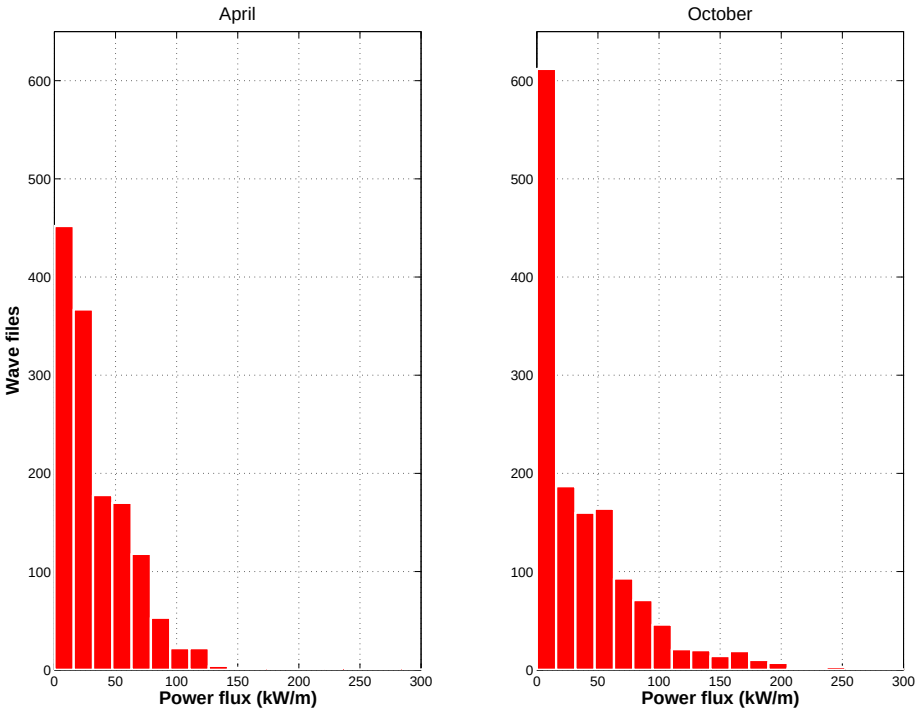

Figure 6-5: *Frequency histogram showing the wave power flux in April and October*

6.2.1 Creating the Wave Excitation Force Signal

The simulation model uses the wave excitation force as the input to the hydrodynamic model. However, the raw data provided by EMEC is for the heave displacement of the wave so it is necessary to create a wave excitation force signal to correspond to this wave displacement. The FFT of the wave displacement gives the discrete frequency components and their corresponding amplitude and phase.

Assuming a finite number of wave components, the wave excitation force coefficient ($\Gamma(\omega_i)$, equation 3.14) of each wave component can be calculated from the corresponding wave amplitude (X_{w_i}) and frequency (ω_i). It is assigned with the correct phase component (φ_i) so the wave force signal corresponds to the original wave displacement signal.

$$f_{e_i}(t) = \Gamma(\omega_i) X_{w_i}(\omega_i) \cos(\omega_i t + \varphi_i) \tag{6.6}$$

and

$$f_e(t) = \sum_{i=1}^{n} \Gamma(\omega_i) X_w(\omega_i) \cos(\omega_i t + \varphi_i) \tag{6.7}$$

Figure 6-6 shows a 600 s section of an example EMEC file with the wave displacement and the calculated wave excitation force. In the time domain, Figure 6-7 shows that the WEC behaves in a similar manner to that in irregular waves produced by the random phase method (Section 5.2). The induced body stall and Coulomb type PTO force is still evident.

However, because the wave profile is non repeating the energy stored in the accumulators will not average out over a fixed time period like previously. Therefore, to negate the effect of the added energy stored in the accumulators giving an inaccurate result for the generated power (P_{gen}) and PTO efficiency (η_{pto}) the model is analysed over the largest possible time period with limits that correspond to similar levels of stored energy in accumulator 'A'.

6.3 PTO Tuning in Real Seas

Section 5.3 demonstrated a relationship between the peak wave period (T_p) and the optimum PTO damping (α_{opt}) for waves created using the Pierson-Moskowitz spectrum and the random phase method. It is important to determine if this, or any other relationship, exists for real wave data. Therefore, a number of wave

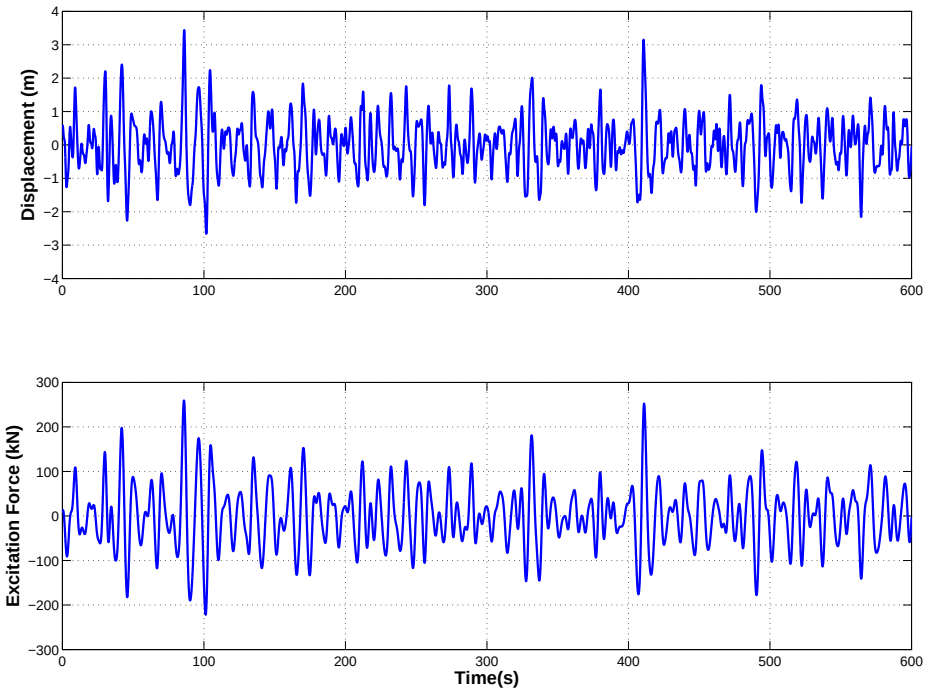

Figure 6-6: *Wave displacement and excitation force for an example EMEC file*

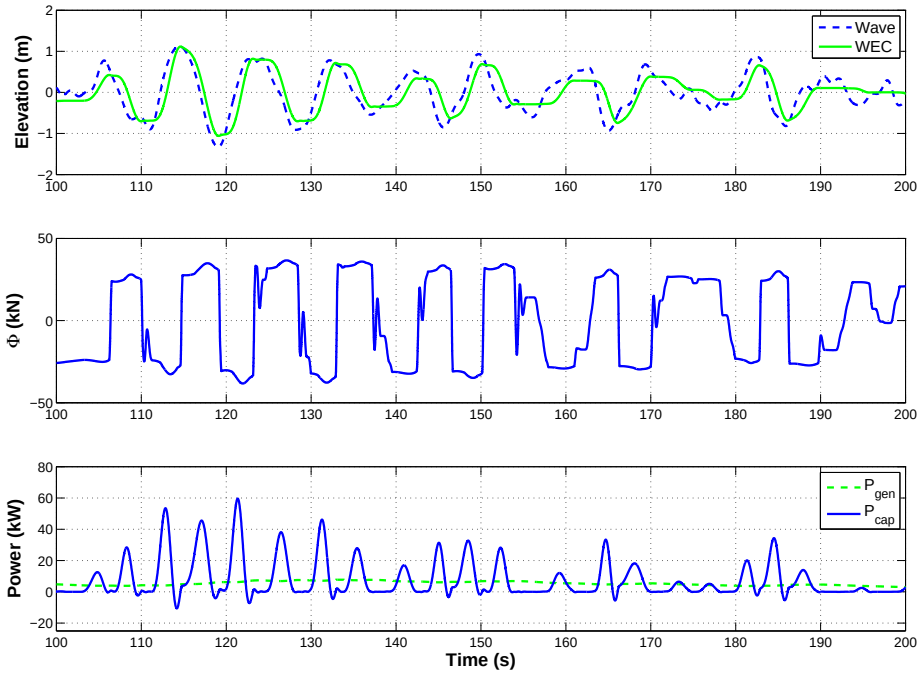

Figure 6-7: *WEC and PTO behaviour in the example EMEC file*

files were chosen in both months with $H_s \approx 2.5\,\text{m}$ and T_p ranging from 8 - 14 s approximately. Information on these files is given in Appendix B. For each of the wave files the optimisation algorithm is used to maximise P_{gen} and give α_{opt} to determine any trends between it and the wave parameters.

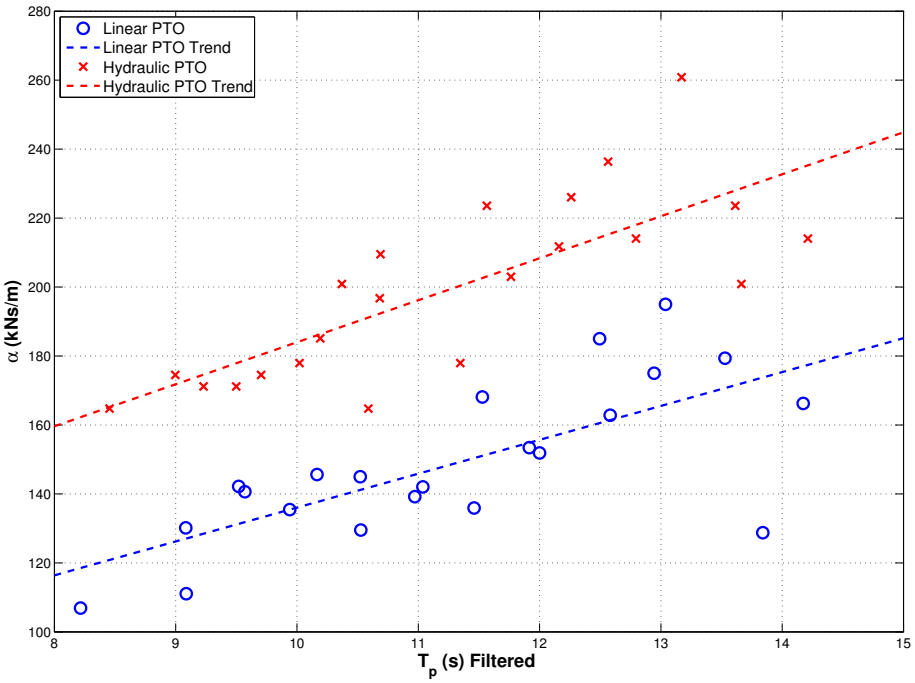

Figure 6-8: *Optimum PTO damping vs peak wave period with filtered spectrum*

Wave Parameter	Linear PTO	Hydraulic PTO
T_p (Filtered)	71.8	74.9
T_p (Unfiltered)	89.3	95.3
T_e	29.2	56.1

Table 6.2: *Norm of the residuals for the fit between the optimum PTO damping and the different wave parameters*

Figures 6-8, 6-9 and 6-10 show a similar optimisation trend between the linear and hydraulic PTO with a relatively constant offset between the two. The correlation between T_p and α_{opt} is better when T_p is calculated from the filtered spectrum. However, Table 6.2 shows that the norm of the residuals, an indicator of the goodness of the correlation, is lowest for the fit between the energy period (T_e) and α_{opt}. Even with filtering, two distinct peaks may remain in the spectrum, like Figure 6-13, so the PTO may best be tuned to a frequency between these

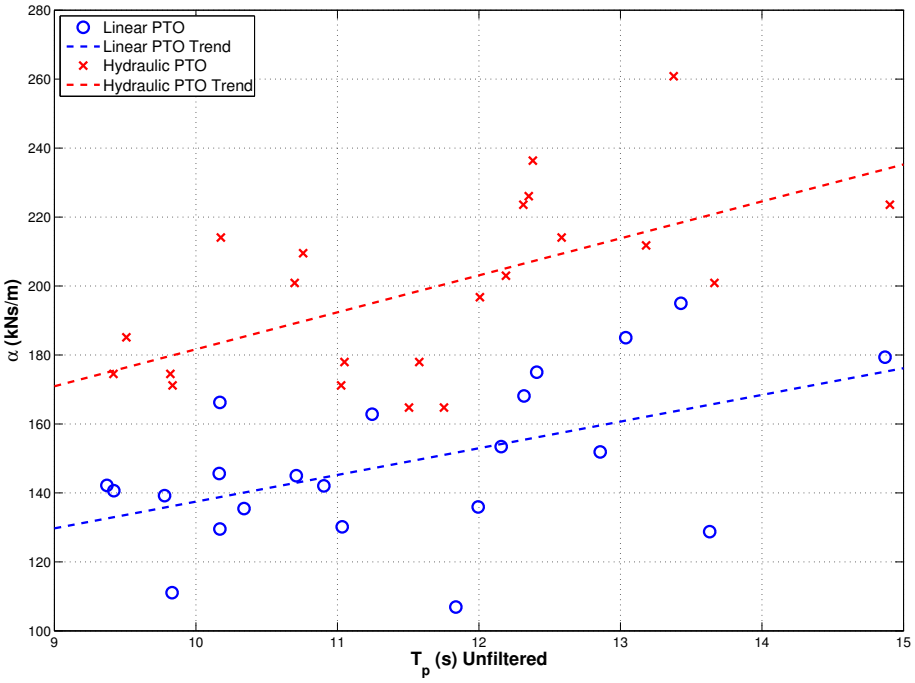

Figure 6-9: *Optimum PTO damping vs peak wave period with unfiltered spectrum*

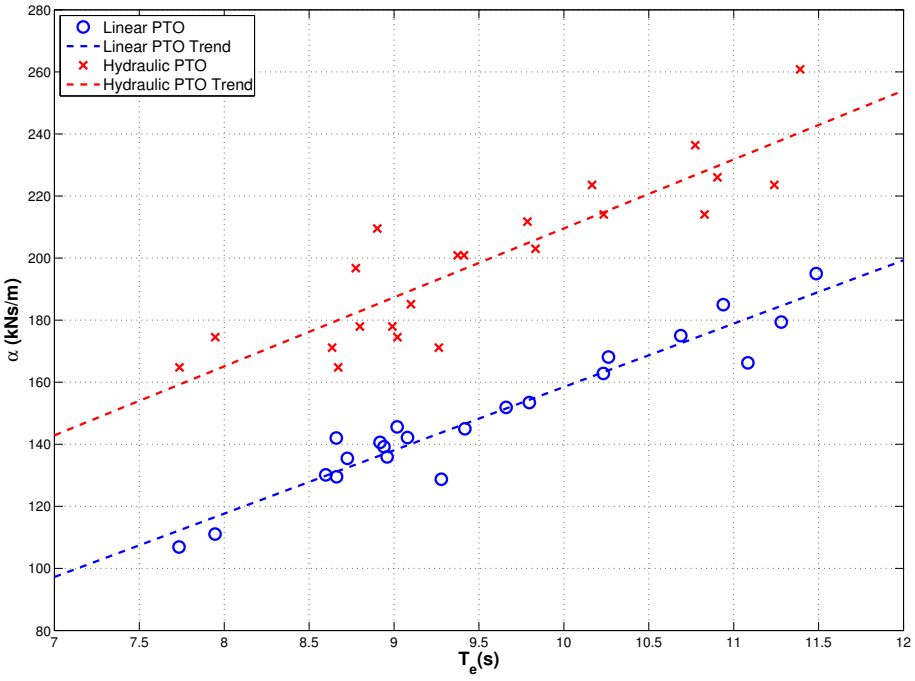

Figure 6-10: *Optimum PTO damping vs energy period*

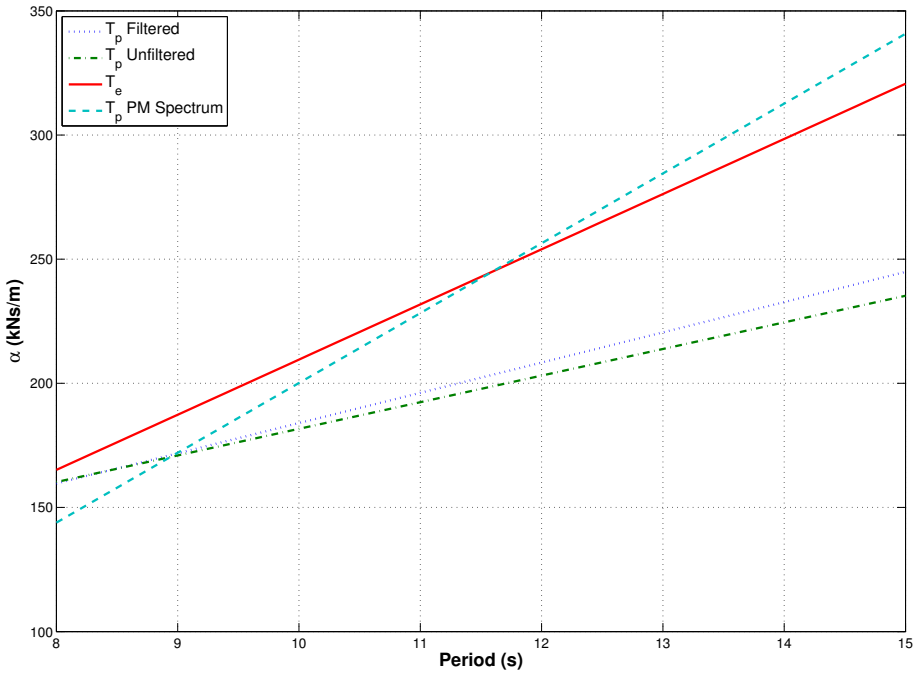

Figure 6-11: *Comparing the optimum PTO damping trends (for the hydraulic PTO) for different wave parameters*

two peaks, instead of the peak frequency, so it can benefit from the high energy at both these frequencies. These types of spectrum are mainly responsible for the outliers in Figures 6-8 and 6-9 and are the reason for the poorer correlation. The energy period is less affected by these types of spectrum and therefore produces a better correlation.

When comparing all the trend lines, it is clear from Figure 6-11 that the filtered T_p and unfiltered T_p trends are very similar. It also shows that the trend for T_e and T_p using the Pierson-Moskowitz spectrum in Chapter 5.3 are similar.

In terms of power, Figure 6-12 indicates that P_{gen} displays a minor drop with T_p, which is a similar tendancy to before (Figure 5-6). P_{gen} for the hydraulic PTO is approximately 60% of P_{gen} for the linear PTO. However, it is important to note that the efficiency of the hydraulic PTO for these wave files is approximately 55-60% so the power captured by both PTOs is approximately the same.

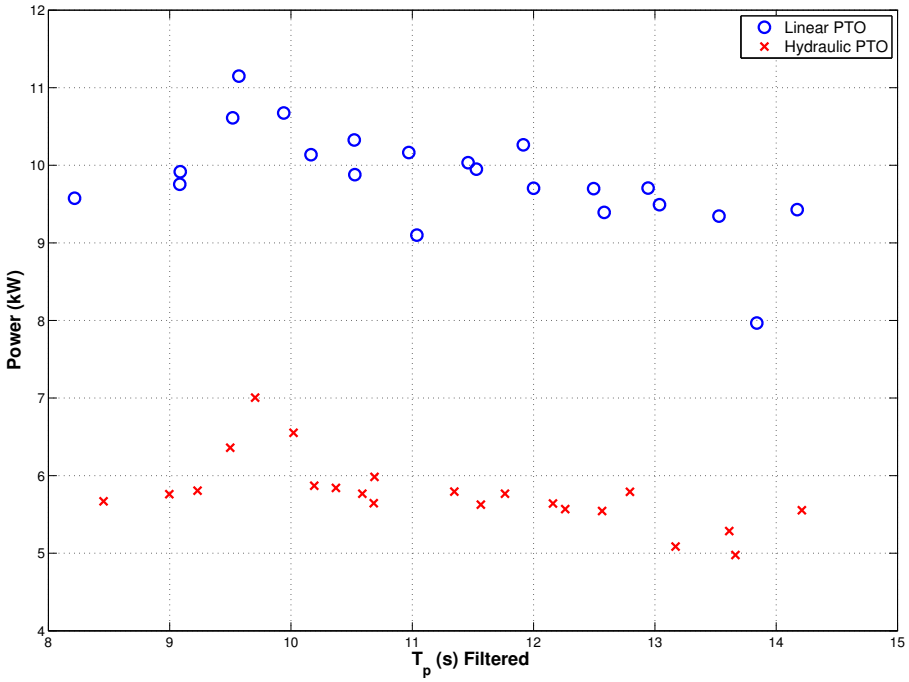

Figure 6-12: *Maximum power generated vs peak wave period for the linear and hydraulic PTO*

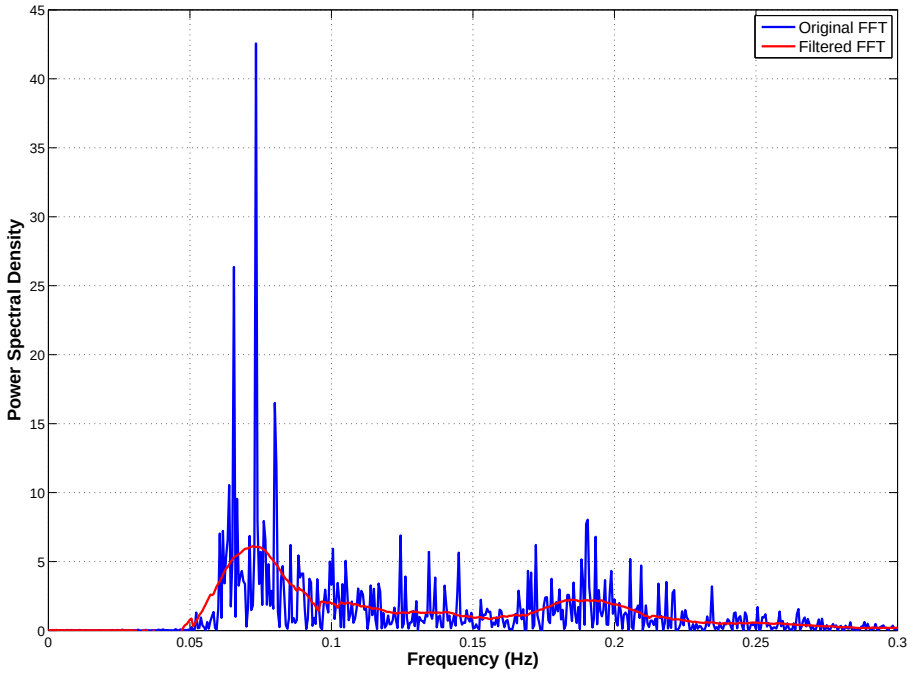

Figure 6-13: *Frequency spectrum of one EMEC file with two distinct peaks*

6.4 Real Time PTO tuning

The results have shown that a PTO can be tuned, to maximise power generation, by using T_e over a 30 minute time period. It is therefore beneficial to discover the best time period for which the PTO should be tuned. Four EMEC files, that were not used previously to determine the tuning trends, are chosen to investigate real time PTO tuning. Their parameters are presented in Table 6.3 and their filtered spectra are shown in Figure 6-14.

Wave Parameter	Sea States			
	1	2	3	4
Date & Time	10/04 03:30	21/04 20:30	05/04 13:30	12/04 13:30
H_s (m)	1.24	1.98	3.10	4.34
(Filtered) T_p (s)	11.92	10.34	11.61	12.95
T_e (s)	10.18	9.72	8.83	10.45

Table 6.3: *Parameters of the four EMEC files chosen for the real time PTO tuning*

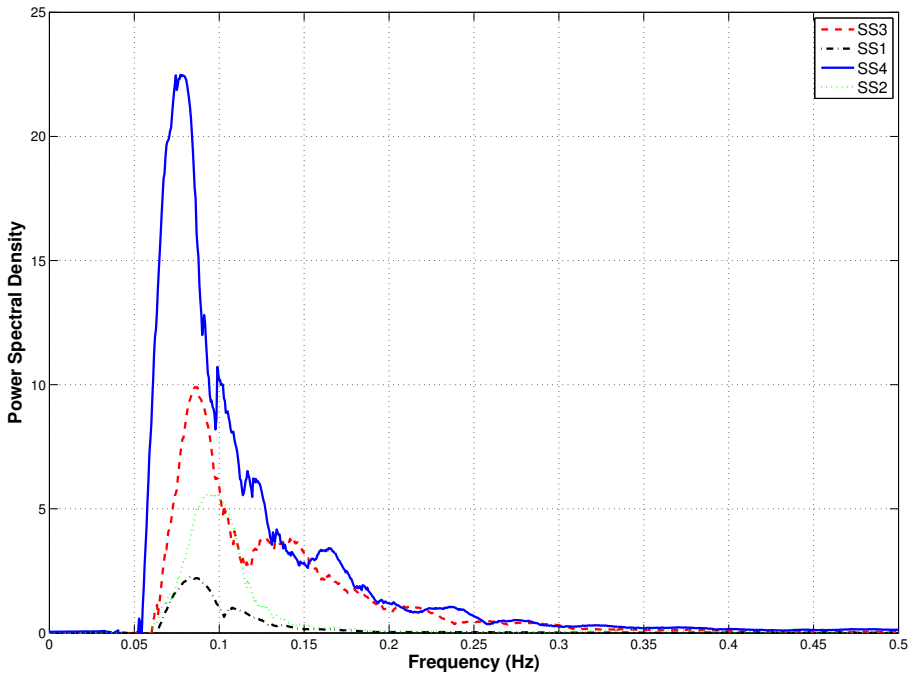

Figure 6-14: *Filtered spectra of the four EMEC files chosen for the real time PTO tuning*

Previous work into real time PTO tuning has shown an approximate doubling in power capture with a linear PTO by using an estimated wave frequency, cal-

culated on a 20 s moving average, rather than the constant energy frequency of the spectrum [10]. The estimated wave frequency is calculated using a windowed FFT of the wave displacement. Furthermore, it has been shown that active tuning methods generally outperform passive methods with a linear PTO. Passive methods assume the PTO settings to be fixed whereas the active methods assume that PTO settings can be constantly varying. The best active tuning technique uses a sliding FFT of the wave displacement with a sampling window of 200 s. In practice, however, it assumes future knowledge of the incident waves so it would require measurement of wave conditions upwind of the device [35].

Most recently, work has been presented which illustrates the advantages of estimating the suitable wave frequency information by using signal processing and filtering of the wave displacement signal [65]. It estimates the wave frequency information without future knowledge of the wave profile using the zero-upcrossing method to update the linear PTO settings every 2 - 3 s. The zero-upcrossing method measures each point at which the wave profile crosses the zero line upward. That point is taken as the start of an individual wave and the next zero-upcrossing point is taken as the end of that wave. The time period between the two adjacent zero-upcrossing points is defined as the wave period for that individual wave and the vertical distance between the highest and lowest points between the adjacent zero-upcrossing points is defined as the wave height.

In all the work to date it is assumed that the PTO is linear and the desired settings are achieved instantly. This work investigates methods to calculate wave frequency information which is then used as the input to an open loop controller for the tuning of the hydraulic PTO. The PTO damping (α) is adjusted according to the relationship to T_e established in Figure 6-10. This relationship is used as it provided the best correlation.

A base-line passive method uses the PTO damping for the mean site energy frequency (T_e= 9.20 s). The mean site energy frequency is calculated from the two months of data which have been collected. Ideally this would be an average over a number of years of full data but this is not available. Four active methods are investigated which assume that future prediction of wave displacement is not possible, so the PTO is tuned to the energy frequency calculated from a time period (window length) of preceding wave displacement data which is updated every 20 s.

It is assumed that the demand signal for α is transmitted to the PTO instantaneously but any change in motor displacement (D_m) or generator load (C_g) to

produce the required α will be subject to the dynamics stated previously (equation 5.16). Furthermore, closed loop motor control is implemented, like in Section 5.4, to maximise P_{trans}. The overall tuning and control arrangement is shown in Figure 6-15.

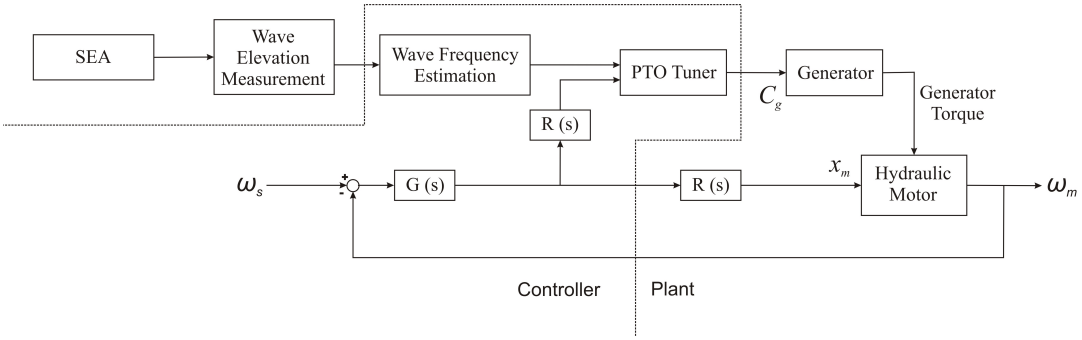

Figure 6-15: *PTO Tuning and Motor Control Block Diagram*

Strategy	Notation	Window Length
Passive	P	Site Average
Active	A1	30 mins
	A2	10 mins
	A3	3 mins
	A4	30 s

Table 6.4: *Parameters of the five tuning strategies for the hydraulic PTO*

Strategy	Power (kW)			Efficiency (%)		
	P_{cap}	P_{gen}	P_{trans}	η_{pto}	η_{trans}	η_{tot}
P	1.13	0.18	0.18	16.2	98.7	16.0
A1	1.11	0.17	0.17	15.6	98.4	15.4
A2	1.12	0.18	0.17	15.7	98.6	15.5
A3	1.10	0.16	0.16	14.6	98.6	14.4
A4	1.10	0.16	0.16	14.6	98.5	14.4

Table 6.5: *Results for SS1 comparing the different tuning methods*

In general, the results show that there is only a marginal gain, if any, from using active tuning methods (Tables 6.5 to 6.9). The captured power (P_{cap}) is effectively the same for all the methods but there are slight variances in the generated (P_{gen}) and transmitted power (P_{trans}). The biggest gain is for the highest energy sea state (SS4) where the active methods out perform the passive method by at least 20% (in terms of P_{trans}). This is probably because T_e for SS4 has the biggest difference from the site average value.

Strategy	Power (kW)			Efficiency (%)		
	P_{cap}	P_{gen}	P_{trans}	η_{pto}	η_{trans}	η_{tot}
P	6.21	3.41	3.40	54.8	99.7	54.7
A1	6.17	3.42	3.42	55.4	100	55.4
A2	6.16	3.42	3.42	55.4	100	55.4
A3	6.15	3.41	3.41	55.5	100	55.5
A4	6.16	3.41	3.38	55.3	99.2	55.3

Table 6.6: *Results for SS2 comparing the different tuning methods*

Strategy	Power (kW)			Efficiency (%)		
	P_{cap}	P_{gen}	P_{trans}	η_{pto}	η_{trans}	η_{tot}
P	15.7	9.38	6.75	59.6	72.0	42.9
A1	15.8	9.26	6.48	58.6	70.0	41.0
A2	15.8	9.26	6.43	58.6	69.4	40.7
A3	15.8	9.32	6.67	59.0	71.5	42.2
A4	15.7	9.27	6.64	58.9	71.6	42.2

Table 6.7: *Results for SS3 comparing the different tuning methods*

Strategy	Power (kW)			Efficiency (%)		
	P_{cap}	P_{gen}	P_{trans}	η_{pto}	η_{trans}	η_{tot}
P	28.2	16.5	4.81	58.5	29.1	17.0
A1	28.3	17.4	6.43	61.4	37.0	22.7
A2	28.3	17.4	6.51	61.6	37.5	23.1
A3	28.3	17.3	6.27	61.2	36.2	22.2
A4	28.2	17.1	5.89	60.5	34.5	20.8

Table 6.8: *Results for SS4 comparing the different tuning methods*

Strategy	Sea States				Average
	1	2	3	4	
P	0.18	3.40	6.75	4.82	3.79
A1	0.17	3.42	6.48	6.43	4.12
A2	0.17	3.42	6.43	6.51	4.13
A3	0.16	3.41	6.67	6.27	4.13
A4	0.16	3.38	6.64	5.89	4.02

Table 6.9: *The transmitted power in kW for each sea state using the active and passive tuning methods*

Figure 6-16 shows how the estimated energy period (T_e) and PTO damping (α) vary with time for the different control strategies. For A4 there are large fluctuations in T_e between consecutive discrete values but these variations reduce as the window length of the strategies increases.

For SS4 the largest P_{trans} is for method A2. For shorter window lengths, like A4, there can be large transient waves which have a major affect on the estimated T_e. A2 gives a good balance between determining an underlying change in wave frequency but it analyses enough preceding data to not be affected by large transients.

The advantages of using a shorter window length is the reduction in the capacity required to store preceding data but with the passive method there is no requirement for data storage or online calculations. The results for these sea states show only a minor reduction in transmitted power with the passive method but this is expected to increase as the energy period shows more discrepancy to the average site value.

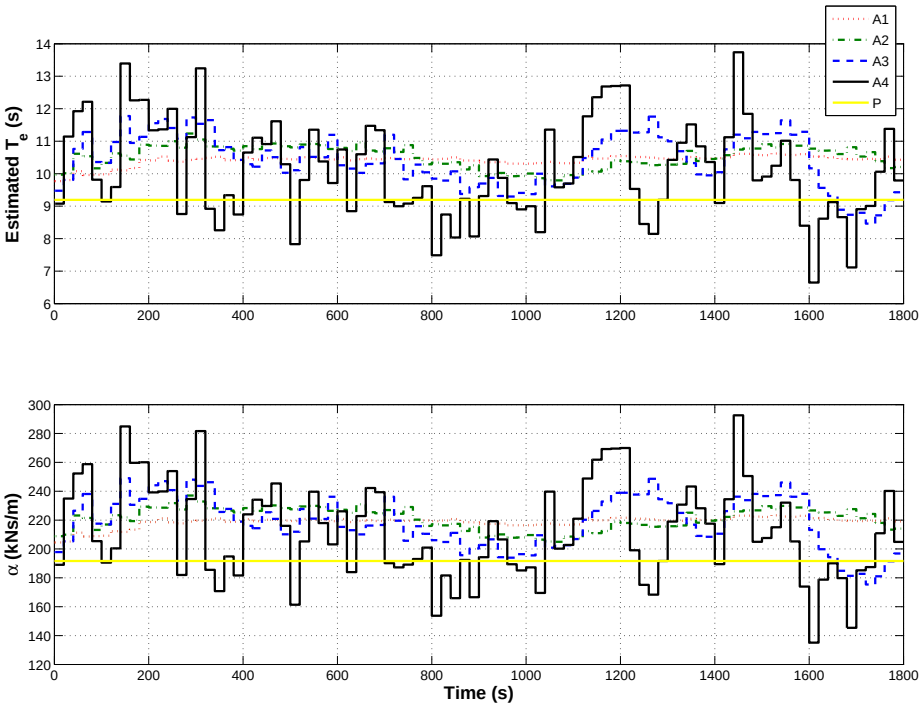

Figure 6-16: *Estimated T_e and corresponding α for the control strategies for SS4*

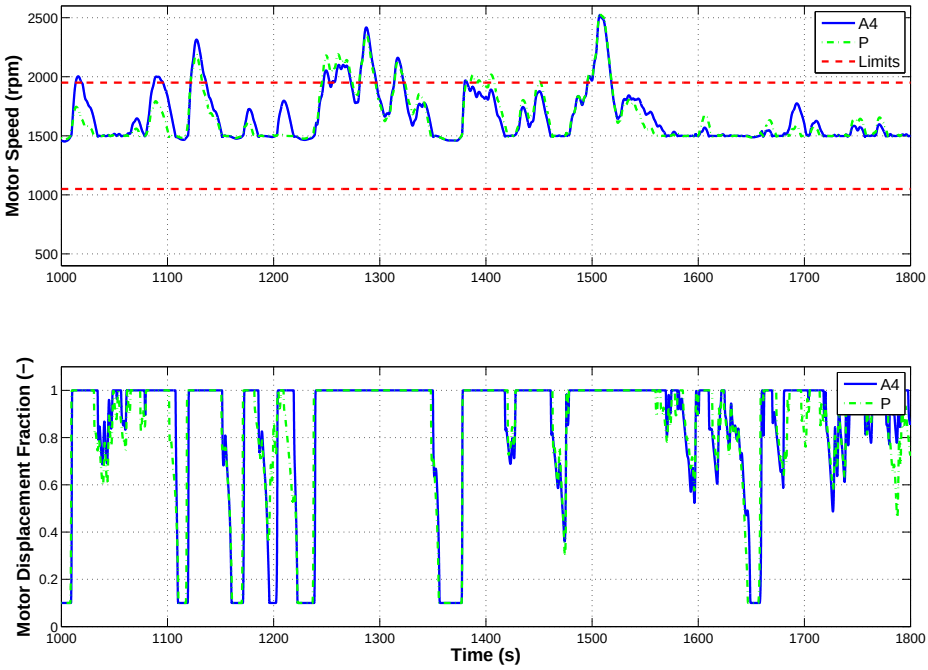

Figure 6-17: *Comparison of motor displacement fraction and motor speed for control strategies P and A4 for SS3*

6.4.1 PTO Tuning To Future Wave Data

Results show that active tuning of the PTO, using preceding wave displacement data, does not provide a meaningful gain in P_{trans} compared to passive tuning. However, if the future wave displacement could be predicted by measurement buoys upwind of the WEC or by wave prediction algorithms, would this provide a large gain in generated power? Previous work has shown this to be true for a linear PTO [35] but this work will investigate if it is valid for a hydraulic PTO model.

The tuning method predicts T_e from a future window length of 20 s and it uses the same trend to modify α accordingly. The results, presented in Table 6.10, indicate that there is only a minimal gain from using a future wave prediction method when compared to the passive tuning method. The future method only gives a higher P_{trans} for SS4 compared to the passive method and it constantly performs worse than the active methods, which use the preceding wave data.

Therefore, this indicates that there is no gain from using algorithms or nearby measurement buoys to predict the future wave behaviour. Overall, the best tuning

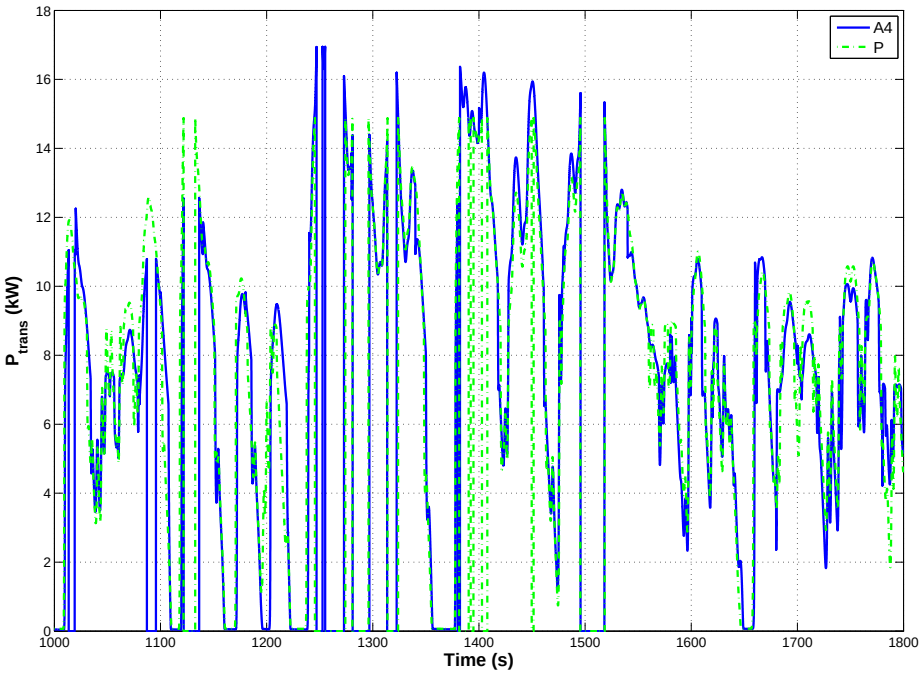

Figure 6-18: *Comparison of transmitted power for control strategies P and A4 for SS3*

Strategy	Power (kW)	Sea States			
		1	2	3	4
Future	P_{cap}	0.97	6.19	15.7	28.4
	P_{gen}	0.11	3.38	8.99	17.1
	P_{trans}	0.10	3.37	5.79	5.41
Passive	P_{cap}	1.13	6.21	15.7	28.2
	P_{gen}	0.18	3.41	9.38	16.53
	P_{trans}	0.18	3.40	6.75	4.82

Table 6.10: *The power for each sea state for the future and passive tuning methods*

method is an active method which determines only a fundamental change in the energy frequency of the waves and therefore gradually changes the PTO damping to tune the device correctly. It is important to note that the presented P_{trans} values are still subject to the inefficiencies of the generator.

6.5 Concluding Remarks

Wave data, recorded at the European Marine Energy Centre, was presented at the start of the Chapter. The derivation of important wave parameters was explained and results presented for two months of data from 2011, which highlighted key differences between the two months. The calculation of the wave excitation force from the raw wave displacement was presented. This was required as it is the input to the simulation model of the device. The simulation model was then used to determine the relationship between the peak and energy wave period and the optimum PTO damping for a number of wave files with varying parameters. The best fit and most similar trend to Chapter 5 was found by comparing the wave energy period and the PTO damping.

An open loop tuning method was then investigated, which uses preceding wave displacement data to tune the PTO according to the wave energy frequency. Different time periods of data were analysed for the active methods and compared to a passive method which tuned the PTO to an average site frequency. The results show that the tuning of a hydraulic PTO to an estimated wave frequency is a difficult task. Even if the wave frequency can be estimated accurately and the PTO damping adjusted immediately, the PTO force will not change instantly due to the dynamics of the hydraulic PTO. It may therefore be sufficient to adjust the PTO damping according to an estimated wave frequency over a longer time frame, which will detect a fundamental change in the wave frequency rather than react to each transient wave.

Section 6.3 shows that there is an optimum PTO damping, to maximise power generation, which is dependent on the energy period of the incoming waves. That section of work assumed the knowledge of future wave conditions was possible and the data was analysed for a 30 minute period. The PTO was, therefore, not tuned to each individual wave but to the wave frequency with the highest available energy over this period. However, Section 6.4 shows that the tuning of the PTO to an estimated energy period using preceding wave data does not necessarily improve power generation. This is for a number of reasons:

- **The random nature of waves**. Previous wave data may show no correlation to the future wave data
- **The PTO force magnitude does not change instantly**. Due to the dynamics of the PTO, there is a delay between varying the PTO damping

and a change in the PTO force magnitude. Therefore, the active tuning methods with the large changes in PTO damping may not have sufficient time to achieve the desired change in PTO force.

- **There is minimal variation in the generated power from a small change in PTO damping**. The constant PTO damping for the passive method is around the mean value for each of the active methods so the PTO is never completely de-tuned (Figure 6-16) and the power values are therefore very similar.

The best active method was one which analysed a sufficiently long preceding period of data to determine any fundamental change in wave frequency and so did not react to each individual wave. Power generation is expected to improve from using active tuning as the energy frequency of the waves deviates further from the average site value. Knowledge of the future waves provided no improvement.

Finally, the results have illustrated again that there is a large power loss in the PTO. This is due to two main reasons:

- **The inefficiency of the PTO**. There is significant power loss in the components of the PTO especially the hydraulic motor. For example, in low energy seas the small motor displacement required to maintain the synchronous speed means that the motor efficiency is always very low so the mechanical power that is captured by the PTO can not be converted efficiently.

- **The transmission of generated power to the electrical generator**. In high energy seas, there is a significant drop between the generated power and the transmitted power because the motor displacement is not large enough to maintain the synchronous speed. Therefore, even though the PTO efficiency is adequate, a significant portion of the generated power will be lost (Figures 6-17 and 6-18).

CHAPTER 7

EXPERIMENTAL PTO TUNING

To validate the simulation results, the dynamics of a hydraulic PTO were investigated on an experimental rig. The design of the experimental PTO rig is presented and measured behaviour is compared to a simulation model of the rig. The PTO is then incorporated into a hardware-in-the-loop model, where the hydrodynamic action of the buoy is modelled by simulation but the action of the hydraulic PTO is real. The study focuses on tuning the PTO to maximise power generation by altering the force that it produces.

7.1 Experimental Setup and Procedure

A scaled-down PTO was developed and tested using a laboratory rig. The rig was designed and built by the author, who also collected the data. The wave force was simulated in real-time and applied to the PTO using a hydraulic actuator. This actuator is under closed-loop PI position control. The driving actuator has a velocity limit of approximately 0.35 m/s due to the limitations of the pump and servo valve that control it.

The full scale hydraulic PTO model used throughout the simulation work included an equal area actuator. However, an unequal area actuator, with area ratio approximately 2:1, was used for the experimental PTO. Therefore, the rectifying circuit has been modified to ensure a similar flow is produced in both extension and retraction whilst maintaining a similar overall PTO behaviour. A similar design was proposed for a regenerative shock absorber in race cars [80]. Figure 7-1 illustrates the hydraulic circuit for the experimental PTO, with the

modified rectifying circuit highlighted.

This design means that the piston chamber (2) re-feeds the annulus chamber (1) in compression mode (i.e linear actuator retraction). Therefore, during compression mode the flow produced by the boost pump is re-circulated to tank and the rectified flow is approximately half of the piston flow due to the area ratio. In extension mode the rectified flow equals the annulus flow and the LP accumulator recharges the piston chamber. The boost pump re-feeds the hydraulic motor case drain flow and prevents cavitation.

As with an equal area actuator, the rectifying circuit means that irrespective of the direction of piston motion the hydraulic motor turns in the same direction. Furthermore, the accumulators provide the same power smoothing function but they are reduced in volume.

In contrast to the simulated PTO, the hydraulic motor on the experimental PTO is a fixed displacement gear motor and the load applied to the DC generator is constant. Therefore, to enable the PTO force to be variable a throttle valve is included before the hydraulic motor. By adjusting the throttle valve, the system pressure can be varied to alter the PTO force. This has the same effect as varying the displacement of the hydraulic motor or the generator load in the simulated PTO. However, the throttle valve adds a significant pressure loss to the system, which needs to be accounted for when investigating PTO efficiency. Table 7.1 provides a summary of the component values.

Six transducers measure the pressure at suitable points in the hydraulic circuit.

- Piston chambers (P1 and P2)
- Before and after the high pressure accumulator (P3 and P4)
- Before and after the hydraulic motor (P5 and P6)

Two flow meters (F1 and F2) are placed before and after the high pressure accumulator to measure the smoothing effect and a load cell is attached to the hydraulic piston to measure the force which it produces. Piston position is measured using an LVDT. All the sensors were calibrated offline before being connected to the rig to ensure accuracy. The signals were recorded with a sampling frequency of 1000 Hz and low pass filtered using a 6th order phase compensated Butterworth filter with a 5 Hz cut off frequency.

Figures 7-2 and 7-3 are photographs of the rig, which help to show the overall design and arrangement.

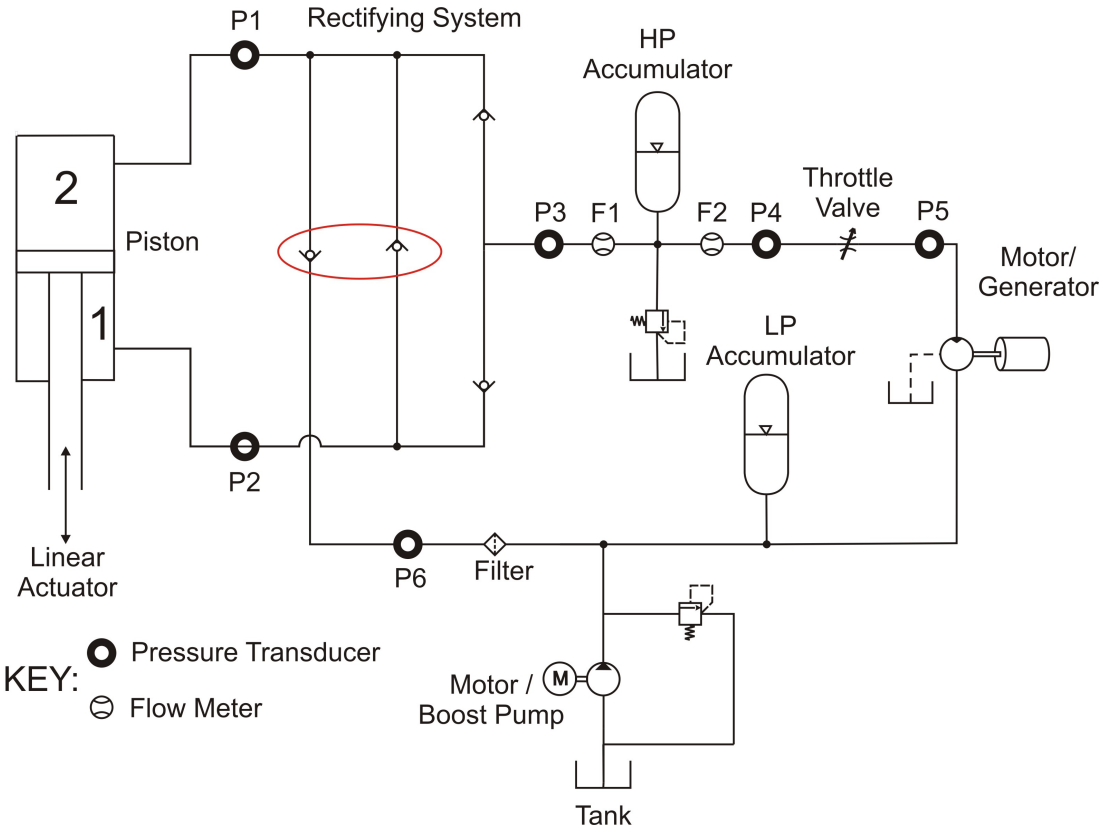

Figure 7-1: *The hydraulic circuit diagram for the experimental PTO*

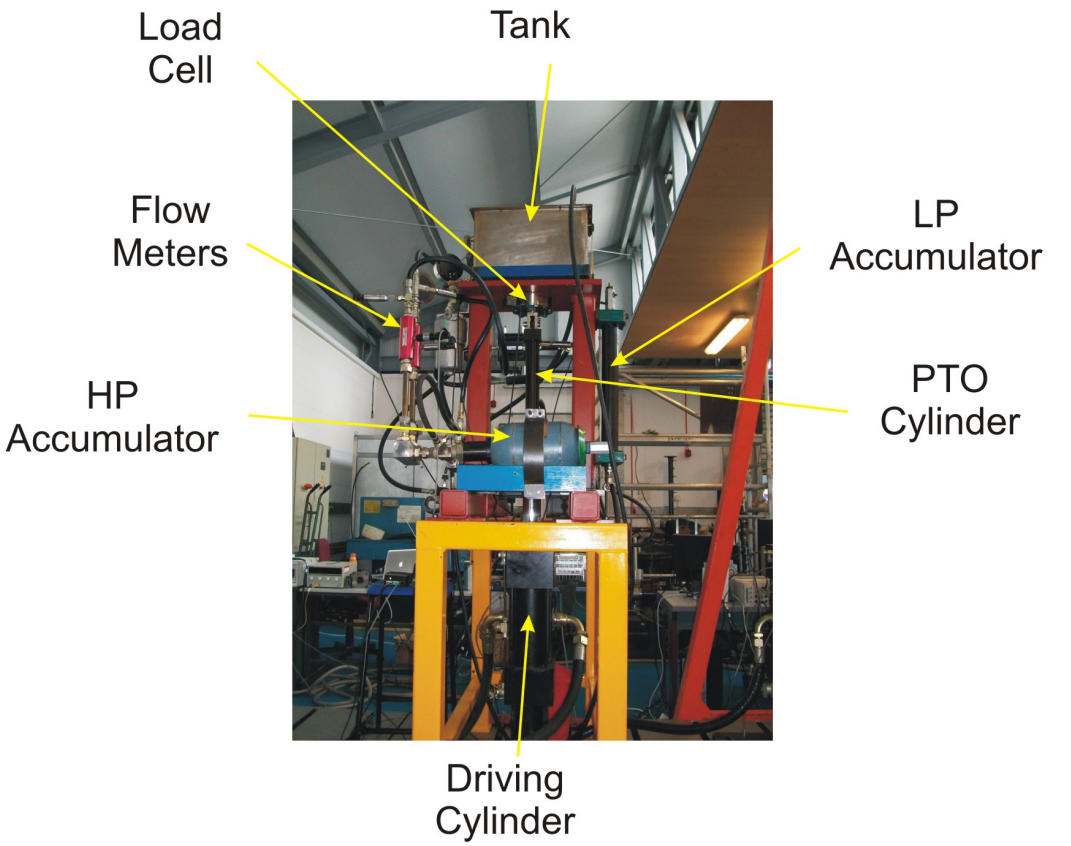

Figure 7-2: *Front view of the PTO rig*

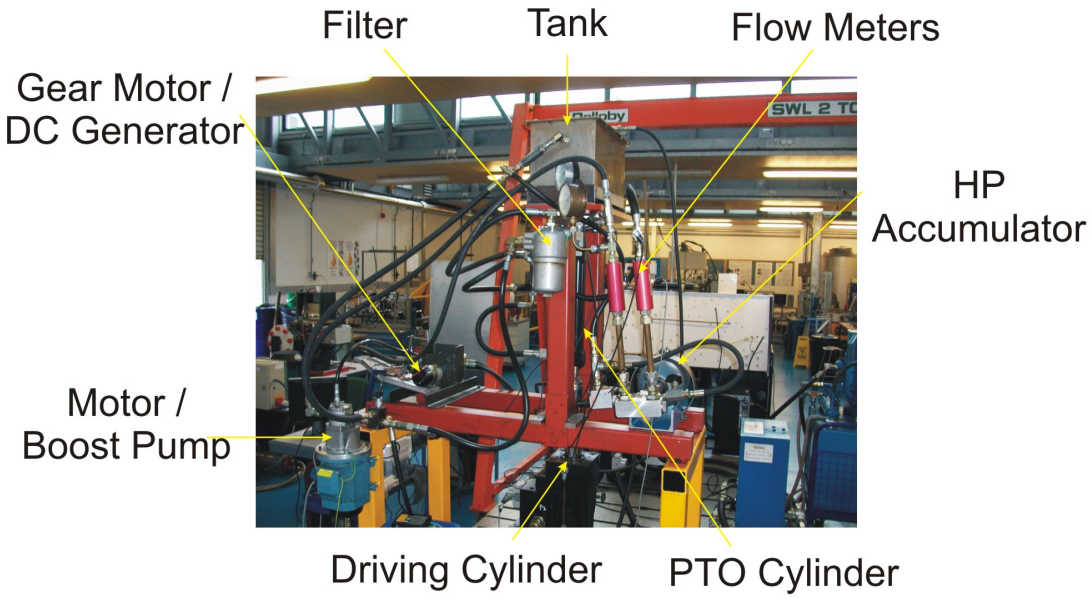

Figure 7-3: *Side view of the PTO rig*

Maximum system pressure	100 bar
PTO Cylinder	
Bore Diameter	40 mm
Rod Diameter	28 mm
Stroke	±150 mm
HP Gas Accumulator	
Pre-charge Pressure	10 bar
Volume	3.8 L
LP Gas accumulator	
Pre-charge Pressure	2 bar
Volume	1.0 L
Gear Motor	
Capacity	4.0 cc/rev
DC Generator	
Rated Power	90 W
Rated Speed	3000 rpm
Resistance	0.6 Ω
Boost Pump	
Capacity	4.0 cc/rev
Rated Flow	6 lpm
Relief valve pressure	7 bar
Driving Cylinder	
Maximum Force	20 kN
Maximum Velocity	≈ 0.35 m/s
Stroke	±125 mm

Table 7.1: *Experimental PTO and Rig main component values*

7.2 PTO Modelling

One of the main motivations for the experimental work is to use the data to validate the simulation results, and in particular the PTO tuning. Because the PTO rig is scaled and the PTO design has been modified, a new simulation model was created in Simulink to replicate the design and size of the PTO rig. The simulation model has been created with some assumptions.

- There are no pressure losses in the pipes
- A constant generator load has been estimated from the resistance of the DC generator on the rig
- The hydraulic motor efficiency is assumed to be constant

The piston stroke of the rig is a tenth of the stroke in the full scale simulation model so, to maintain an equivalent piston velocity in the rig, the frequency of the input wave has been increased. However, it is important to note the velocity limit of the driving actuator. For model validation, the actuator position of the driving cylinder was used as the input signal to the rig. Figures 7-4 to 7-6 show the result for a sine wave amplitude of 125 mm and a frequency of 0.33 Hz.

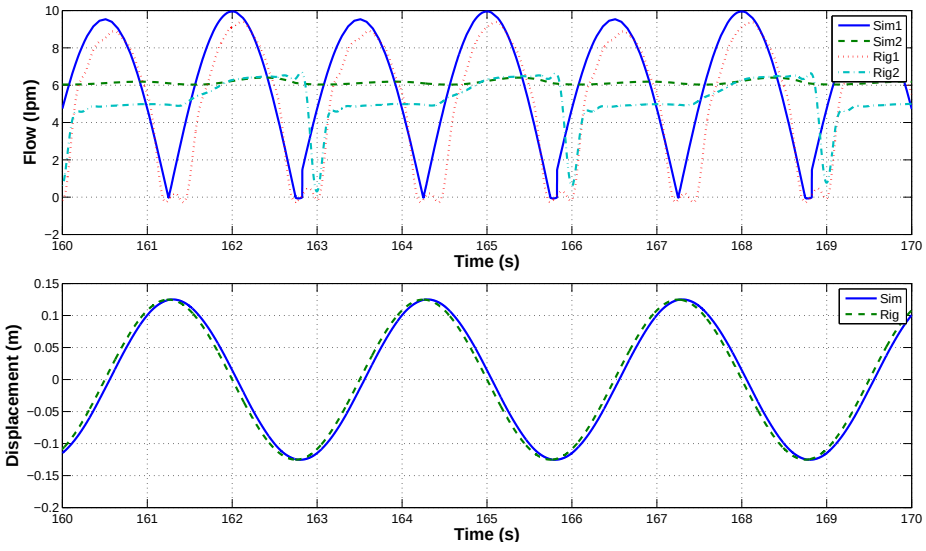

Figure 7-4: *Top: Flow meters 1 and 2. Bottom: Actuator position*

The only comparable results in the literature are presented in [28] so all the results gained by a rig of this kind are valuable. The experimental results give a

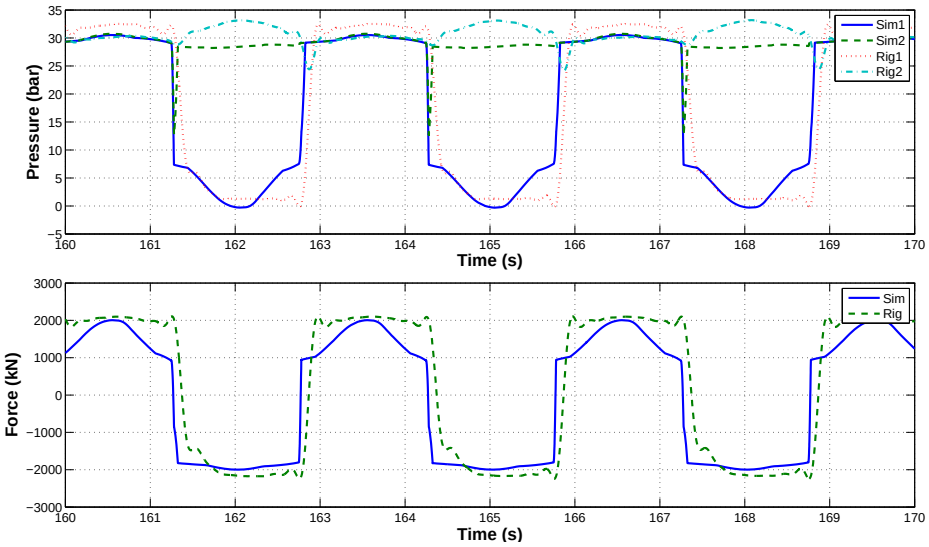

Figure 7-5: *Top: Piston chamber pressures (P1 and P2). Bottom: PTO Force*

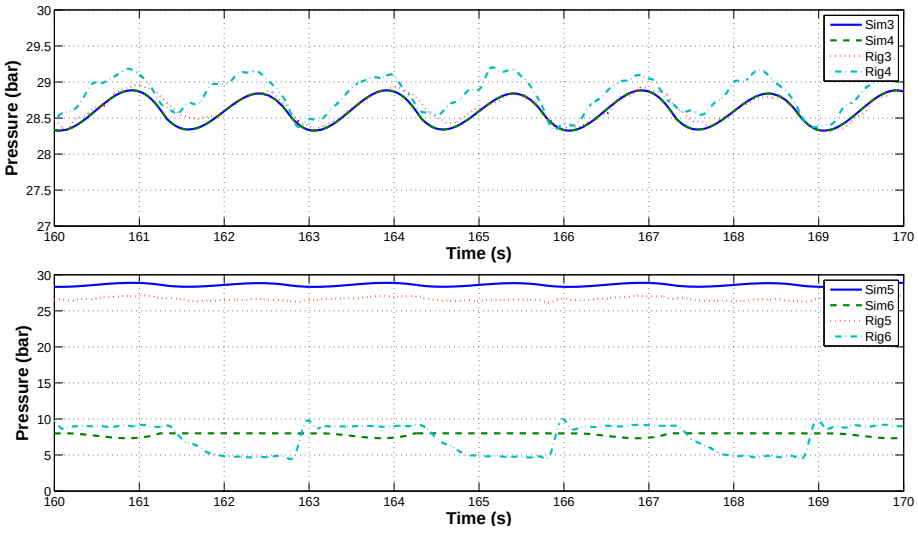

Figure 7-6: *System Pressures. Top: P3 and P4. Bottom: P5 and P6*

good validation to the simulation model and are comparable to the results found in [28]. Figure 7-4 shows that the driving actuator is able to follow the input signal as it is within the velocity limit. The rectified flow (F1) and flow to the motor (F2) are slightly lower for the rig than the simulation. This may be a result of increased piston friction in the rig. Additionally, the dynamic performance of the flow meters is poor so there is a phase delay between the two signals.

Figure 7-5 reveals that the piston chamber pressures show a good correlation. For the experimental results, there is a larger pressure drop across the check valve on the compression stroke when the piston chamber re-feeds the annulus chamber but the shape and magnitude of the signals are similar. This means that the PTO force signals are very similar with both exhibiting a Coulomb type damping force.

Figure 7-6 indicates the same pressure before and after the accumulator for the simulation. There is a slight pressure increase with the experimental results, which is assumed to be because of a small calibration error and due to the accumulator. The results verify the desired smoothing effect of the accumulators with the relatively constant pressure and oil flow to the hydraulic motor.

The throttle valve is fully open for this test so for the simulation P5 = P4. However, on the rig there is a pressure drop in the pipework which is not accounted for in the simulation. The pressure drop across the motor (P5 - P6) is similar for both cases. However, P6 shows a larger fluctuation with the experimental results. When the check valve opens on the extension stroke to allow the low pressure accumulator and boost pump to re-circulate oil to the piston, there is a pressure drop due to the pipe and filter. This pressure drop is not accounted for in the simulation. Therefore, the pressure relief valve on the simulation has been set slightly lower to account for this and give a similar piston chamber pressure.

It is noted that the results of the experimental rig are not shown in comparison to the non-linear idealised PTO model in this work. When these results are compared there is an appreciable reduction in the system pressure and therefore PTO force amplitude. For both models there is a similar pressure difference across the hydraulic motor due to the same generator damping but due to the idealised nature of the hydraulic components there are no pressure losses in the rectifying valves and the hydraulic cylinder so the PTO force is reduced for the idealised model.

7.3 Hardware-in-the-Loop Model

To investigate how the experimental PTO would interface with a real device it is necessary to use a hardware-in-the-loop system (HIL). This enables the full action of the device to be replicated without a wave tank. A real-time model calculates the buoy position from the estimated wave force and measured PTO force acting on the buoy mass. The buoy position is used as a demand signal for the driving actuator position control loop. $G(s)$ is the transfer function of the position controller as given in equation 5.15. The arrangement is shown in Figure 7-7.

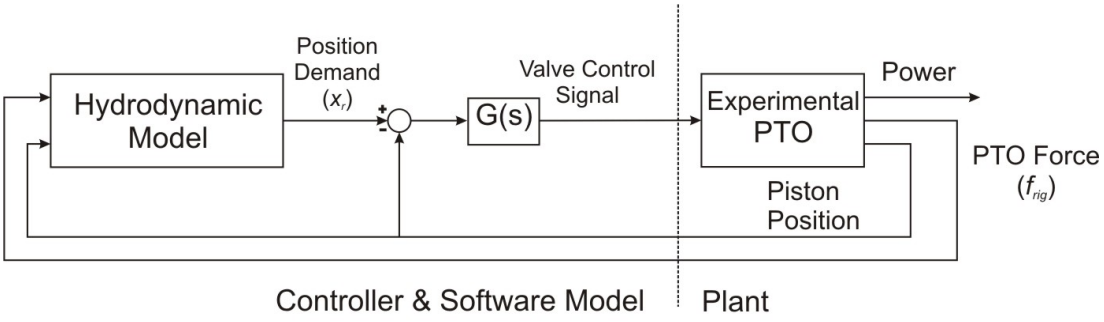

Figure 7-7: *Hardware in the loop system*

As the experimental PTO is scaled down, scaling factors must be incorporated into the model to maintain a piston velocity which is equivalent to the full size simulated model. Furthermore, the wave forces must be scaled to maintain the correct magnitude to ensure the overall behaviour of the device is equivalent to the full size system. As only regular waves will be simulated, the following expression (equation 3.15) is valid

$$(m + A)\ddot{x} + B\dot{x} + \rho g S x = f_e + f_m \tag{7.1}$$

Transforming into the frequency domain:

$$\left(-(m + A)\omega^2 + B\omega + \rho g S\right) X(j\omega) = F_e(j\omega) + F_m(j\omega) \tag{7.2}$$

Introducing a displacement scaling factor (k_z) and a frequency scaling factor (k_ω) such that:

$$k_z = \frac{x}{x_r} \tag{7.3}$$

$$k_\omega = \frac{\omega_r}{\omega} \tag{7.4}$$

$$f_{rig} = \frac{f_m}{k_z} \tag{7.5}$$

where ω_r is the rig frequency of the wave, x_r is the rig displacement and f_{rig} is the PTO force produced by the rig. Therefore the equation of motion for the rig can be re-written as:

$$\left[\frac{-(m+A)}{k_\omega^2}\omega_r^2 + \frac{B}{k_\omega}\omega_r + \rho g S\right] X_r(j\omega) = \frac{F_e(j\omega)}{k_z} + F_{rig}(j\omega) \tag{7.6}$$

The magnitude of the excitation force (f_e) is calculated using the original wave frequency but its frequency is adjusted according to the frequency scaling factor (k_ω). It is understood that F_{rig} will not be sinusoidal in reality but it is assumed that the model can be implemented using the transfer function in equation 7.6. Ideally, the measured position and the position demand would be the same. For this work the measured piston position is used in the hydrodynamic model but further analysis is required to determine if using the position demand would cause any major change.

Wave Excitation Force		Scaling Factors	
Period (s)	Amplitude (m)	k_r	k_ω
10	1.0	10	5

Table 7.2: *The wave parameters and scaling factors used to verify the HIL model*

The wave input and scaling factors given in Table 7.2 are used to validate the HIL model. Figures 7-8 to 7-10 are generated with a relatively open throttle to ensure a low system pressure and PTO force. Figure 7-8 shows a strong correlation between the piston position for the offline simulation and rig. This indicates that the dynamics required by the HIL model are within the capabilities of the driving actuator. Figure 7-9 reveals a good equivalence between the piston chamber pressures and the PTO force. There is a slight phase difference because of the instantaneous change in pressure for the simulation model.

Figure 7-10 shows a larger pressure drop across the rectifying circuit for the experimental result and it indicates the same minor pressure increase across the accumulator. For the simulation, there is a larger pressure drop across the throttle valve, which compensates for the zero pressure drop in the pipes. The pressure drop across the motor is marginally larger for the simulation to compensate for the pressure drop between P6 and P1 on the rig. This ensures that the piston pressures and PTO force are equivalent.

Figure 7-8 reveals a larger phase difference between the simulated and experimental rectified flows (F1) due to the poor dynamic performance of the flow meters. For the simulation, there is an appreciable difference in the rectified flow magnitude for the different directions of motion for the simulation. This is due to a non-symmetrical velocity signal, which is a function of the non-symmetrical PTO force signal. This is not the case for the experimental rig so the rectified flow magnitudes are similar.

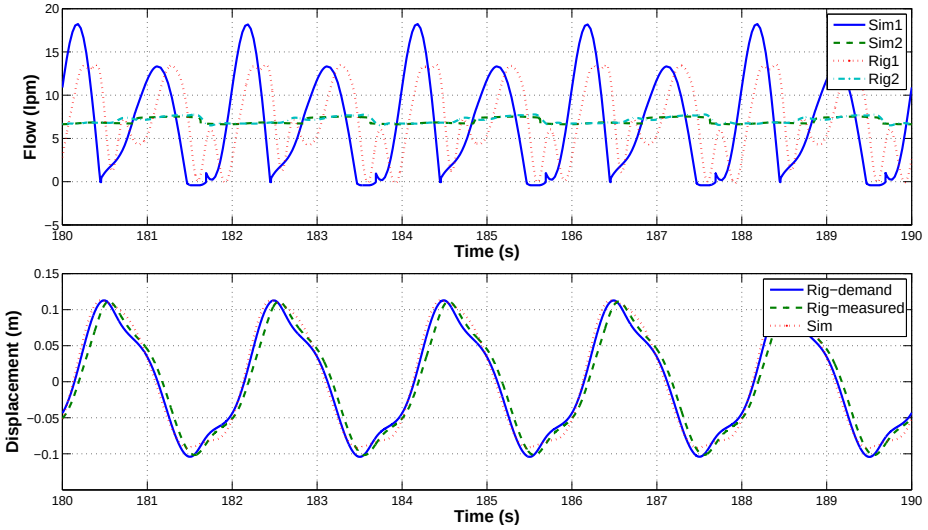

Figure 7-8: *Low Pressure- Top: Flows (F1 and F2), Bottom: Piston position*

Figures 7-11 to 7-13 are generated with a more throttled flow to give a higher system pressure and larger PTO force. It is clear that with this higher PTO force, there is a contrast between the piston dynamics for the HIL and offline simulation models. The piston displacement for the simulation model is larger because the velocity amplitude is greater than the capability of the driving actuator for the HIL model. Therefore, the HIL model settles to a different steady state because the rig can not produce the same dynamics, which has an effect on the wave forces in the closed loop model. If the displacement scaling factor is reduced to reduce the piston velocity the flow becomes too low for the flow meter to give a reliable reading.

Both HIL and offline simulation results show an induced body stall effect because the PTO force is larger than the wave force for a greater period of the wave cycle. Furthermore, the rectified flow is different for the two models because of the different piston dynamics.

Figure 7-12 indicates similar piston chamber pressures but there are oscilla-

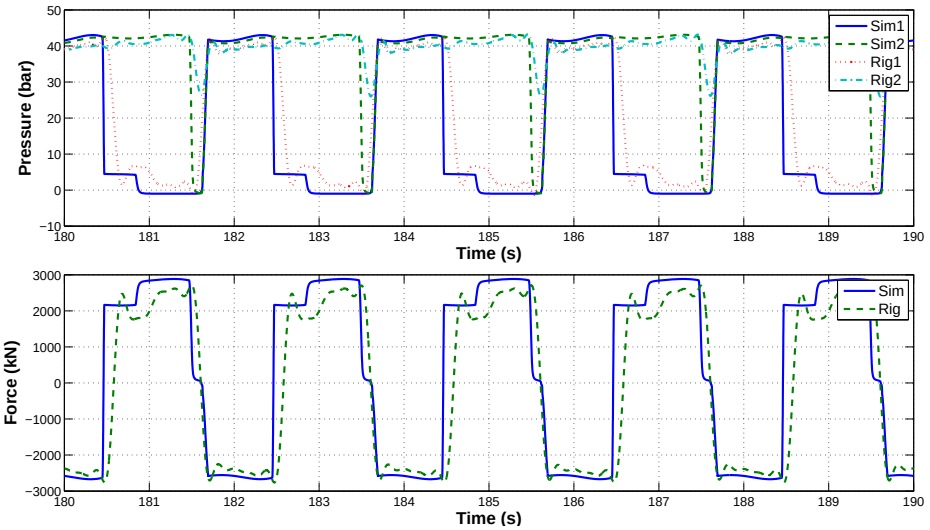

Figure 7-9: *Low Pressure- Top: Piston chamber pressures (P1 and P2). Bottom: PTO Force*

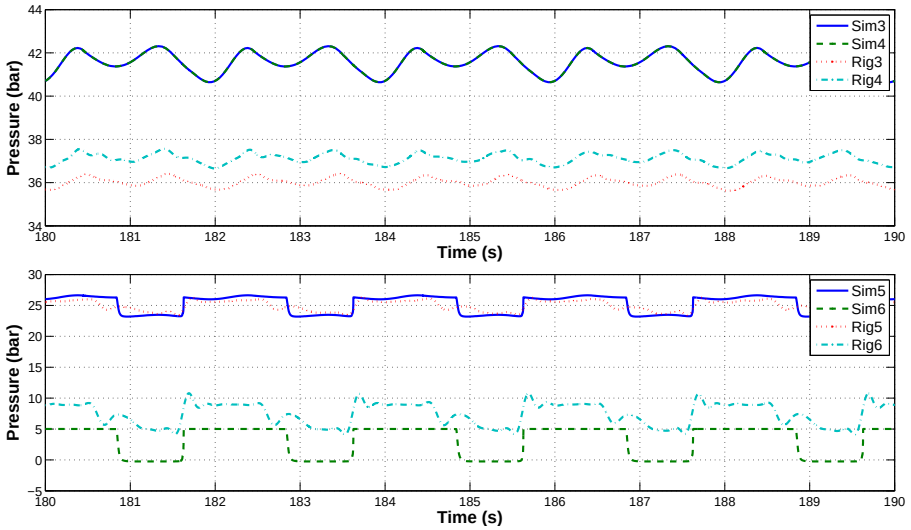

Figure 7-10: *Low Pressure- System Pressures. Top: P3 and P4. Bottom: P5 and P6*

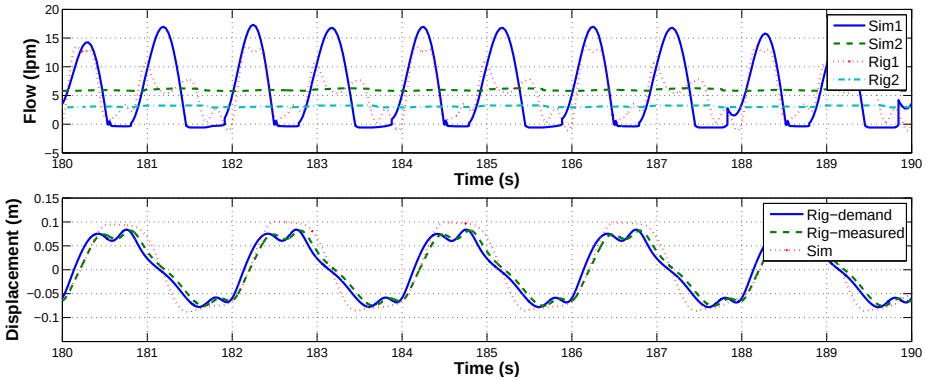

Figure 7-11: *High Pressure- Top: Flows (F1 and F2), Bottom: Piston position*

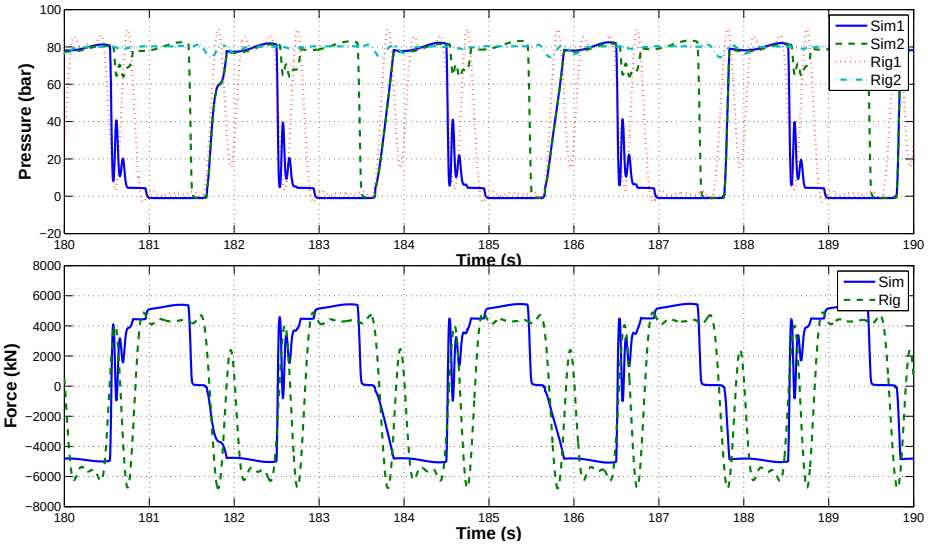

Figure 7-12: *High Pressure- Top: Piston chamber pressures (P1 and P2). Bottom: PTO Force*

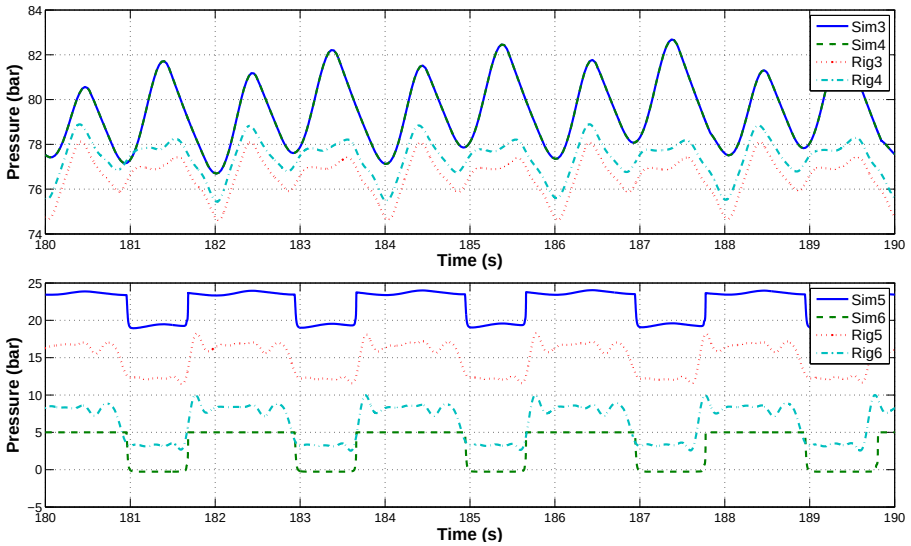

Figure 7-13: *High Pressure- System Pressures. Top: P3 and P4. Bottom: P5 and P6*

tions for the experimental result due to the piston dynamics. The PTO force gives a good agreement. Figure 7-13 points toward a similar pressure drop across the rectifying circuit. The individual pressure drops across the throttle valve and motor are marginally different but the total pressure drop is similar for both models.

It is clear that the main limitation in the HIL system is the velocity amplitude of the driving cylinder. It is expected that if this velocity amplitude could be increased the experimental result would also match the simulation model for the higher system pressure.

Overall, the experimental results are consistent with the PTO behaviour found, by simulation, in Section 3.3.1. The experimental PTO produces the same Coulomb type damping force and the accumulators provide the desired smoothing effect to the rectified flow and system pressure.

7.4 Experimental PTO Tuning

To examine the tuning of the experimental PTO, the PTO force must be altered by throttling the flow. The generated power is assumed to be equal to the hydraulic fluid power before it is dissipated through the throttle valve. It is calculated as the pressure drop across the throttle valve and motor multiplied by the mean flow out of the accumulator, which at steady state is equal to the

mean flow into the accumulator. The same wave parameters and scaling factors are used as before (Table 7.2).

Figure 7-14 reveals a comparable tuning trend between the HIL system and offline simulation. Generated power is lower for the experimental result because of the extra pressure losses in the rectifying circuit and reduced flow due to the added piston friction and the lower piston velocities at the higher PTO forces. However, the results indicate a similar optimum PTO force amplitude for both models. The full results are given in Appendix C.

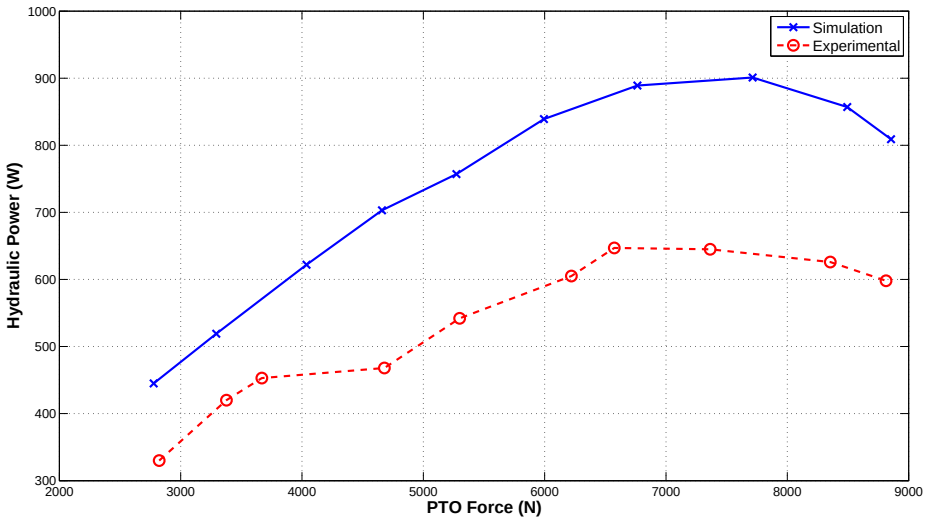

Figure 7-14: *Hydraulic Power against PTO force for the simulation and experimental HIL models*

7.5 Concluding Remarks

This chapter displayed the experimental results for a PTO test rig developed in the laboratory. The PTO design was modified due to size restrictions and component availability. A circuit design suitable for an unequal area cylinder was used. A driving actuator was used to replicate the wave force and hence remove the need for a wave tank.

The main motivation of the experimental work was to validate the simulation results. Firstly, a sine wave input was used to investigate the behaviour of the experimental PTO and the results were found to be in good agreement with a PTO simulation. A hardware-in-the-loop system was created to investigate how the experimental PTO would interact with a hydrodynamic model of a heaving buoy. The hydrodynamic force was simulated using real-time software but scaling factors needed to be introduced to enable this to be used with the small scale experimental PTO. The HIL model gave good agreement for a low PTO force but this reduced for a high PTO force because the velocity of the driving actuator was insufficient. However, the experimental results still demonstrate the effect of the PTO force on the system dynamics with a higher PTO force causing a greater induced body stall. By altering the PTO force, the generated power could be affected and the device could be tuned to an incoming wave condition.

Overall the experimental results give confidence in the simulation results which have been found previously. The behaviour and tuning effect of the PTO follow the same trends as for the simulation. Furthermore, it is assumed that if the limitations of the driving actuator could be removed then the experimental results would give a better correlation at higher piston velocities.

CHAPTER 8

CONCLUSIONS

Wave energy converters (WECs) have been developed as a means to extract energy from the sea and generate electricity from a renewable source. The resultant devices that have been designed vary in their mode of operation and method of energy capture but they all require a process of converting the mechanical motion into electrical energy. Hydraulic power take-off units (PTOs) have been proposed for this process but their operation has not been investigated in great detail.

Therefore, the scope of this PhD research was to develop a simulation model to investigate the hydrodynamic interaction of a heaving buoy coupled to a realistic hydraulic PTO. This model could then be used to investigate buoy and PTO behaviour in different wave conditions and methods to maximise power generation. Furthermore, the verification of a simulation model against experimental results would provide a greater overall confidence in the research.

The thesis has been divided into a number of chapters. Chapter 3 presented the modelling of the device. It introduces the hydrodynamic modelling of a point absorber using linear wave theory and the realistic modelling of a hydraulic PTO with losses included. Results demonstrated the behaviour of the buoy in regular waves and the predicted PTO efficiency. Chapter 4 demonstrates the tuning of a hydraulic PTO to the wave frequency by adjusting the hydraulic motor displacement to maximise power generation in regular waves. Chapter 5 investigates the behaviour of the WEC in irregular waves created using wave spectra. The tuning, sizing and control of the hydraulic PTO to maximise power generation is then demonstrated in irregular waves. Chapter 6 presents real wave data collected from Scotland. It reveals the wave parameters for different sets of

data and it presents a real time tuning algorithm to maximise power generation from analysis of previous wave data. Finally, chapter 7 describes the experimental work which has been performed. The design of the test rig and experimental PTO is presented with results compared to an offline simulation model. A hardware-in-the-loop system is used to investigate the behaviour of the WEC without a wave tank and it demonstrates the PTO tuning to maximise power generation in regular waves.

8.1 Research Achievements

Most previous work in the area has assumed the PTO to be linear and not subject to any force limits or energy losses that would affect power generation. This simplest, linear PTO concept was therefore considered first in regular waves. Results showed it to behave like a viscous damper and produce a sinusoidal force, which causes the action of the buoy to also be sinusoidal.

The hydraulic PTO employed in this work uses a linear actuator, directly coupled to the buoy, behaving as a linear pump to drive a variable displacement hydraulic motor and generator. Flow rectification and smoothing accumulators are included to give a smoother power output by decoupling the power capture and generation elements of the PTO. For this arrangement, results indicate that the PTO reaches a pseudo steady state with the system pressure oscillating around an average value. A Coulomb type resisting force is produced by the PTO which causes the action of the WEC to not be sinusoidal with results revealing an induced body stall at the ends of the motion when the force produced by the PTO exceeds the total wave force. PTO efficiency is shown to have a significant effect on power generation but it remains fairly constant in all wave conditions.

There are two main ways to improve power generation in WECs; by improving power capture or by improving PTO efficiency. To improve power capture various control methods have been proposed by previous researchers. Reactive phase control is a way to achieve resonance through a negative spring force. This is possible for a linear PTO but for this hydraulic PTO arrangement a negative spring force cannot be produced.

However, force control can be achieved by altering the effective damping of the PTO, which is best accomplished by varying the hydraulic motor displacement. Results show that there is an optimal PTO damping to maximise power generation which is only dependent on the incoming wave frequency. This value

varies for the linear and hydraulic PTOs but the optimal PTO force amplitude is constant. This implies that there is the same optimal PTO force, which must be produced to maximise power generation but it is produced by different damping values for the distinct PTO models.

The WEC was then investigated in irregular waves to understand its behaviour and determine any control methods to improve power generation. Results revealed that, even with the large smoothing accumulators, no pseudo steady state is reached due to the highly irregular magnitude of the captured power. Induced body stall was still observed but the duration is always varying and is dependent on the PTO force and the incoming wave force. For this work, the wave profile was created using the Pierson-Moskowitz spectrum and results revealed that the device can be tuned to the peak wave frequency of the spectrum by varying the hydraulic motor displacement. However, the optimal PTO damping values are different to the values for regular waves.

A control strategy was proposed to maintain the motor speed at the synchronous speed of the generator, by altering the fraction of the motor displacement, to maintain the maximum flow of electrical power to the grid, assuming the use a doubly fed induction generator. To maintain the optimal PTO damping, the generator load must be altered at the same rate as the hydraulic motor displacement to ensure maximum power capture is maintained. Results revealed large gains in transmitted power but the hydraulic motor must also be sized appropriately for maximum PTO efficiency.

Real wave data was then used to represent irregular waves because it is random and non-repeating. Two months of data from the European Marine Energy Centre in Scotland were analysed to reveal the hourly variations in key wave parameters at different times of the year. Again PTO tuning was investigated, with results revealing the best correlation between the optimal PTO damping and the energy period of the waves over a 30-minute period, when the future knowledge of wave conditions was assumed.

Real time PTO tuning methods were then investigated to determine their advantages for power generation. A passive method, which uses a constant PTO damping for the mean site energy frequency, was compared to active methods which tune the PTO to the energy frequency calculated from a time period of preceding wave data which is updated every 20 s. The active methods were found to only give minimal gains over the passive tuning method but the performance of the active tuning methods is expected to improve as the energy period exhibits a

larger difference from the average site value. The best active method uses a time period with sufficient data to determine a long term change in wave frequency and so does not react to each individual wave.

Results also revealed significant power losses in both sea states extremes. In low energy seas, the small fraction of motor displacement required to maintain the synchronous speed causes poor motor efficiency. This may be deemed acceptable due to the small wave powers involved but these wave conditions are most frequent. However, in high energy seas, the motor displacement is not large enough to maintain the synchronous speed so much of the power generated is lost, as indicated by the low transmission efficiency. This may also be deemed acceptable due to the rare occurrences of such sea conditions but the powers involved are much greater. Overall, the results showed a maximum total PTO efficiency of approximately 60% for an average sea state.

A scaled experimental PTO was developed to validate the simulation work. The PTO test rig was driven by a hardware-in-the-loop system so the interaction of a real PTO with a hydrodynamic model of the buoy could be investigated. A limitation on the driving actuator meant that the experimental PTO produced differing results for certain conditions but overall the results gave a good validation of the simulation results. The experimental PTO produces a Coulomb type damping force whose magnitude has an effect on power generation. Results indicated a good correlation for the PTO tuning in regular waves between the HIL system and offline simulation model, which increases confidence in the full scale PTO simulation results.

8.2 Further Work

Overall, PTO efficiency can possibly be improved in all sea conditions by altering the PTO design. Two possible solutions are:

- Using a variable displacement hydraulic motor with high efficiency over the full operating range. For example the Digital Displacement motors developed by Artemis could be implemented in such a device [64]. This could mean a constantly high motor efficiency that would give power gains, especially in the low energy sea states.

- Multiple generation modules of different sizes could be incorporated into a single PTO. The effective motor displacement could therefore be varied

over a larger range by switching in and out modules using hydraulic valves. In low energy seas, it would mean a better sized PTO to maintain the synchronous speed and a high motor efficiency. However, it would also mean that the synchronous speed could be maintained in high energy seas so generated power would not be wasted by a generator.

It is noticeable that the level of captured power is appreciably lower than the incoming wave power. The captured power could be increased by incorporating a declutching control strategy [57]. The design of hydraulic PTOs lend themselves to this control strategy but work needs to be done to determine the generated power gains and the exact implementation of this strategy in real sea conditions.

Additionally, it is important to determine where these devices will be located so that annual wave conditions can be measured and the annual average generated power can be predicted. It is imperative to determine this value instead of the device rated power, as it will give a far better indication of their economic viability.

The author realises that the PTO model in this work has been defined by numerous parameters so all the results presented are for a single PTO sizing. Therefore, even though these settings make good physical sense, it would be interesting to perform a sensitivity analysis on the sizing of the PTO components. This could be performed using an open or closed loop Monte Carlo simulation based on random variation of the most important component sizes.

Finally, the experimental rig used in this work could be developed further in a number of ways. By increasing the velocity limit of the driving actuator to make all piston dynamics achievable would mean that PTO tuning could be investigated more thoroughly. Furthermore, to investigate the PTO efficiency the throttle valve must be removed and a variable displacement motor and generator load incorporated. This arrangement would also mean that a motor speed control strategy could be explored for irregular wave inputs.

APPENDIX A

FURTHER WAVE DATA ANALYSIS

The following terms can also be calculated from the frequency moments of the spectrum and their values for both months are shown in Figures A-1, A-2 and A-3.

The mean zero crossing period (T_z) is given by:

$$T_z = \sqrt{\frac{m_0}{m_2}} \tag{A.1}$$

The integral period (T_i) is given by:

$$T_i = \sqrt{\frac{m_{-2}}{m_0}} \tag{A.2}$$

The mean period (T_m) is given by:

$$T_1 = \frac{m_0}{m_1} \tag{A.3}$$

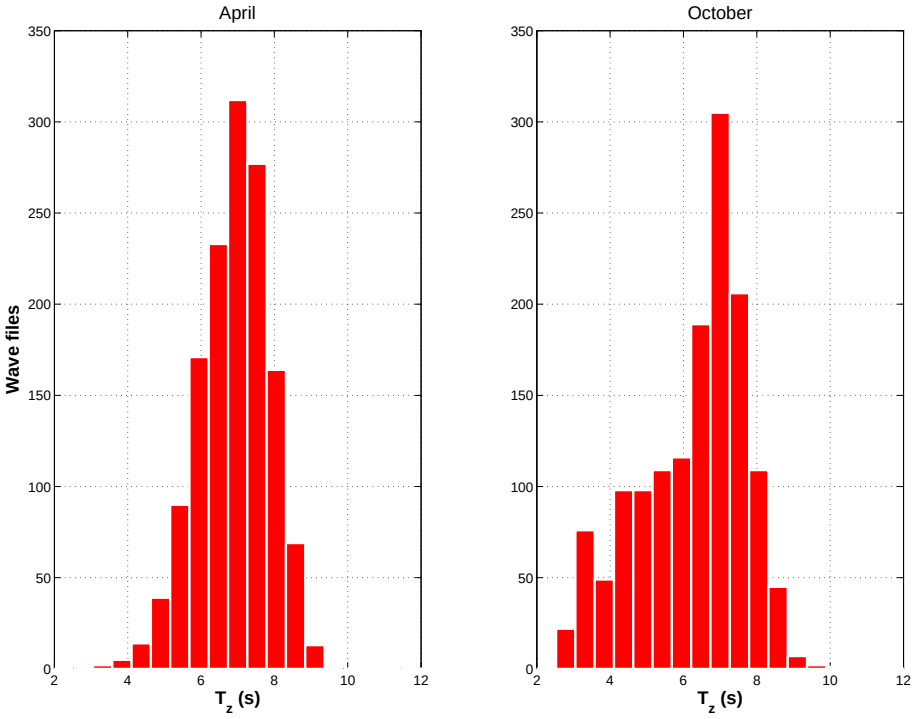

Figure A-1: *Frequency histogram showing the mean zero crossing period in April and October*

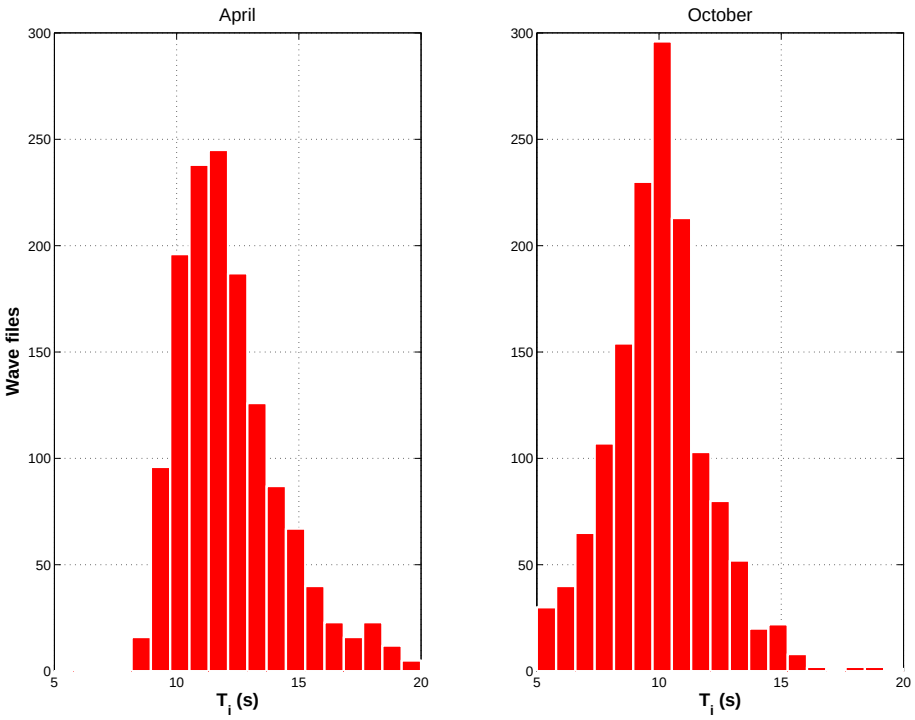

Figure A-2: *Frequency histogram showing the integral period in April and October*

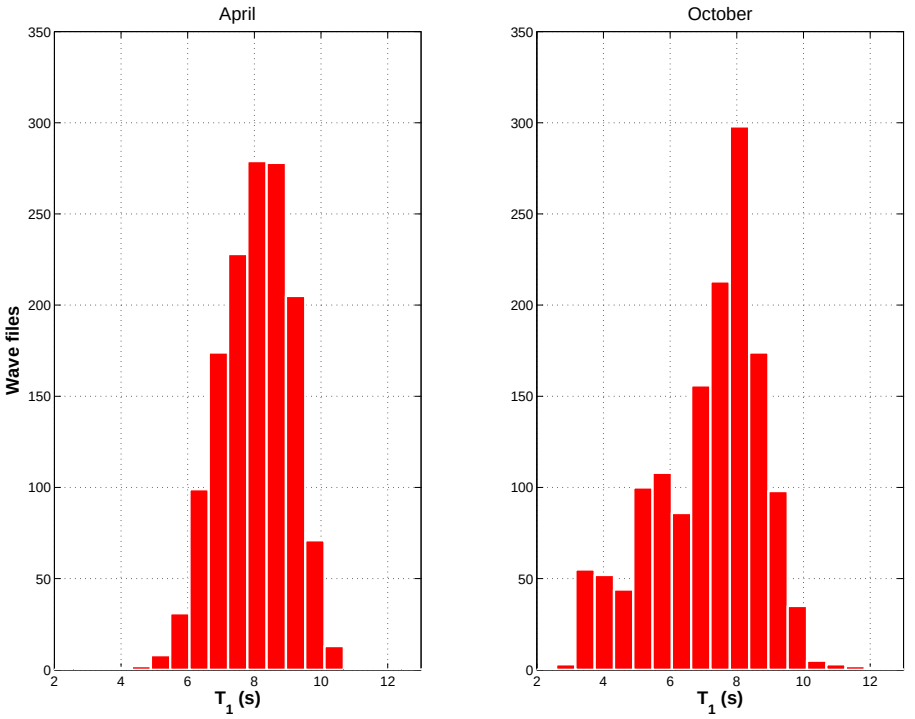

Figure A-3: *Frequency histogram showing the mean period in April and October*

A.1 Hourly Variation of Data

Figures A-4, A-5 and A-6 shows the hourly variation of H_s, T_p and T_e for the two months.

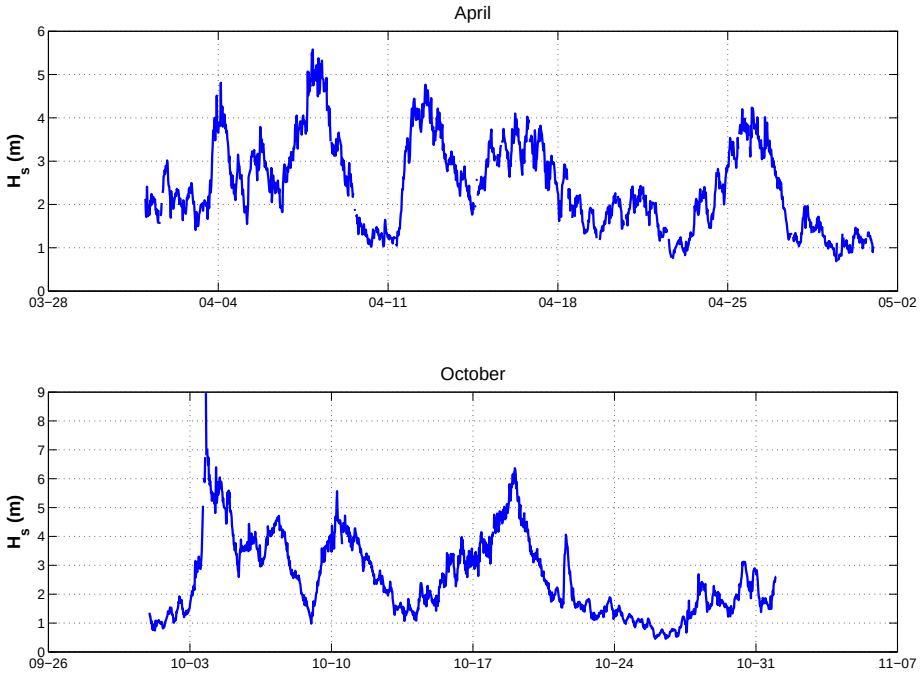

Figure A-4: *Hourly variation of H_s for April and October*

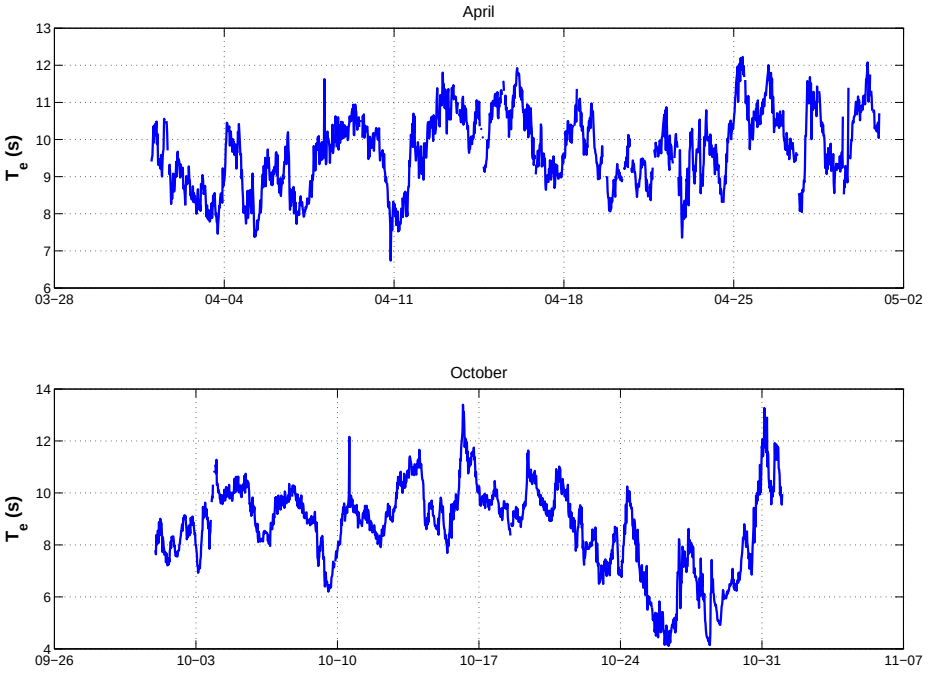

Figure A-5: *Hourly variation of T_e for April and October*

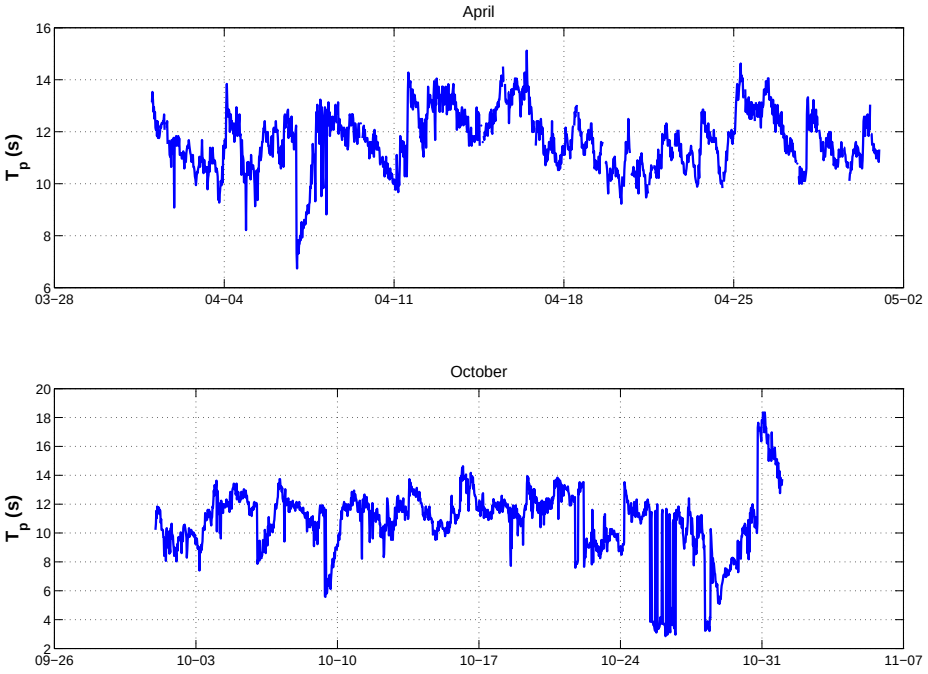

Figure A-6: *Hourly variation of T_p for April and October*

APPENDIX B

WAVE FILE INFORMATION FOR PTO TUNING

Month	Date	Time	Filtered T_p
April	21st	05:30	8.40
	28th	20:30	9.00
	14th	08:00	9.52
	8th	13:30	10.05
	13th	01:00	10.52
	8th	15:00	10.97
	21st	01:00	11.53
	12th	17:00	12.08
	20th	21:30	12.58
	12th	14:00	12.94
	12th	18:30	13.23
	21st	05:00	14.28
October	24th	10:30	7.86
	20th	23:00	8.69
	3rd	08:00	9.52
	3rd	07:30	10.00
	5th	05:30	10.52
	4th	17:00	10.97
	3rd	12:00	11.53
	24th	02:00	12.00
	2nd	11:00	12.50
	28th	05:30	12.94
	18th	13:00	13.42
	18th	12:30	14.05

Table B.1: *Dates, times and peak period of the EMEC files used in the PTO tuning in Section 6.3*

APPENDIX C

EXPERIMENTAL PTO TUNING

Pressure (bar)	PTO Force (N)	Flow (lpm)	Hydraulic Power (W)
41.6	2777	7.01	445
49.5	3293	6.76	519
60.9	4037	6.49	622
70.5	4659	6.30	703
79.4	5273	5.98	757
90.9	5994	5.77	839
102.3	6764	5.41	889
116.8	7714	4.77	901
129.5	8494	4.10	857
135.4	8855	3.69	809

Table C.1: *The full results for the offline simulation model in Section 7.4*

Pressure (bar)	PTO Force (N)	Flow (lpm)	Hydraulic Power (W)
38.9	2823	7.14	330
46.3	3377	7.07	420
49.1	3669	7.00	453
60.7	4679	5.51	468
66.0	5299	5.47	542
72.1	6220	5.58	605
85.0	6574	4.96	647
94.8	7364	4.40	645
110.0	8354	4.33	626
115.1	8814	4.21	598

Table C.2: *The full results for the HIL model in Section 7.4*

REFERENCES

[1] T.W. Thorpe. An overview of wave energy technologies: status, performance and costs. *Wave Power: moving towards Commercial Viability*, 30 November 1999.

[2] Opt- ocean power technologies. Obtained from: `http://www.oceanpowermagazine.net` on 18/07/12.

[3] Aws- archimedes wave swing. Obtained from: `http://atsariam.blogspot.co.uk` on 18/07/12.

[4] Pelamiswave. Obtained from: `http://www.rechargenews.com` on 18/07/12.

[5] Salter's duck. Obtained from: `http://www.marketoracle.co.uk` on 10/10/12.

[6] Aquamarine power- oyster. Obtained from: `http://www.dpenergy.com` on 18/07/12.

[7] Oscillating water column. Obtained from: `http://www.esru.strath.ac.uk` on 18/07/12.

[8] Wave dragon overtopper. Obtained from: `http://www.wavedragon.net` on 18/07/12.

[9] B. Drew, A.R. Plummer, and M.N. Sahinkaya. A review of wave energy converter technology. *Proceedings of the Institution of Mechanical Engineers, Part A: Journal of Power and Energy*, 223(8):887–902, 2009.

[10] H. Yavuz, A. McCabe, G. Aggidis, and M.B. Widden. Calculation of the performance of resonant wave energy converters in real seas. *Proceedings of the Institution of Mechanical Engineers, Part M: Journal of Engineering for the Maritime Environment*, 220(3):117–128, 2006.

[11] M. McCormick. *Ocean Wave Energy Conversion*. Dover Publications, 1981.

[12] Anon. "Accelerating marine energy". Technical report, The Carbon Trust, July 2011.

[13] S. Barstow, D. Mollison, and J. Cruz. The Wave Energy Resource. In J. Cruz, editor, *Ocean Wave Energy: Current Status and Future Perspectives*, chapter 4, pages 93–132. Springer, 2008.

[14] J. Falnes. A review of wave-energy extraction. *Marine Structures*, 20:185–201, 2007.

[15] B. Count, editor. *Power from Sea Waves*. Academic Press, London, UK, 1980.

[16] R. Pelc and R.M. Fujita. Renewable energy from the ocean. *Marine Policy*, 26(6):471–479, 2002.

[17] S. Salter. Looking Back. In J. Cruz, editor, *Ocean Wave Energy: Current Status and Future Perspectives*, chapter 2, pages 7–39. Springer, 2008.

[18] J. Twidell and T. Weir. *Renewable Energy Resources*. Taylor and Francis, London, UK, second edition, 2006.

[19] A.F.O. Falcão. Wave energy utilization: A review of the technologies. *Renewable and Sustainable Energy Reviews*, 14:899–918, 2010.

[20] S.H. Salter, J.R.M. Taylor, and N.J. Caldwell. Power conversion mechanisms for wave energy. *Proceedings of the Institution of Mechanical Engineers, Part M: Journal of Engineering for the Maritime Environment*, 216(1):1–27, 2002.

[21] M.A. Mueller. Electrical generators for direct drive wave energy converters. *Generation, Transmission and Distribution, IEE Proceedings-*, 149(4):446–456, 2002.

[22] R. Crozier, H. Bailer, M. Mueller, E. Spooner, P. McKeever, and A. McDonald. Hydrodynamic and Electromechanical Simulation of a WEC with a Novel Non-Linear PTO. In *Proceedings of the 9th European Wave and Tidal Energy Conference (EWTEC)*, Southampton, UK, September 2011.

[23] H. Polinder, M.E.C. Damen, and F. Gardner. Linear PM Generator system for wave energy conversion in the AWS. *Energy Conversion, IEEE Transactions on*, 19(3):583–589, 2004.

[24] H. Polinder, M.E.C. Damen, and F. Gardner. Design, modelling and test results of the AWS PM linear generator. *European Transactions on Electrical Power*, 15:245–256, 2005.

[25] N. Iwabuchi, A. Kawahara, T. Kume, T. Kabashima, and N. Nagasaka. A Novel High-Torque Reluctance Motor with Rare-Earth Magnet. *IEEE Transactions on Industry Applications*, 145(6), May/June 1994.

[26] M. Leijon, H. Bernhoff, O. Agren, J. Isberg, J. Sundberg, M. Berg, K.E. Karlsson, and A. Wolfbrandt. Multiphysics simulation of wave energy to electric energy conversion by permanent magnet linear generator. *Energy Conversion, IEEE Transactions on*, 20(1):219–224, 2005.

[27] D.L. O'Sullivan and T. Lewis. Electrical Machine Options in Offshore Floating Wave Energy Converter Turbo-Generators. In *Proceedings of the 10th World Renewable Energy Congres (WREC X)*, pages 1102–1107, 2008.

[28] R. Henderson. Design, simulation, and testing of a novel hydraulic power take-off system for the Pelamis wave energy converter. *Renewable Energy*, 31(2):271–283, February 2006.

[29] J. Taylor. Hydraulics. In J. Cruz, editor, *Ocean Wave Energy: Current Status and Future Perspectives*, chapter 6.3, pages 241–260. Springer, 2008.

[30] C. Josset, A. Babarit, and A.H. Clément. A wave-to-wire model of the SEAREV wave energy converter. *Proceedings of the Institution of Mechanical Engineers, Part M: Journal of Engineering for the Maritime Environment*, 221:81–93, 2007.

[31] A.R. Plummer and M. Schlotter. Investigating the Performance of a Hydraulic Power Take-Off. In *Proceedings of the 8th European Wave and Tidal Energy Conference (EWTEC)*, Uppsala, Sweden, 2009.

[32] The european wave energy centre. Obtained from: `http://www.emec.org.uk` on 30/09/09.

[33] PelamisWave. Pelamiswave. Obtained from: `http://www.pelamiswave.com` on 27/09/09.

[34] J. Callaghan and R. Boud. "Future Marine Energy: Results of the Marine Energy Challenge: Cost competitiveness and growth of wave and tidal stream energy". Technical report, The Carbon Trust, January 2006.

[35] H. Yavuz, T.J. Stallard, A.P. McCabe, and G. Aggidis. Time series analysis-based adaptive tuning techniques for a heaving wave energy converter in irregular seas. *Proceedings of the Institution of Mechanical Engineers, Part A: Journal of Power and Energy*, 221(1):77–90, 2007.

[36] M.J.L. Greenhow. The hydrodynamic interactions of spherical wave-power devices in surface waves, booktitle=Power from Sea Waves. pages 287–343. Academic Press, London, 1980.

[37] E.R. Jeffreys. Device Characterisation. In B. Count, editor, *Power from Sea Waves*, pages 413–438. Academic Press, London, 1980.

[38] J. Falnes. *Ocean Waves and Oscillating Systems*. Cambridge University Press, Cambridge, UK, 2002.

[39] W. E. Cummins. The Impulse Response Function and Ship Motions. *Schiffstechnik*, 9:101–109, 1962.

[40] M. O'Cathain, B.J. Leira, J.V. Ringwood, and J-C Golloteaux. A modelling methodology for multi-body systems with application to wave-energy devices. *Ocean Engineering*, 35:1381–1387, July 2008.

[41] G. Thomas. The Theory Behind the Conversion of Ocean Wave Energy: A Review. In J. Cruz, editor, *Ocean Wave Energy: Current Status and Future Perspectives*, chapter 3, pages 41–91. Springer, 2008.

[42] A.F.O. Falcão. Modelling and control of oscillating-body wave energy converters with hydraulic power take-off and gas accumulator. *Ocean Engineering*, 24:2021–2032, 2007.

[43] A.F.O. Falcão. Phase control through load control of oscillating-body wave energy converters with hydraulic PTO system. *Ocean Engineering*, 35:358–366, 2008.

[44] A. Babarit, G. Duclos, and A.H. Clément. Comparison of latching control strategies for a heaving wave energy device in random sea. *Applied Ocean Research*, 26(5):227–238, 2005.

[45] G. Duclos, A. Babarit, and A.H. Clément. Optimizing the Power Take Off of a Wave Energy Converter With Regard to the Wave Climate. *Journal of Offshore Mechanics and Arctic Engineering*, 128:56, 2006.

[46] B.F.M. Child and V. Venugopal. Optimal configurations of wave energy device arrays. *Ocean Engineering*, 37:1402–1417, 2010.

[47] B. Borgarino, A. Babarit, and P. Ferrant. Impact of the seperating distance between interacting wave energy converters on the overall energy extraction of an array. In *Proceedings of the 9th European Wave and Tidal Energy Conference (EWTEC)*, Southampton, UK, September 2011.

[48] B.F.M. Child and M. Livingstone. The development of a tool for optimising arrays of wave energy converters. In *Proceedings of the 9th European Wave and Tidal Energy Conference (EWTEC)*, Southampton, UK, September 2011.

[49] U.A. Korde. Efficient primary energy conversion in irregular waves. *Ocean Engineering*, 26(7):625–651, 1999.

[50] J. Falnes. Optimum control of oscillation of wave-energy converters. *International Journal of Offshore and Polar Engineering*, 12(2):147–154, 2002.

[51] U.A. Korde. Control system applications in wave energy conversion. *OCEANS 2000 MTS/IEEE Conference and Exhibition*, 3, 2000.

[52] K Budal and Falnes J. Interacting point absorbers with controlled motion. In B. Count, editor, *Power from Sea Waves*, pages 381–399. Academic Press, London, 1980.

[53] A. Babarit and A.H. Clément. Optimal latching control of a wave energy device in regular and irregular waves. *Applied Ocean Research*, 28(2):77–91, 2006.

[54] M Livingstone and A.R. Plummer. The Design, Simulation and Control of a Wave Energy Converter. In *Proceedings of the 7th International Fluid Power Conference*, Aachen, Germany, 2010.

[55] M. Folley and T. Whittaker. The control of wave energy converters using active bipolar damping. *Proceedings of the Institution of Mechanical Engineers, Part M: Journal of Engineering for the Maritime Environment*, 223(4):479–487, 2009.

[56] A. Babarit, H. Mouslim, M. Guglielmi, and A.H. Clément. Simulation of the SEAREV Wave Energy Converter with a by-pass control of its hydraulic Power Take Off. In *Proceedings of the 10th World Renewable Energy Congress (WREC X)*, pages 1004–1009, Glasgow, UK, July 2009.

[57] A. Babarit, M. Guglielmi, and A.H. Clément. Declutching control of a wave energy converter. *Ocean Engineering*, 36:1015–1024, 2009.

[58] K. Gunn, J. Taylor, and C. Lingwood. An independent validation of the optimality of latching and de-clutching control by evolutionary methods. In *Proceedings of the 9th European Wave and Tidal Energy Conference (EWTEC)*, Southampton, UK, September 2011.

[59] A.P. McCabe and G.A. Aggidis. Optimum mean power output of a point-absorber wave energy converter in irregular waves. *Proceedings of the Institution of Mechanical Engineers, Part A: Journal of Power and Energy*, 223(7):773–781, 2009.

[60] P. Ricci, J. Lopez, M. Santos, J.L. Villate, P. Ruiz-Minguela, F. Salcedo, and A.F.O. Falcão. Control Strategies of a simple Point-Abrsorber Connected to a Hydraulic Power Take-Off . In *Proceedings of the 8th European Wave and Tidal Energy Conference (EWTEC)*, Uppsala, Sweden, 2009.

[61] Y Kamizuru and H Murrenhoff. Improved Control Strategy for Hydrostatic Transmissions in Wave Power Plants. In *Proceedings of the Twelth Scandinavian International Conference on Fluid Power*, Tampere, Finland, May 2011.

[62] K. Schlemmer, F. Fuchshumer, N. Böhmer, R. Costello, and C. Villegas. Design and Control of a Hydraulic Power Take-off for an Axi-symmetric

Heaving Point Absorber. In *Proceedings of the 9th European Wave and Tidal Energy Conference (EWTEC)*, Southampton, UK, September 2011.

[63] R.H Hansen, T.O Andersen, and H.C Pedersen. Model Based Design of Efficient Power Take-Off Systems for Wave Energy Converters. In *Proceedings of the Twelth Scandinavian International Conference on Fluid Power*, Tampere, Finland, May 2011.

[64] R. Costello, J.V. Ringwood, and J. Weber. Comparison of Two Alternative Hydraulic PTO Concepts for Wave Energy Conversion. In *Proceedings of the 9th European Wave and Tidal Energy Conference (EWTEC)*, Southampton, UK, September 2011.

[65] H. Yavuz, S. Mistikoglu, and T. Stallard. Processing irregular wave measurements to enhance point absorber power capture performance. *Ocean Engineering*, 38:684–698, 2011.

[66] A. Babarit and J. Hals. On the maximum and actual capture width ratio of wave energy converters. In *Proceedings of the 9th European Wave and Tidal Energy Conference (EWTEC)*, Southampton, UK, September 2011.

[67] A. Hulme. The Wave forces acting on a floating hemisphere undergoing forced periodic oscillations. *The Journal of Fluid Mechanics*, 121:443–463, 1982.

[68] M. Eriksson, J. Isberg, and M. Leijon. Hydrodynamic modelling of a direct drive wave energy converter. *International Journal of Engineering Science*, 43:1377–1387, 2005.

[69] M Ivantysynova. Energy Losses of Modern Displacement Machines- a New Approach of Modelling. In *Proceedings of the Seventh Scandinavian International Conference on Fluid Power, SICFP' 01*, Linkoping, Sweden, May 2001.

[70] W.E. Wilson. Performance criteria for positive displacement pumps and fluid motors. *Trans. Am. Soc. Mech. Eng*, 71(2), 1949.

[71] D McCandlish and R.E Dorey. The mathematical modelling of hydrostatic pumps and motors. *Proceedings of the Institution Mechanical Engineers*, 198B(10), 1983.

[72] W.B Wan Nik, M.A Maleque, F.N Ani, and H.H Masjuki. Experminetal investigation on system performance using palm oil as hydraulic fluid. *Industrial Lubrication and Tribology*, 59(5):200–208, 2007.

[73] Y. Goda. Statistical Properties and Spectra of Sea Waves. In *Advanced Series And Design Of Maritime Structures*, volume 15, chapter 2, pages 12–44. 2000.

[74] M.J. Ketabdari and A. Ranginkaman. Measurements of wind-wave growth and swell decay during the Joint North Sea Wave Project (JONSWAP). *Deutsche Hydr. Zeit Reihe A*, 8(12), 1973.

[75] W.J. Jr Pierson and L. Moskowitz. A proposed spectral form for fully developed wind seas based on the similarity theory of S.A. Kitaigoroskii. *Journal of Geophysical Research*, 69(24):5181–5190, 1964.

[76] M.J. Ketabdari and A. Ranginkaman. Simulation of Random Irregular Sea Waves for Numerical and Physical Models Using Digital Filters. *Transaction B: Mechanical Enginerring*, 16(3):240–247, 2009.

[77] A. Petersson. *Analysis, Modeling and Control of Doubly-Fed Induction Generators for Wind Turbines*. PhD thesis, Chalmers University of Technology, 2005.

[78] Edward Pitt. Assessment of Wave Energy Resource. Technical report, European Marine Energy Centre, 2009.

[79] A. Savitzky and M.J.E. Golay. Smoothing and Differentiation of Data by Simplified Least Squares Procedures. *Analytical Chemistry*, 36(8):1627–1639, 1964.

[80] J-C. Mare and P-E. Berthe. Design, virtual prototyping and test of a regnerative shock absorber for race cars. In *Proceedings of the 22nd Fluid Power and Motion Control Symposium (FPMC)*, pages 447–460, Bath, England, September 2010.